

1 **The Fucino 250-170 ka tephra record: new insights on peri-Tyrrhenian explosive**
2 **volcanism, central Mediterranean tephrochronology, and timing of the MIS 8-6 climate**
3 **variability**

4

5 Lorenzo Monaco^{a, b}, Niklas Leicher^c, Danilo M. Palladino^d, Ilenia Arienzo^e, Fabrizio Marra^f, Maurizio Petrelli^g, Sebastien Nomade^h,
6 Alison Pereiraⁱ, Gianluca Sottili^d, Sandro Conticelli^j, Massimo D'Antonio^k, Alessandro Fabbri^l, Brian R. Jicha^m, Giorgio Mannella^a,
7 Paola Petrosino^k, Polychronis C. Tzedakisⁿ, Bernd Wagner^c, Giovanni Zanchetta^a, Biagio Giaccio^{b, f, *}

8

9

Affiliations

10

a Dipartimento di Scienze della Terra, University of Pisa, Pisa, Italy

11

b Istituto di Geologia Ambientale e Geoingegneria, CNR-IGAG, Monterotondo, Rome, Italy

12

c Institute of Geology and Mineralogy, University of Cologne, Cologne, Germany

13

d Dipartimento di Scienze della Terra, "Sapienza" - University of Rome, Rome, Italy

14

e Istituto Nazionale di Geofisica e Vulcanologia, Osservatorio Vesuviano, Naples, Italy

15

f Istituto Nazionale di Geofisica e Vulcanologia, INGV, Rome, Italy

16

g Dipartimento di Fisica e Geologia, University of Perugia, Perugia, Italy

17

h Laboratoire de Sciences du Climat et de l'Environnement, UMR 8212, CEA-UVSQ, IPSL and Université de Paris-Saclay, Gif-sur-Yvette, France

18

i Université Paris-Saclay, CNRS, UMR 8148, Laboratoire GEOPS, Orsay, 91405, France

19

j Dipartimento di Scienze della Terra, Università degli Studi di Firenze, Florence, Italy

20

k Dipartimento di Scienze della Terra, dell'Ambiente e delle Risorse, Università degli Studi di Napoli Federico II, Naples, Italy

21

l Institute of Petrology and Structural Geology, Faculty of Science, Charles University, Albertov 6, 12843 Prague, Czech Republic

22

m Department of Geoscience, University of Wisconsin-Madison, Madison, Wisconsin, USA

23

n Environmental Change Research Centre, University College London, London, UK

24

** Corresponding author*

25

26 **ABSTRACT**

27 The Fucino Basin, central Italy, with its long and continuous history of Quaternary sediment accumulation, is
28 one of the richest Mediterranean Middle Pleistocene tephra records. Here we present a new detailed
29 investigation of tephra layers of the 250-170 thousand years before present (ka) interval, corresponding to the
30 entire Marine Isotope Stage (MIS) 7 and parts of the MIS 8 and MIS 6. The investigated tephra layers have
31 been characterised in terms of major, minor and trace elements, Sr-Nd isotopic compositions and ⁴⁰Ar/³⁹Ar
32 ages. For correlation purposes, glass compositions and several new ⁴⁰Ar/³⁹Ar ages of selected proximal
33 pyroclastic units spanning the same temporal interval from Vulsini, Sabatini, and Vico volcanic systems, central
34 Italy, were measured. The late MIS 8-early MIS 6 Fucino tephras were backtracked to their corresponding
35 volcanic sources, which include the Vulsini, Vico, Sabatini, Roccamonfina, Ischia and Campi Flegrei volcanic
36 systems. While some of these tephra layers have been correlated to specific eruption units, other layers are
37 currently not documented or described in near vent sections, thus highlighting previously unrecognised events
38 generated by these volcanic systems. Furthermore, the new high precision ⁴⁰Ar/³⁹Ar ages provide improved
39 temporal constraints for Fucino making it one of the most detailed and chronologically best constrained tephra

40 record for central Mediterranean MIS 7 tephrochronology. The investigated Fucino record thus provides new
41 integrative information for reconstructing the explosive history of Italian volcanoes during the investigated
42 interval. Furthermore, the geochronological constrains provide the basis for future paleoclimatic investigations
43 at local and regional scale.

44

45 **1. Introduction**

46 Past changes in the Earth's climate system are being explored in ever greater temporal detail to obtain a
47 better understanding of the role of the orbital forcing and the interaction dynamics among its different
48 components (e.g., cryosphere and oceanic-atmospheric circulation, and their regional expression and impact).
49 Simultaneous to the advent of this high- to ultrahigh-resolution investigation approach, the urgency of precise
50 and accurate chronologies become crucial. However, for changes before 55 ka, i.e., the current limit of the
51 radiocarbon dating (e.g., [Reimer et al., 2020](#)), the chronology of the proxy records often is still limited by
52 relatively high uncertainties, assumptions, and circular reasonings (e.g., astronomical tuning procedures).
53 Reducing the uncertainties in dating and correlations, as well as making the chronology of the proxy series
54 independent of any assumptions, is therefore becoming an urgent issue in palaeoclimate studies.

55 In this framework, tephrostratigraphy and tephrochronology, that constitute the methods through which
56 sedimentary successions can be synchronized and dated via geochemical and geochronological tephra
57 fingerprinting (e.g., [Davies et al., 2010](#)), are now considered an outstanding tool for addressing several topics
58 of the Quaternary sciences ([Lowe, 2011](#); [Lane et al., 2017](#)), such as paleoclimatology ([Lane et al., 2013](#);
59 [Blockley et al., 2014](#); [Kutterolf et al., 2019](#)), archaeology ([Giaccio et al., 2008, 2017a](#); [Lane et al., 2014](#); [Pereira
60 et al., 2018](#); [Zanchetta et al., 2018](#); [Villa et al., 2020](#)), and paleogeographic-tectonic evolution (e.g., [Giaccio et
61 al., 2012a](#); [Galli et al., 2017](#); [Bini et al., 2020](#)). Distal tephrostratigraphy is also increasingly being exploited for
62 volcanological purposes, becoming a fundamental and integrative tool for a detailed reconstruction of the
63 history, dynamics, and timing of explosive volcanism (e.g., [Thorarinsson, 1944, 1981a, 1981b](#); [Giaccio et al.,
64 2014](#); [Ponomareva et al., 2015](#); [Albert et al., 2019](#); [Wulf et al., 2020](#); [Monaco et al., 2021](#)).

65 However, such a great potential strongly depends on the completeness and quality of the available tephra
66 geochemical and geochronological datasets that allow their unambiguous identification through diagnostic
67 features, among which the geochemical glass composition is one of the most powerful (e.g., [Smith and
68 Westgate, 1968](#); [Hayward, 2011](#); [Lowe et al., 2017](#); [Pearce et al., 2019](#)).

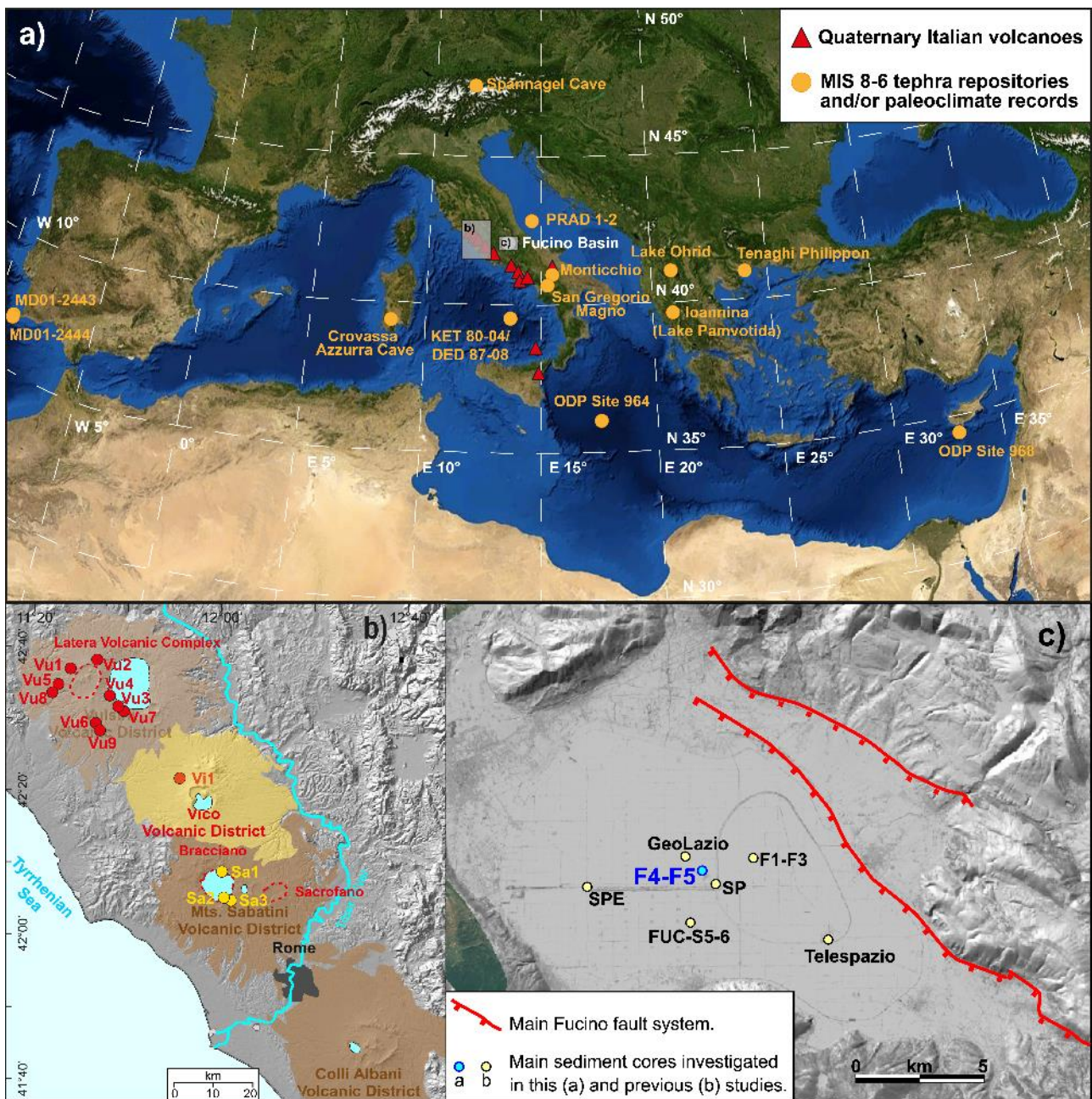
69 Although tephrochronology can be applied to all regions of the Earth characterised by intense and frequent
70 volcanism (e.g., [Shane, 2000](#); [de Fontaine et al., 2007](#); [Wastegård et al., 2013](#); [Albert et al., 2018](#); [De](#)

71 [Maisonneuve & Bergal-Kuvikas, 2020](#); [Chen et al., 2022](#); [Sunyé-Puchol et al., 2022](#)), the Mediterranean area
72 ([Fig. 1a](#)) is as an ideal region for its development and application. Its complex geodynamic setting, the diffuse
73 and geochemically diverse Quaternary magmatism (e.g., [Wilson and Bianchini, 1999](#)), and abundant
74 continental and marine basins acting as fundamental traps for sediments and tephra layers, make this region
75 particularly well-suited for the application of tephrochronology (e.g., [Paterne et al., 1986, 1988, 2008](#); [Wulf et
76 al., 2004, 2008, 2012](#); [Bourne et al., 2010, 2015](#); [Satow et al., 2015](#); [Petrosino et al., 2016](#); [Giaccio et al.,
77 2017a, 2019](#); [Leicher et al., 2019, 2021](#); [Vakhrameeva et al., 2021](#)). Furthermore, the alkaline magmas feeding
78 the peri-Tyrrhenian potassic Quaternary volcanoes (e.g., [Peccerillo, 2017](#)) generated products bearing K-rich
79 minerals (e.g., sanidine and leucite), which are ideal for direct $^{40}\text{Ar}/^{39}\text{Ar}$ dating. The significant technological
80 developments of noble gas mass spectrometers over the last decade, such as the introduction of the multi-
81 collector spectrometer Isotopx NGX-600 ([Mixon et al., 2022](#)), have improved the effectiveness of the method
82 and the possibility of getting direct, high-precision $^{40}\text{Ar}/^{39}\text{Ar}$ dating of fine-grained distal tephra (e.g., [Albert et
83 al., 2019](#); [Monaco et al., 2022](#)).

84 Among the numerous distal archives, the lacustrine succession hosted in the Fucino Basin, central Italy ([Fig.
85 1c](#)), proves to be the richest Mediterranean Middle Pleistocene tephra records ([Giaccio et al., 2017a, 2019](#); [Di
86 Roberto et al., 2018](#); [Del Carlo et al., 2020](#); [Monaco et al., 2021](#)). Here we present a detailed investigation of
87 the tephra succession spanning the ~250-170 ka interval from the Fucino lake sediments recovered in the F4-
88 F5 core documenting the last 430 ka ([Giaccio et al., 2019](#); [Monaco et al., 2021](#)). The selected interval spans
89 from the late MIS 8 to the early MIS 6 glacial periods and thus encompasses the whole MIS 7 interglacial
90 complex.

91 This interval includes 21 tephra layers (n=21) that were all geochemically characterised in terms of major and
92 minor element compositions. For selected layers, we also provided the trace element (n=7), the Sr-Nd isotopic
93 compositions (n=10), and $^{40}\text{Ar}/^{39}\text{Ar}$ ages (n=3). Furthermore, to improve the reference geochemical dataset
94 required for establishing reliable proximal-distal correlations of the Fucino tephra with the corresponding near-
95 vent volcanic deposits, we also provided new glass analyses and $^{40}\text{Ar}/^{39}\text{Ar}$ ages (n=6) of proximal pyroclastic
96 units ([Fig. 1b](#)) that were all emplaced during the 250-150 ka time interval here considered. These deposits
97 were generated from the Latera Volcanic Complex (LVC, Vulsini Volcano; [Vezzoli et al., 1987](#)), the Sabatini
98 Volcanic District (SVD; [Sottili et al., 2010](#)), and Vico volcano (i.e., Farine Formation Unit of [Sollevanti, 1983](#)).
99 For improving the correlations among Mediterranean records, we also present new glass compositions
100 acquired by EPMA-WDS (Electron Probe Micro Analyser-Wavelength Dispersive Spectroscopy) of tephra OH-
101 DP-0725 from the Lake Ohrid sediment succession (Albania, North Macedonia), which was previously

102 investigated only by SEM-EDS (Scanning Electron Microscope-Energy Dispersive Spectroscopy) and
 103 attributed to Campi Flegrei/Pantelleria (Leicher et al., 2019, 2021). Whilst we correlate some of the Fucino
 104 tephras to eruptions generated at Vulsini, Vico, Sabatini, Roccamonfina, Ischia, and Campi Flegrei volcanoes,
 105 other tephras are attributed to eruptions that have not yet been documented in proximal settings or are
 106 geochronologically and geochemically poorly characterised. The results of this study are discussed both in
 107 terms of the volcanic histories and recurrence time intervals at the peri-Tyrrhenian Quaternary volcanoes and
 108 of tephrochronological constraints for the Mediterranean MIS 7 sedimentary archives.
 109



110
 111 **Figure 1.** Reference maps. **a)** Map of the Central Mediterranean with the location of the Fucino Basin, the continental and insular
 112 Quaternary Italian volcanic districts and other sites cited in the text. **b)** Location of the Latera Volcanic Complex (LVC), Vico volcano, and

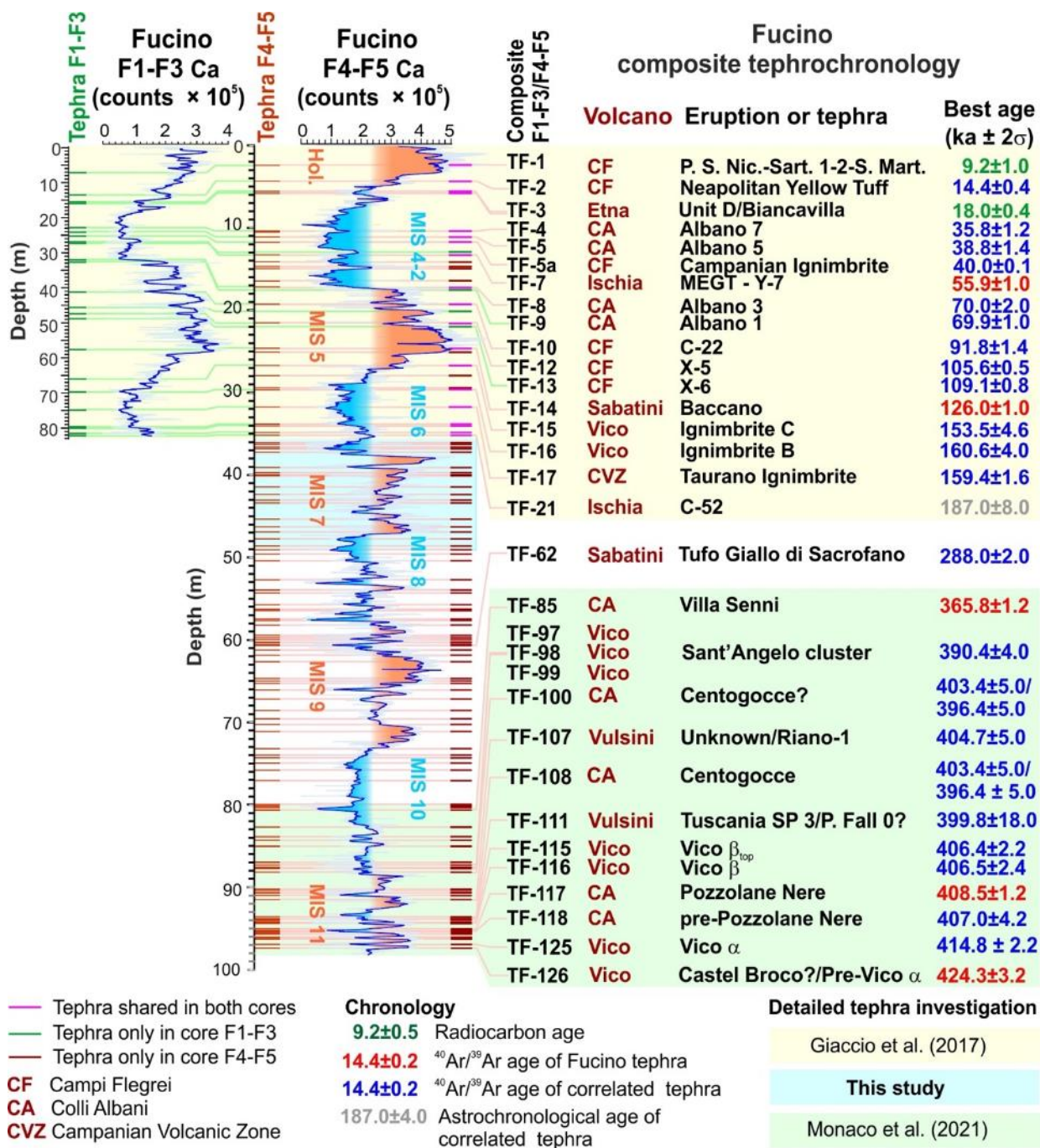
113 Bracciano and Sacrofano (SVD) centres, along with locations of investigated sections. c) Fucino Plain with the locations of the F4-F5 and
114 other drilling sites.
115

116 2. Geological setting and tephrochronological framework of the Fucino Basin

117 The Fucino Basin is one of the largest intermountain tectonic basins in central Italy (Fig. 1c) and formed
118 during the extensional stretching of the Apennine chain following the opening of the Tyrrhenian Basin (e.g.,
119 Doglioni et al., 1996). Starting in the Late Pliocene-Lower Pleistocene, extensional tectonic, mainly acting
120 along E-W, NE-SW, and NW-SE oriented high-angle normal faults, caused the stretching of the mountain
121 chain (e.g., D'Agostino et al., 2001) and opening of several intermountain basins, including the Fucino Basin
122 (Galadini and Galli, 2000; Boncio et al., 2004; Giaccio et al., 2012b; Amato et al., 2014). The Plio-Quaternary
123 tectonic and sedimentary evolution of the Fucino Basin was driven by the *Fucino Fault System* (FFS, Galadini
124 and Galli, 2000; Fig. 1c), which depicts a semi-graben architecture where the thickness of the Plio-Quaternary
125 sedimentary infilling increases up to ~900 m from west to east toward the depocenter (Cavinato et al., 2002;
126 Patacca et al., 2008). The Fucino Basin was likely characterised by continuous sedimentation (Giaccio et al.,
127 2017a, 2019; Mannella et al., 2019) since the Plio-Pleistocene and hosted a lake, *Lacus Fucinus*, until the 19th
128 century CE, when it was drained by the Torlonia family.

129 Two cores were recovered at the F4-F5 drilling site in the central area of the basin (42°00'06" N, 13°32'18" E,
130 Fig. 1c) and combined into a 98 m-long composite profile based on optical information and geochemical data
131 obtained from XRF scanning (Giaccio et al. 2019). Drilling site selection strategy and recovery procedure are
132 reported in Giaccio et al. (2019). The F4-F5 composite profile contains at least 130 tephra layers (Giaccio et
133 al., 2019; Fig. 2). The sediment succession from F4-F5 was ascribed to the last 430 ka (Fig. 2; Giaccio et al.,
134 2019) based on correlations with tephra layers from the nearby F1-F3 record covering the last 190 ka (Giaccio
135 et al., 2017a), and on a detailed geochemical and geochronological characterisation of 32 tephra layers from
136 the lowermost portion of the F4-F5 record, spanning the 430-365 ka time interval or the MIS 11 period (Monaco
137 et al., 2021; Fig. 2). Tephra layers from this interval were attributed to the Vulsini, Vico, Sabatini, Colli Albani,
138 and Roccamonfina volcanic districts, providing new detailed chronological constraints for the frequent
139 explosive activity of these volcanoes.

140



141

142

143

Figure 2. Composite F1-F3/F4-F5 tephra record. Data source: Giaccio et al. (2017a, 2019), Monaco et al. (2021) and references therein.

Table 1. Data summary of the investigated F4-F5 Fucino tephra, along with Ohrid tephra OH-DP-0725 and proximal LVC, Vico and SVD pyroclastic units.

Distal tephra							
Location	Tephra	Core section and depth (cm)	Composite Depth (m)	Type of analysis			
				Glass-WDS (EPMA)	Trace elements (LA-ICP-MS)	Sr and Nd isotopes (TIMS)	⁴⁰ Ar/ ³⁹ Ar
Fucino Basin (F4-F5)	TF-17a ^b	F4-22 60.00-62.00	31.74	Yes	No	No	No
	TF-18a ^b	F4-23 107.8-111.0	33.79	Yes	Yes	Yes	No
	TF-19a ^b	F5-23 61.50-67.00	34.01	Yes	Yes	Yes	No
	TF-21a ^b	F4-24 45.50-48.93	34.83	Yes	Yes	No	No
	TF-21a ^b	F4-24 79.50-81.50	35.15	Yes	No	No	No
	TF-22a ^b	F5-25 111.5-114.7	36.04	Yes	No	Yes	Yes
	TF-23 ^b	F5-24 130.8-134.3	36.24	Yes	No	No	No
	TF-24 ^b	F4-25 66.20-68.50	36.59	Yes	Yes	No	No
	TF-25 ^b	F4-25 78.90-87.70	36.78	Yes	Yes	No	No
	TF-26 ^b	F4-25 127.0-129.0	37.20	Yes	No	Yes	No
	TF-27 ^b	F4-26 136.0-142.0	39.05	Yes	Yes	Yes	Yes
	TF-28 ^b	F4-27 28.00-33.00	39.66	Yes	No	No	No
	TF-29 ^b	F4-27 59.00-60.20	39.94	Yes	No	No	No
	TF-30 ^b	F5-27 03.00-07.50	40.07	Yes	No	No	No
	TF-31 ^b	F4-28 42.00-43.80	41.41	Yes	No	Yes	No
	TF-32 ^b	F4-28 132.0-136.0	42.30	Yes	Yes	Yes	Yes
	TF-33 ^b	F4-29 45.70-47.70	43.00	Yes	No	No	No
	TF-35 ^b	F5-29 71.20-71.80	43.70	Yes	No	No	No
	TF-35b ^b	F4-30 79.96-97.45	45.24	Yes	No	No	No
	TF-37 ^b	F4-31 20.23-22.76	46.23	Yes	No	No	No
TF-43 ^b	F4-32 149.8-151.5	49.02	Yes	Yes	Yes	No	
Lake Ohrid	OH-DP-0725 ^{b,c}	1D-32H-2 1.25-3.75	72.50	Yes	No	No	No
Proximal volcanic units							
Volcanic system	Unit	Section location	Coordinates				
LVC	Pitigliano ^b	Case Collina quarry	42°38'31"N 11°43'54"E	Yes	Yes	Yes	No
	Onano ^b	Grotte di Castro-Onano road cut Poggio Falchetto-Bonini	42°40'41"N 11°51'10"E	Yes	Yes	Yes	Yes
			42°35'08"N 11°51'24"E				
	Grotte di Castro ^b	Poggio delle Forche	42°33'11"N 11°53'02"E	Yes	Yes	Yes	Yes
	Sorano ^b	Rio Maggiore road cut	42°37'07"N 11°40'13"E	Yes	Yes	Yes	No
	Sovana ^b	Rio Maggiore road cut	42°37'07"N 11°40'13"E	Yes	No	No	Yes
	Farnese ^b	Arlena di Castro-Tessenanno road cut Rio Maggiore road cut	42°27'46"N 11°48'18"E	Yes	Yes	Yes	Yes
			42°37'07"N 11°40'13"E				
	Stenzano ^b	Rio Maggiore road cut	42°37'07"N 11°40'13"E	Yes	No	No	No
	Canino ^b	Monte di Marta Fosso la Nova road cut Pian di Vico	42°32'05"N 11°54'56"E	Yes	Yes	Yes	Yes
42°35'54"N 11°38'46"E 42°25'08"N 11°48'41"E							
SVD	TR-CR-2 ^b	Trevignano Romano-Centro Rapaci	42°10'23"N	Yes	Yes	Yes	No
	TR-CR-1 ^b		12°14'47"E	Yes	Yes	Yes	No
	Vigna di Valle ^b	Anguillara Sabazia	42°05'29"N 12°16'16"E	Yes	No	Yes	No
	Pizzo Prato ^b	Anguillara Sabazia-Mola Vecchia	42°05'25"N 12°16'55"E	Yes	No	No	No
Vico	Farine Formation	San Martino al Cimino train station	42°22'58"N 12°06'26"E	Yes	No	No	No

^a: [Giaccio et al. \(2017a\)](#); ^b: this study; ^c: [Leicher et al. \(2021\)](#). Abbreviations: LVC = Latera Volcanic Complex; SVD = Sabatini Volcanic District.

Table 2. Thickness, lithological and mineralogical features, and TAS classification of the twenty-one tephra layers deposited at the F4-F5 site in the Fucino Basin during the MIS 8-6 interval.

Tephra	Thickness (cm)	Composite depth (m)	Core section and depth (cm)	Lithology		Rock type (main)
				Juvenile clasts	Minerals	
TF-17a	2.00	31.74	F4-22 60.00-62.00	White and grey pumice	Kfs>cpx>bmca	Ph
TF-18	3.20	33.79	F4-23 107.8-111.0	Grey pumice	Kfs>cpx	Ph
TF-19	5.50	34.01	F5-23 61.50-67.00	Grey pumice	Kfs>cpx>bmca	Ph
TF-21	3.43	34.83	F4-24 45.50-48.93/ F5-23 145-147	White pumice	Kfs>bmca	Tr
TF-21a	2.00	35.15	F4-24 79.50-81.50	transparent-white – brownish shards and pumice	Kfs>cpx>bmca	Ph-Tr
TF-22	3.20	36.04	F5-24 111.5-114.7	White pumice and grey scoria	Kfs>bmca	Ph-Tph-Lat
TF-23	3.50	36.24	F5-24 130.8-134.3	Transparent shards white pumice	Kfs>plg >bmca>x	Tr
TF-24	2.30	36.59	F4-25 66.20-68.50	White pumice	Kfs>bmca	Ph
TF-25	8.80	36.78	F4-25 78.90-87.70	White pumice	Kfs>bmca	Ph
TF-26	2.00	37.20	F4-25 127.00-129.00	White and grey pumice	Kfs>cpx>bmca	Tr-Ph
TF-27	6.00	39.05	F4-26 136.0-142.0 F4-27 28.00-33.00/	White pumice	Bmca>kfs	Ph-Tph-Tr-Lat
TF-28	5.00	39.66	F5-26 132.27-136.25	White pumice	Bmca>kfs	Ph-Tph-Tr-Lat
TF-29	1.20	39.94	F4-27 59.00-60.20	Grey pumice	Bmca>kfs	Sho-Lat
TF-30	4.50	40.07	F5-27 3.00-7.50/ F4-27 68.99-73.25	White and grey pumice	Kfs>bmca>cpx	Ph-Tr
TF-31	1.80	41.41	F4-28 42.00-43.80	White and grey pumice	Kfs>bmca>cpx	Ph-Tr-Tph-Pht
TF-32	4.00	42.30	F4-28 133.0-134.5	Grey pumice	Kfs>bmca>cpx	Tph-Ph-Tr-Lat
TF-33	2.00	43.00	F4-29 45.75-47.75	white and grey pumice, transparent shards	Kfs>cpx>bmca	Ph
TF-35	0.60	43.70	F5-29 71.20-71.80	White pumice	Kfs>bmca	Tr
TF-35b*	17.5	45.24	F4-30 79.96-97.45	Very few material	No	Ph
TF-37	2.53	46.23	F4-31 20.23-22.76	white and grey pumice, grey-black scoria	Kfs>cpx>bmca	Pht-Tph-Ph-Tr
TF-43	1.70	49.02	F4-32 149.8-151.5	White pumice	Bmca>kfs	Tr

151
152
153

*: Bioturbated layer, real tephra thickness is not quantifiable. Rock type abbreviations: Ph = phonolite; Tr = trachyte; Tph = tephriphonolite; Pht = phonotephrite; Lat = latite; Sho = shoshonite. Mineral abbreviations: Kfs = K-feldspar; bmca = black mica; cpx = clinopyroxene.

Table 3. Location, lithological features and TAS classification of the LVC, Vico and SVD investigated proximal units.

Outcrop/ Location	Coordinates	Unit	Sub-unit/ sample	Lithology		Rock type (main)
				Juvenile clasts	Free crystals	
Case Collina Quarry (Vu1)	42°38'31"N 11°43'54"E	Pitigliano	Tuff	Black scoria	Kfs	Ph-Tr
			Basal pumice fall	White pumice	Kfs	Ph-Tr
Grotte di Castro- Onano road cut (Vu2)	42°40'41"N 11°51'10"E	Onano	Spatter flow	Black spatter	Kfs	Sho
Poggio Falchetto-Bonini (Vu3)	42°35'08"N 11°51'24"E		Lower sillar- mid	Grey and white pumice	Cpx>kfs	Ph-Tph-Pht
		Lower sillar- base	Grey and white pumice	Kfs>bmca>cpx	Ph-Tph	
Poggio delle Forche (Vu4)	42°33'11"N 11°53'02"E	Grotte di Castro	Basal fall-top	White pumice	Kfs	Ph-Tr
			Basal fall-base	Dark grey scoria	Cpx	Pht-Te-Trb
Rio Maggiore road cut (Vu5)	42°37'07"N 11°40'13"E	Sorano	Ash flow-main body	White pumice	Kfs>bmca	Ph-Tr
			Ash flow-base	White pumice	Bmca>cpx	Ph-Tr
Rio Maggiore road cut (Vu5)	42°37'07"N 11°40'13"E	Sovana*	Black pumice flow "BUS"	Black scoria	Kfs>Lc	Ph
			White pumice	Kfs	Ph	
Arlena di Castro- Tessennano road cut (Vu6)	42°27'46"N 11°48'18"E	Farnese	Pumice flow	Light grey pumice	Kfs>cpx	Ph
Rio Maggiore road cut (Vu5)	42°37'07"N 11°40'13"E		Pumice fall F	White pumice	Kfs>cpx	Ph
Rio Maggiore road cut (Vu5)	42°37'07"N 11°40'13"E	Stenzano	Pyroclastic flow	White pumice	Kfs>bmca	Tr
Monte di Marta (Vu7)	42°32'05"N 11°54'56"E	Canino	Fall C	White pumice	Kfs>cpx>bmca	Tr
Fosso la Nova road cut (Vu8)	42°35'54"N 11°38'46"E		Upper Flow	Black scoria	Kfs	Tr
Pian di Vico (Vu9)	42°25'08"N 11°48'41"E		Main Flow	Light grey-pink pumice	Kfs>cpx	Tr
			Upper Fall B	White pumice	Kfs>cpx	Tr
			Lower Fall B	White pumice	Kfs>cpx	Tr
Trevignano Romano, Centro Rapaci (Sa1)	42°10'23"N 12°14'47"E	TR-CR-2	TR-CR-2	White pumice	Kfs	Ph
Anguillara Sabazia (Sa2)	42°05'29"N 12°16'16"E	Vigna di Valle	Scoria Fall Top	Grey scoria	Kfs>cpx	Ph
			Base	White pumice	Kfs>cpx	Ph
			White pumice	Kfs	Ph	
Anguillara Sabazia-Mola Vecchia (Sa3)	42°05'25"N 12°16'55"E	Pizzo Prato	Surge-pumice layer	White pumice	Kfs>cpx	Ph-Lat
			Surge-base	White pumice	Kfs>cpx	Ph
San Martino al Cimino train station (Vi1)	42°22'58"N 12°06'26"E	Farine Formation	Lower Flow	White pumice	Kfs>cpx	Ph
			Fall Top	White pumice	Kfs>bmca>cpx	Ph-Tr
San Martino al Cimino train station (Vi1)	42°22'58"N 12°06'26"E	Farine Formation	Fall Base	White pumice	Kfs>cpx	Ph-Tr
			Pyroclastic flow	White-brownish pumice	Kfs>cpx>bmca	Ph-Tr

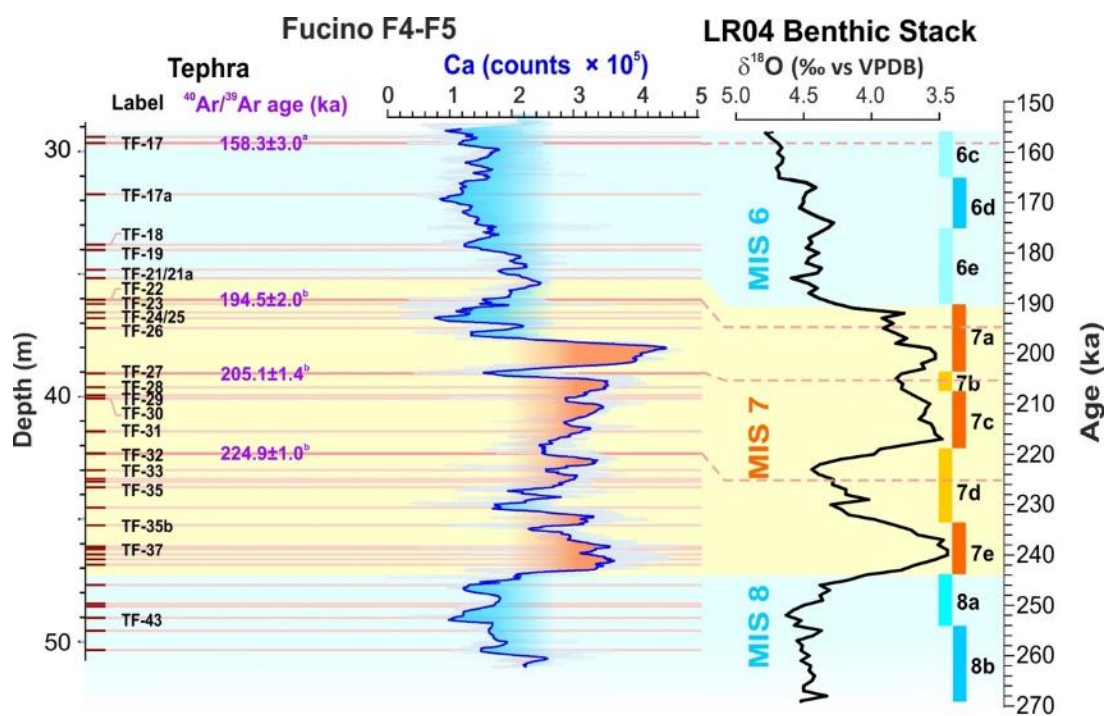
155
156
157
158

*Palladino et al., 2014. Rock type abbreviations: Tr = trachyte; Ph = phonolite; Tph = tephriphonolite; Pht = phonotephrite; Lat = latite; Sho = shoshonite; Te = tephrite; Trb = trachybasalt. Mineral abbreviations: Kfs = K-feldspar; bmca = black mica; cpx = clinopyroxene; Lc = leucite.

159

3. Materials and methods

160 In this study, 21 Fucino tephra layers and 13 proximal units, from the Vulsini, Sabatini and Vico volcanic
 161 systems, have been characterised in terms of major (n=34) and trace (n=16) element compositions, Sr-Nd
 162 isotopes (n=17) and $^{40}\text{Ar}/^{39}\text{Ar}$ dating (n=9). A summary of the performed analysis is reported in [Table 1](#), while
 163 detailed information on the instruments utilized and applied settings is provided in Supplementary Materials-
 164 1.
 165



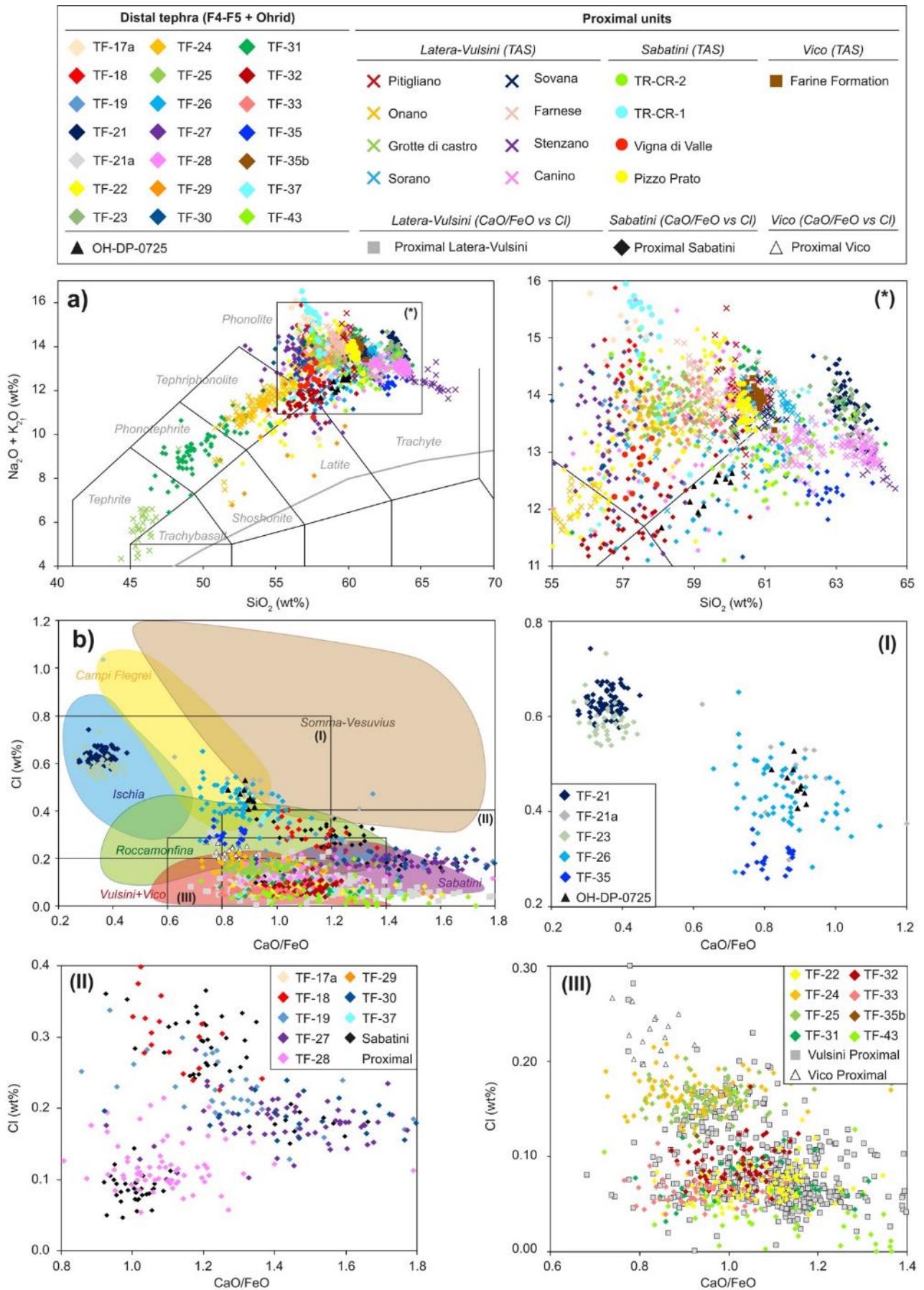
166
 167 **Figure 3.** Detailed tephrostratigraphy and Ca counts from XRF scanning ([Giaccio et al., 2019](#)) of the investigated MIS 8-MIS 6 interval
 168 from Fucino F4-F5 core compared with LR04 Benthic Stack ([Lisiecki and Raymo, 2005](#)). The available (^a [Giaccio et al., 2017a](#)) and new
 169 (^b this study) direct $^{40}\text{Ar}/^{39}\text{Ar}$ age determinations of the Fucino tephra are also shown.
 170

171 4. Results

172 4.1. Major and minor element composition

173 The analysed tephra layers and proximal units are shown in the *Total Alkali vs Silica* classification diagram
 174 (TAS, [Le Maitre et al., 2002](#); [Fig. 4a](#)). The 21 Fucino tephra locates within the fields of the high-K series
 175 ([Appleton, 1972](#)), and can thus be classified as potassic tephrites, phonotephrites, tephriphonolites, phonolites
 176 and trachytes, but also as latites and shoshonites (e.g., TF-22, TF-27, and TF-29). In particular, the
 177 investigated Fucino tephra are mainly phonolithic and trachytic in composition ([Fig. 4a](#); [Supplementary Fig.](#)
 178 [S1a](#)), with variable amounts of alkali contents and ratios, all with $\text{K}_2\text{O}/\text{Na}_2\text{O} \geq 1$, except for TF-21 and TF-23
 179 where $\text{K}_2\text{O}/\text{Na}_2\text{O} < 1$ ([Fig. S3a](#)).

180



181

182

183

184

Figure 4. Classification and discrimination diagrams for Fucino MIS 8-6 investigated tephra, the proximal pyroclastic units of Latera Volcanic Complex (LVC), Vico volcano (Farine Formation unit), and Sabatini Volcanic District (SVD), and Ohrid tephra OH-DP-0725. **a)** Total Alkali vs Silica (TAS; Le Maitre et al., 2002). **b)** CaO/FeO vs Cl (Giaccio et al., 2017a)

185

186 The eight investigated LVC units are classified as K-phonolites and K-trachytes, but also as potassic
187 tephriphonolites (Onano unit) and tephrites-trachybasalts (Grotte di Castro Basal Fall sub-unit; Fig. 4a,
188 Supplementary Fig. S1b). The four SVD units are all phonolitic in composition (Fig. 4a, Supplementary Fig.
189 S1b), with similar amounts of K₂O and Na₂O K₂O/Na₂O = 1, except for Pizzo Prato unit where K₂O/Na₂O is >
190 2 (Fig. S3b). The Farine Formation unit from Vico volcano has a fairly homogeneous phonolitic-trachytic
191 composition (Fig. 4a, Supplementary Fig. S1b), with 60-62 wt.% SiO₂, 13-15 wt.% alkali sum and mean
192 K₂O/Na₂O ratio of 1.58 ± 0.18 (2 s.d.; Fig. S3b). Finally, Ohrid tephra OH-DP-0725 is trachytic in composition
193 (Fig. 4a), with K₂O/Na₂O > 1 (mean = 1.81 ± 0.13 [2 s.d.]). Leicher et al. (2021) reported both a phonolitic and
194 a rhyolitic component, the latter not observed in the sample analysed in this study. Full analytical data can be
195 found in Supplementary Materials-2.

196

197 4.2. Trace element compositions

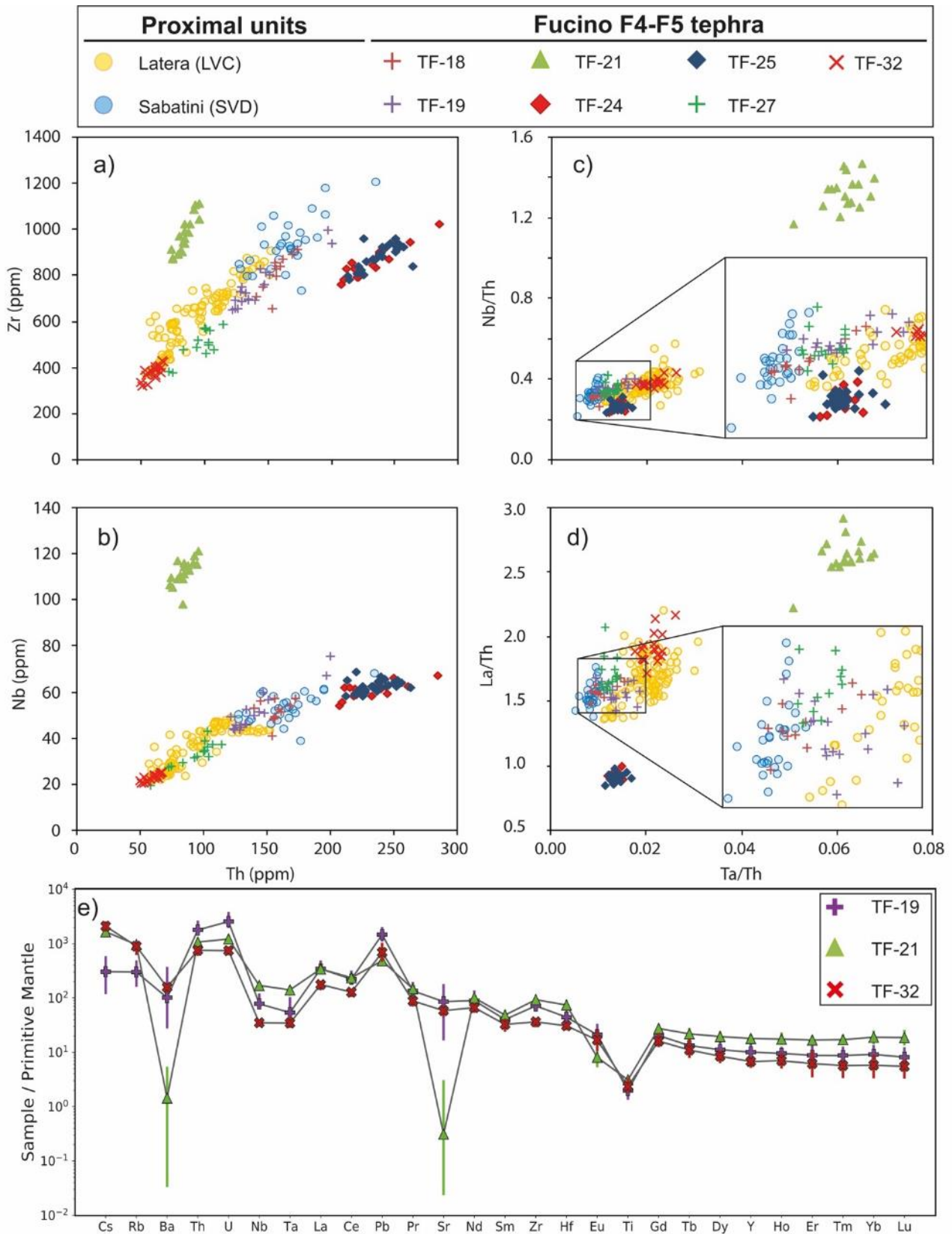
198 Seven out of the eight Fucino tephra and all eight proximal LVC and SVD units selected for trace element
199 data analysis, provided sufficient analytical points (i.e., > 10-15) for their characterisation, whereas only 1 point
200 could be obtained for TF-43 (not shown in Fig. 5), preventing us from determining its trace element
201 composition.

202 The analysed Fucino tephra form three distinguished clusters (Fig. 5a-b). TF-18, 19, 27 and 32 form a
203 common cluster, but have different Th concentrations (TF-18 = 140-173 ppm; TF-19 122-200; TF-27 = 58-115
204 ppm; TF-32 = 50-68 ppm) if compared with other incompatible trace elements (Fig. 5a-b). Indeed, tephra layers
205 TF-18 and TF-19 are more enriched in Th (Th = 140-173 ppm and 122-200 ppm respectively), with respect to
206 TF-27 (58-115 ppm) and TF-32 (50-68 ppm). Tephra TF-21 form a cluster less enriched in Th (75-93 ppm,
207 amongst the lowest) whilst being more enriched in Zr (869-1113 ppm, Fig. 5a), Nb (98-121 ppm, Fig. 5b) and
208 Ta (4.3-5.3 ppm) with respect to all the other tephra. Furthermore, it displays the highest ratios of High Field
209 Strength Elements (HFSE) and Light Rare-Earth Elements (LREE) to Th (e.g., Ta/Th = 0.05-0.07; Nb/Th =
210 1.17-1.47 [Fig. 5c]; La/Th = 2.22-2.91 [Fig. 5d]; Ce/Th = 4.07-4.97). Finally, phonolitic tephra TF-24 and TF-
211 25 form a separate cluster, being the most enriched in Th, ranging respectively from 208-285 ppm and 214-
212 264 ppm, compared to all the other tephra having ≤ 200 ppm of Th (Fig. 5a-b). TF-24 and TF-25 are also
213 characterised by similar, and basically indistinguishable from one another, ratios of HFSE and LREE to Th
214 (e.g., Nb/Th = 0.24-0.29 for TF-24 and 0.23-0.31 for TF-25 [Fig. 5c]; La/Th = 0.89-0.99 for TF-24 and 0.85-
215 0.98 for TF-25 [Fig. 5d]; Ce/Th = 1.50-1.72 for TF-24 and 1.41-1.59 for TF-25).

216 The LVC pyroclastic units are characterised by very similar incompatible trace element contents, overlapping
217 with those of Fucino tephra (Fig. 5a-b). Overall, Th ranges between 55-155 ppm, Zr between 364-899 ppm
218 (Fig. 5a), Nb between 21-48 ppm (Fig. 5b), and Ta between 1-3 ppm for the LVC units. Ratios of HFSE and
219 LREE to Th overlap with those of TF-32 and partially with TF-18 and TF-19 (Fig. 5c-d).

220 SVD pyroclastic units show a similar variation of incompatible trace elements, with higher Th (i.e., 129-236
221 ppm) with respect to LVC units, overlapping only with tephra layers TF-18 and TF-19 (Fig. 5a-b). However,
222 when employing ratios of HFSE and LREE to Th, a good overlap is observed also for TF-27 (Fig. 5c-d). Full
223 analytical data can be found in Supplementary Materials-2.

224



225

226

227

228

Figure 5. Trace element representative biplots (a to d) and spider (e; normalized to the primitive mantle; McDonough and Sun, 1995) diagram of the selected Fucino F4-F5 tephra and proximal LVC and SVD pyroclastic units.

229

4.3. Isotopic composition

230 *Proximal samples* - From the SVD, the units Vigna Valle, Trevignano Romano Centro Rapaci (TR-CR-1, 2),
 231 and Pizzo Prato (analysed in [Sottili et al., 2019](#)) are characterised by Sr isotopes from c.a 0.7101 to c.a.
 232 0.7112. $^{143}\text{Nd}/^{144}\text{Nd}$ is for all sample c.a. 0.5121. Glass fractions and related feldspar are in isotopic equilibrium
 233 ([Table 4](#)).

234 The Pitigliano, Onano, Grotte di Castro, Farnese, and Fall-C units from LVC have $^{87}\text{Sr}/^{86}\text{Sr}$ ranging from 0.7100
 235 and 0.7078. The lowest ratios belong the Farnese glass fraction, whilst the highest the Canino Fall-C. Farnese
 236 glass and feldspar are in isotopic disequilibrium and are characterized by Sr isotope compositions ranging
 237 from 0.7101 and 0.7103. The possible occurrence of antecrysts can explain such a difference, as often happen
 238 when considering large magma chambers, producing high magnitude eruptions. The $^{143}\text{Nd}/^{144}\text{Nd}$ is c.a. 0.5121
 239 for all samples ([Table 4](#)).

240 *Fucino tephra* - $^{87}\text{Sr}/^{86}\text{Sr}$ ratios ([Fig. 6a](#)) of the Fucino F4-F5 tephra range from 0.70623 (TF-26) and 0.71056
 241 (TF-43), with most of the samples (i.e., excluding TF-26) having $^{87}\text{Sr}/^{86}\text{Sr} > 0.710$ ([Table 4](#)). TF-22, TF-31, TF-
 242 32, and TF-43 show $^{87}\text{Sr}/^{86}\text{Sr} > 0.7103$. Feldspar and light and dark glass fraction of TF-22 display the same
 243 Sr isotopic composition (0.71038). TF-31 is characterized by a small isotope variation, with respect to the
 244 analytical error, between feldspar and glass fraction (c.a. 0.7105). Pyroxene, feldspar, biotite, and glass
 245 fraction from TF-32 have Sr isotopic composition ranging from 0.71036 and 0.71055. Feldspar from TF-43 has
 246 $^{87}\text{Sr}/^{86}\text{Sr}$ of 0.71056. TF-18, TF-19, and TF-27 show similar $^{87}\text{Sr}/^{86}\text{Sr}$ ([Table 4](#)), all < 0.7103 . The lowest values
 247 among these three samples are recorded by TF-27 pyroxene and glass fraction, all characterized by Sr isotope
 248 ratios of 0.7101. TF-26 mineral and glass fractions display $^{87}\text{Sr}/^{86}\text{Sr}$ ranging from 0.70623 (feldspar) and
 249 0.70656 (pyroxene), sensibly lower with respect to all the other tephra. $^{143}\text{Nd}/^{144}\text{Nd}$ ([Fig. 6b](#)) have been
 250 determined for four Fucino tephra (i.e., TF-22, TF-26, TF-27, and TF-32). They are compatible with those of
 251 the proximal samples with the exception of tephra TF-26, which displays the highest $^{143}\text{Nd}/^{144}\text{Nd}$ value among
 252 all samples (i.e., 0.51255). Full analytical data can be found in [Table 4](#).

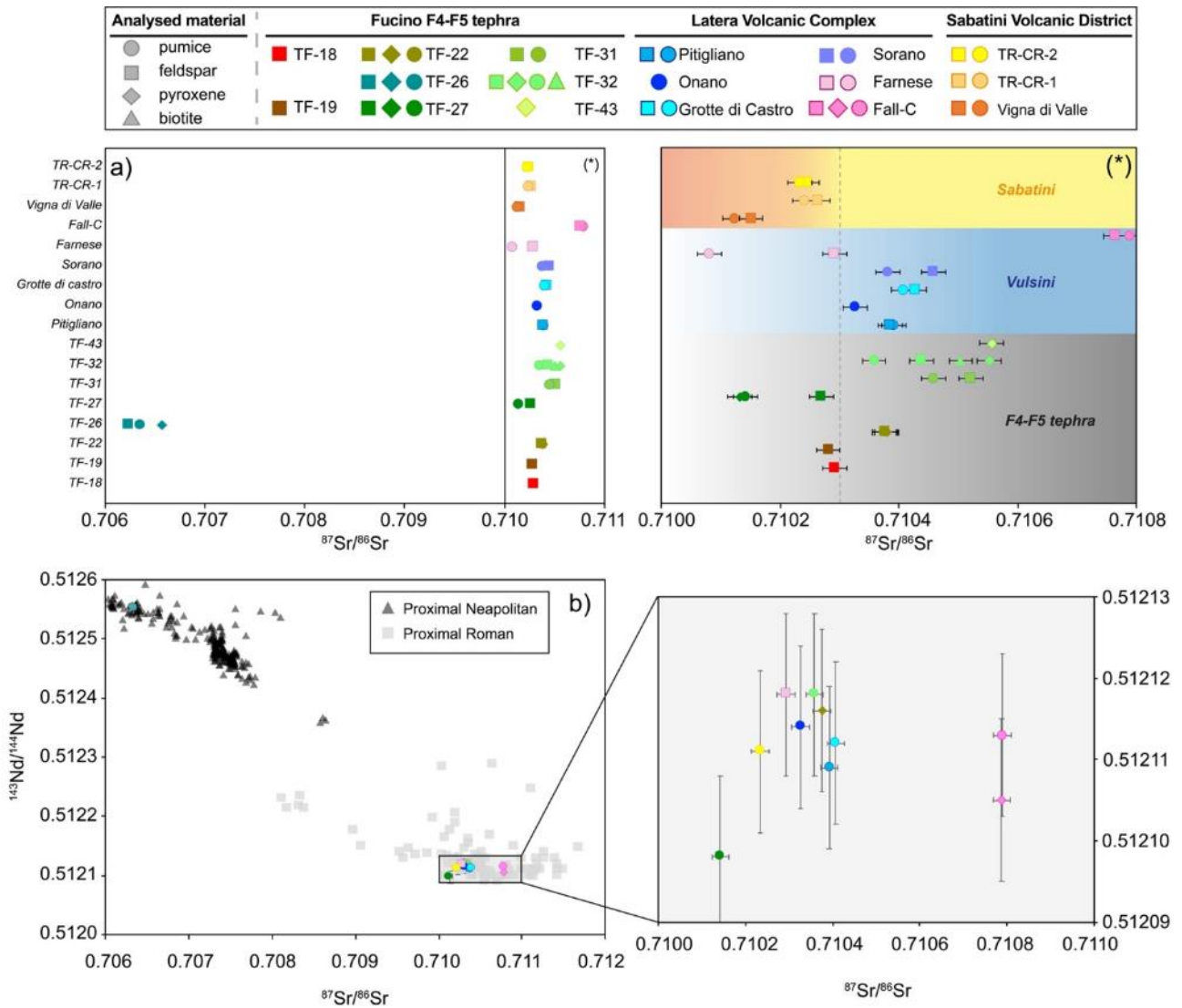
253 Samples from the LVC (i.e., Pitigliano, Onano, Grotte di Castro, Sorano, Farnese, and Canino Fall-C) are
 254 featured by $^{87}\text{Sr}/^{86}\text{Sr} \geq 0.7103$ ([Table 4](#)) and overlap with the Fucino tephra TF-22, TF-31, TF-32, and TF-43.
 255 Finally, TR-CR-2, TR-CR-1, and Vigna di Valle units from the SVD, display similar $^{87}\text{Sr}/^{86}\text{Sr}$ ratios ([Table 4](#)),
 256 overlapping with those of the Fucino tephra TF-18, TF-19, and TF-27.

257

258 **Table 4.** Individual $^{87}\text{Sr}/^{86}\text{Sr}$ and $^{143}\text{Nd}/^{144}\text{Nd}$ isotope ratios for the investigated F4-F5 Fucino tephra, and proximal Vulsini and Sabatini
 259 volcanic systems.

Tephra/Unit	Sub-sample	$^{87}\text{Sr}/^{86}\text{Sr}$	Error	$^{143}\text{Nd}/^{144}\text{Nd}$	Error
Fucino Tephra					
TF-18	Feldspar	0.71029	0,000019		0,00001

TF-19	Feldspar	0,71028	
TF-22	Feldspar	0,71038	0,51212
	Pyroxene	0,71038	
	Pumice	0,71038	
TF-26	Feldspar	0,70623	0,51255
	Pyroxene	0,70657	
	Pumice	0,70635	
TF-27	Feldspar	0,71027	0,51210
	Pyroxene	0,71013	
	Pumice	0,71014	
TF-31	Feldspar	0,71052	
	Pumice	0,71046	
TF-32	Feldspar	0,71044	0,51212
	Pyroxene	0,71055	
	Biotite	0,71050	
	Pumice	0,71036	
TF-43	Feldspar-rich	0,71056	
Proximal Vulsini			
Pitigliano	Feldspar	0,71039	0,51211
	Pumice	0,71039	
Onano	Pumice	0,71033	0,51211
Grotte di Castro	Feldspar	0,71043	0,51211
	Pumice	0,71041	
Sorano	Feldspar	0,71046	
	Pumice	0,71038	
Farnese	Feldspar	0,71029	0,51212
	Pumice	n.a.	
Fall-C	Feldspar	0,71077	0,51211
	Pyroxene	0,71079	
	Pumice	0,71079	
Proximal Sabatini			
TR-CR-2	Feldspar	0,71025	0,51211
	Pumice	0,71023	
TR-CR-1	Feldspar	0,71026	
	Pumice	0,71024	
Vigna di Valle	Feldspar	0,71015	
	Pumice	0,71012	



261

262 **Figure 6.** $^{87}\text{Sr}/^{86}\text{Sr}$ (a) and $^{87}\text{Sr}/^{86}\text{Sr}$ vs $^{143}\text{Nd}/^{144}\text{Nd}$ (b) isotopic composition of the selected Fucino F4-F5 tephra and proximal LVC and
 263 SVD pyroclastic units. $^{87}\text{Sr}/^{86}\text{Sr}$ vs $^{143}\text{Nd}/^{144}\text{Nd}$ literature data from Neapolitan (i.e., Campi Flegrei and Ischia) and Roman (i.e., Vulsini,
 264 Vico, Sabatini and Colli Albani) volcanoes are displayed in b) as a comparison. Literature data source: Neapolitan = [Arienzo et al. \(2009,](#)
 265 [2010, 2015, 2016\), Brown et al. \(2014\), Casalini et al. \(2018\), D'Antonio et al. \(2007, 2013\), Di Renzo et al. \(2011\), Pabst et al. \(2007\),](#)
 266 [Pelullo et al. \(2020\), Tonarini et al. \(2009\); Roman = Di Battistini et al. \(1998\), Gaeta et al. \(2016\), Gasperini et al. \(2002\), Perini et al.](#)
 267 [\(2004\), Sottili et al. \(2019\).](#)

268

269

270 4.4. $^{40}\text{Ar}/^{39}\text{Ar}$ ages

271 **Data reporting** - For consistency with previous studies of Fucino tephra successions ([Giaccio et al.,](#)
 272 [2017a; Giaccio et al., 2019; Monaco et al., 2021](#)), all the new and literature (cited) $^{40}\text{Ar}/^{39}\text{Ar}$ geochronological
 273 data are here reported as relative to an age of 1.1891 Ma for the Alder Creek sanidine, ACs-2 standard
 274 ([Niespolo et al., 2017](#)).

275 **LSCE (Laboratoire de Sciences du Climat et de l'Environnement)** - $^{40}\text{Ar}/^{39}\text{Ar}$ dating results for individual
 276 tephra layers are presented as probability diagrams in [Figure 7](#). Weighted mean age uncertainties are reported
 277 at 2σ , including J uncertainty and were calculated using Isoplot 4.0 ([Ludwig, 2012](#)). For each sample, inverse

278 isochrones have $^{40}\text{Ar}/^{36}\text{Ar}$ initial intercepts that are within uncertainty of that of the atmosphere suggesting that
279 the dated crystals do not contain abundant trapped excess argon.

280 *TF-22* - Crystals extracted from this tephra layer range in length from 200 to 250 μm , which makes them less
281 suitable for single-crystal fusion dating and thus the detection of potential xenocrysts as the argon beam sizes
282 are very small (2 times the ^{40}Ar blank). Despite the low precision of these 8 single crystal fusion dates (Fig. 7),
283 we did not detect any obvious older crystals. We improved the precision by fusing two (6 measurements), and
284 four crystals (6 measurements) at the same time. All experiments with multiple crystals share a similar age
285 within uncertainty, which proves that we were not able to detect any significant older crystal within the analytical
286 uncertainties. These findings are in agreement with the isotopic evidence which suggest isotopic equilibrium
287 between glass and mineral fractions. Finally, to obtain a more precise age, the remaining crystals were
288 analyzed in a small population of 10 to 15 crystals. Including all experiments, we obtained a total of 24 similar
289 ages, allowing us to calculate an accurate and precise weighted mean age of 194.5 ± 2.0 ka (MSWD = 0.3, p
290 = 1.0).

291 *TF-27* - A total of 15 individual crystals were dated. Excluding 4 older crystals, interpreted as xenocrysts (red
292 bars in Fig. 7), a main population constituted by 11 crystals allowed calculation of a weighted mean age of
293 205.1 ± 1.4 ka (MSWD = 1, p = 0.43) for this tephra. The possible occurrence of xenocrysts or antecrysts is
294 confirmed by the relatively high $^{87}\text{Sr}/^{86}\text{Sr}$ obtained for the feldspar with respect to pyroxene and glass fractions.

295 *TF-32* - 19 single crystal ages were obtained for this tephra layer. The probability diagram is complex,
296 multimodal with at least 5 modes with crystals as old as 275 ka (Fig 7). Remarkably, this evidence agrees well
297 with the results of the Sr isotopic investigations performed on different mineral fractions and the related glass.
298 At least three distinct $^{87}\text{Sr}/^{86}\text{Sr}$ ratios have been recognized based on the isotopic composition of $^{87}\text{Sr}/^{86}\text{Sr}$ of
299 glass, feldspar, and pyroxene-biotite, which suggest the occurrence of different crystals populations. The
300 youngest feldspar population includes 9 crystals sharing the same age within uncertainties. Using these
301 crystals, we calculated a weighted mean age of 224.9 ± 1.0 ka (MSWD = 0.8, p = 0.60) that we interpret as
302 the age of deposition of this tephra.

303 *Farnese* - 15 individual crystals were analysed. All of them share the same age within uncertainties as shown
304 by the corresponding almost Gaussian probability diagram (Fig. 7). Using these crystals, we calculated a
305 weighted mean age of 235.6 ± 0.6 ka (MSWD = 0.7, p = 0.8) that we interpret as the age of the Farnese
306 eruption.

307 *Canino Fall-B* - we analysed 15 individual crystals for this sub-unit. Excluding one crystal that shows a sensibly
308 older age and is thus interpreted as a xenocrystal (red bar), all the 14 remaining ones have the same age

309 within uncertainties (Fig. 7). This main population, here interpreted as juvenile crystals, allows us to propose
310 an age of 253.8 ± 0.8 ka (MSWD = 1.1, $p = 0.4$) for the Canino Fall-B sub-unit.

311 *Canino Fall-C* - 11 crystals were individually dated for this sub-unit. Like Canino Fall-B, beside one xenocryst
312 with a low $^{40}\text{Ar}^*$ dated at 276 ka, all remaining crystals display a similar age within uncertainties (Fig. 7) in
313 agreement with the results of the isotopic investigations. Using this main and younger juvenile population of
314 crystals, we have calculated a weighted mean age of 253.1 ± 0.8 ka (MSWD = 1.4, $p = 0.8$) for the Canino
315 Fall-C sub-unit. This age is undistinguishable from the one we obtained for Canino Fall-B, which makes sense
316 as both sub-units belong to the same eruptive phase. The weighted mean age of the Canino eruption, given
317 by both Fall-B and Fall-C sub-units, is thus 253.4 ± 0.8 ka.

318 **UWM (University of Wisconsin-Madison)** - $^{40}\text{Ar}/^{39}\text{Ar}$ dating results for all individual tephra layers are
319 presented as probability diagrams in Figure 7.

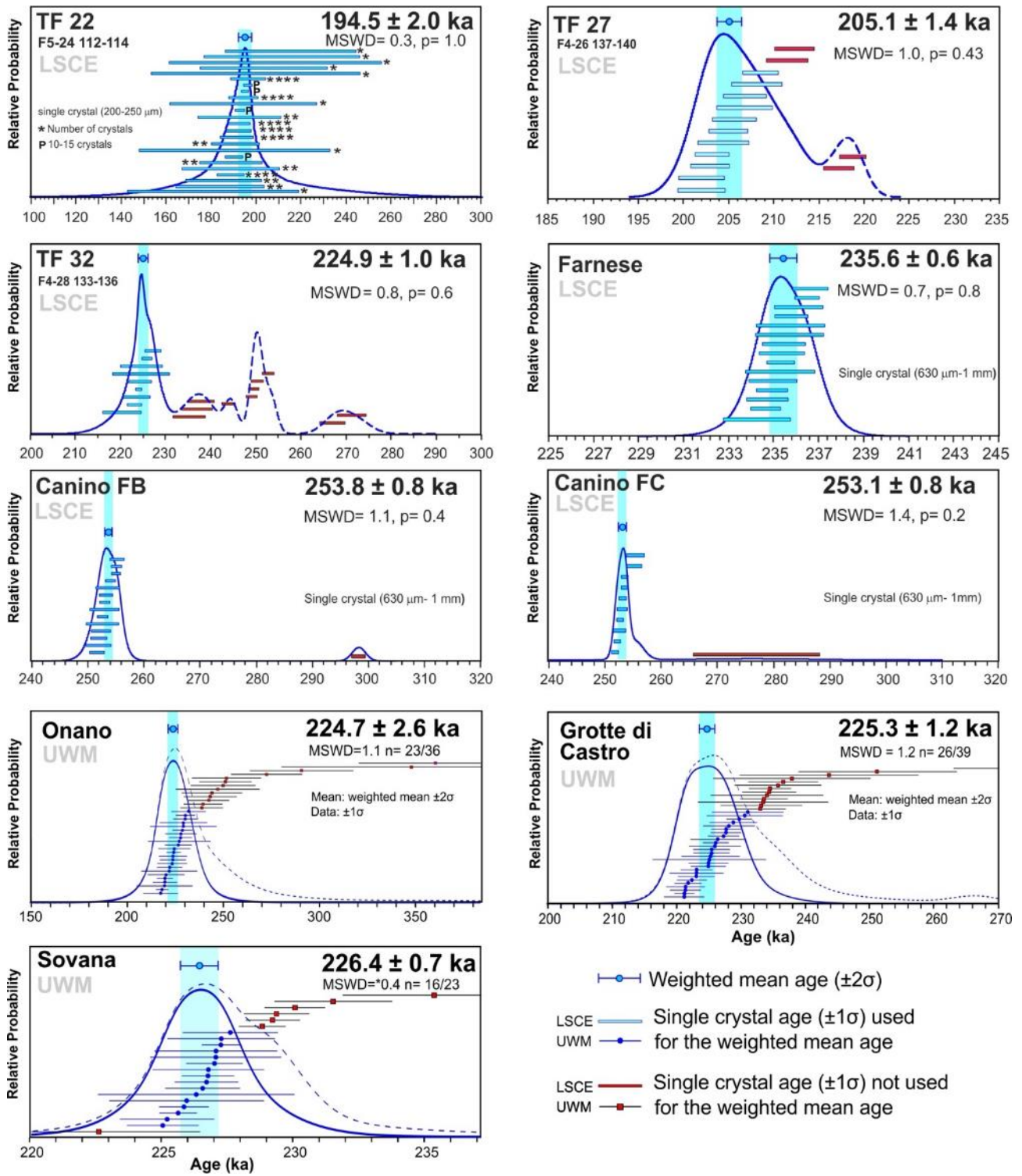
320 *Onano* - 36 crystals were dated for the Onano unit. Of these, 32 were interpreted as juvenile crystals and
321 yielded a weighted mean age of 224.7 ± 2.6 ka (MSWD = 1.1, 2σ ; Fig. 7).

322 *Grotte di Castro* - for this unit, 39 crystals were dated, but only 26 were interpreted as juveniles and yielded a
323 weighted mean age of 225.3 ± 1.2 ka (MSWD = 1.2, 2σ), the remaining 13 crystals being interpreted as older
324 xenocrysts (red squares in Fig. 7).

325 *Sovana* - 23 crystals were dated for this unit. Of these, 16 crystals yielded a weighted mean age of $226.4 \pm$
326 0.7 ka (MSWD = 0.4, 2σ ; Fig. 7), while the remaining 7 crystals were interpreted as older xenocrysts.

327 Full analytical data can be found in Supplementary Materials-3.

328



329
330
331
332
333

Figure 7. Age probability diagrams of tephra layers TF-22, TF-27, and TF-32, and of proximal LVC pyroclastic units Onano, Grotte di Castro, Sovana, Farnese, Canino Fall-B, and Canino Fall-C.

334 **5. Discussion**

335 *5.1. Volcanic sources of the Fucino tephra*

336 *5.1.1. Active volcanoes over the investigated timespan*

337 Volcanoes belonging to the Quaternary potassic peri-Tyrrhenian volcanic region (Fig. 1b) are the most
338 probable sources of all investigated tephra. Indeed, previous investigations (Giaccio et al., 2017a, 2019;
339 Monaco et al., 2021) showed that, to great extent, the majority the Fucino tephra documented so far were
340 sourced from these volcanic systems along with products from the Aeolian Islands (Di Roberto et al., 2018)
341 and Etna volcano (Giaccio et al., 2017a; Del Carlo et al., 2020). Furthermore, almost all these volcanic systems
342 were active in the time interval 250-160 ka (e.g., Peccerillo, 2017).

343 Between ~250 ka and 160 ka, the Latera Caldera (LVC; Vulsini volcanic district; Fig. 1b) produced several
344 Plinian-fall (Palladino and Agosta, 1997) and pyroclastic flow (Sparks, 1975; Palladino and Valentine, 1995)
345 deposits, some of them associated to caldera-forming eruptions (Palladino et al., 2010). These eruptions
346 include, from the oldest to the youngest, those of Canino, Stenzano, Farnese, Sovana, Sorano, Grotte di
347 Castro, Onano, and Pitigliano, the deposits of which were all geochemically characterised in this study. Also,
348 Plinian activity in the eastern Vulsini (Nappi et al., 1994) partially overlapped with the study period.

349 At Vico volcano (Fig. 1b), after a period of ~50 kyr dominated by effusive activity (Lago di Vico lava Formation,
350 305-258 ka, e.g., Perini et al., 2004), which build-up the stratovolcano, a series of explosive, caldera-forming
351 eruptions, i.e., Ignimbrite A/Farine Formation (here analysed), the Ignimbrite B/Ronciglione Formation, and the
352 Ignimbrite C/Sutri Formation (Bertagnini and Sbrana, 1986; Perini et al., 1997; Bear et al., 2009) occurred.

353 At Sabatini (Fig. 1b), two volcanic centres were simultaneously active, i.e., the Sacrofano (~300-200 ka) and
354 Bracciano (~325-200 ka) calderas (Sottili et al., 2019; Marra et al., 2020), both of which had major Plinian
355 (e.g., Magliano Romano Plinian Fall, 312 ± 2 ka; Sottili et al., 2010), caldera-forming eruptions (e.g., Tufo
356 Giallo di Sacrofano, Tufo di Bracciano, Tufo di Pizzo Prato; Sottili et al., 2010, 2019), and minor explosive
357 activity associated to pyroclastic surges, strombolian eruptions and lava flows at parasite cones along the rims
358 of the two calderas.

359 At Colli Albani, the long Tuscolano-Artemisio Phase (de Rita et al., 1988), also known as the Vulcano Laziale
360 period (Giordano and the CARG Team, 2010), spanned the interval 608-351 ka (Marra et al., 2009; Gaeta et
361 al., 2016). It was followed by the Mt. Faete Phase (now Tuscolano-Artemisio-Faete; Giordano and the CARG
362 Team, 2010), characterised by strombolian activity from several edifices coupled to the emplacement of
363 peripheral lava flows in the interval 308-250 ka (Marra et al., 2003; Gaeta et al., 2016), before switching to the
364 Late Hydromagmatic Phase (200-36 ka; Marra et al., 2016), or Via dei Laghi period (Giordano and the CARG
365 Team, 2010), during which the Ariccia (~200 ka), Nemi (~150 ka), Valle Marciana (~100 ka), and Albano (~70-
366 36 ka) maars were active (e.g., Freda et al., 2006; Giaccio et al., 2009; Marra et al., 2016). Products of the
367 Colli Albani volcano are generally characterised by K-foiditic compositions (e.g., Peccerillo, 2017), which are

368 not observed for any of the investigated tephra layers, thus allowing us to exclude this volcanic system as a
369 possible source of the investigated F4-F5 tephra.

370 At Roccamonfina (Fig. 1b), the Upper White Trachytic Tuff (UWTT, ~234 ka; Giannetti and De Casa, 2000)
371 and Yellow Trachytic Tuff (YTT, ~231 ka; Giannetti, 1996) were emplaced, followed by central activity at Mt.
372 Lattani-Mt. Santa Croce latitic scoria cones (173-152 ka; Ruchon et al., 2008).

373 In the Campanian Plain, activity is documented by a series of ignimbrite deposits, including the Seiano (~250
374 ka), Moschiano (~188 ka) and Taurano (~160 ka) ignimbrites (De Vivo et al., 2001; Rolandi et al., 2003), and
375 other pyroclastic deposits (i.e., Taurano Layered Tuff Series, 207-188 ka; De Vivo et al., 2001; Belkin et al.,
376 2016). Such a Middle Pleistocene activity in the Campania area is referred to the diffused, so-called
377 Campanian Volcanic Zone (CVZ) by Rolandi et al. (2003), although younger pyroclastic deposits (92-109 ka),
378 similarly spread in the Campanian Plain, have been recently confidentially ascribed to the Campi Flegrei
379 activity (Monaco et al., 2022). Therefore, rather than ascribing this Middle Pleistocene activity to a poorly
380 defined zone of diffused volcanism, we prefer to identify its source within the Neapolitan volcanic area (NVA),
381 i.e., an area that roughly envelops the present volcanic centers of the Campi Flegrei, Ischia and Procida.
382 Finally, at Ischia, southern Italy, several Plinian Fall deposits emplaced by this volcano are documented in the
383 island itself and neighbouring areas. The deposits better preserved on the island date back to 75 ka (e.g.,
384 Brown et al., 2008, 2014), but with evidence of an activity as old as at least 150 ka, and lasting up to historical
385 times (e.g., Poli et al., 1987; Sbrana et al., 2018).

386

387 5.1.2. Geochemical signatures and volcanic sources

388 Potassic tephrites, phonotephrites, tephriphonolites, phonolites, trachytes, shoshonites, and latites
389 compositions (Fig. 4a) are quite common to all the peri-Tyrrhenian Quaternary potassic volcanoes (e.g.,
390 Peccerillo, 2017). To identify and discriminate the volcanic source of the Fucino tephra, we employed the
391 CaO/FeO vs Cl classification diagram (Fig. 4b; Giaccio et al., 2017a), which allows discrimination of products
392 with 52-67 wt.% of SiO₂ of the Latium (i.e., Vulsini, Vico and Sabatini), Roccamonfina and Neapolitan (i.e.,
393 Ischia, Campi Flegrei and Somma-Vesuvius) volcanoes from each other. In Figure 4b (see also Supplementary
394 Fig. S2a), the 21 Fucino tephra can be divided as follow.

395 Tephra layers TF-21 and TF-23, which are distinguished from all the others by a K₂O/Na₂O ratio < 1 (Fig. S3a),
396 are both characterised by a CaO/FeO ratio < 0.5 and Cl ranging between 0.54-0.74 wt.%, compatible with
397 products from Ischia volcano (Fig. 4b; Fig. S2a). An origin from Ischia for TF-21 was already pointed out by

398 [Giaccio et al. \(2017a\)](#), and is also suggested by the high ratios of HFSE and LREE to Th ([Fig. 5c-d](#)), and the
399 anomaly of Ba and Sr ([Fig. 5e](#)).

400 Tephra TF-21a and TF-26 have CaO/FeO ratios ranging between 0.6 and 1.3, and Cl contents of 0.27-0.63
401 wt.% and 0.27-0.65 wt.%, respectively ([Fig. 4b](#); [Fig. S2a](#)), which would suggest a NVA origin for both and
402 specifically in Campi Flegrei. Indeed, TF-26 $^{87}\text{Sr}/^{86}\text{Sr}$ and $^{143}\text{Nd}/^{144}\text{Nd}$ values ([Fig. 6a-b](#)) are compatible with
403 literature data on old volcanic rocks from the Neapolitan volcanoes.

404 TF-35 has an intermediate CaO/FeO ratio of 0.74-0.88 and Cl content of 0.26-0.36 wt.% ([Fig. 4b](#); [Fig. S2a](#)),
405 which is compatible with either a Roccamonfina or NVA origin.

406 Tephra layers TF-17a, TF-18, TF-19, TF-27, and TF-30 have a wider CaO/FeO range, generally ≥ 1 , and
407 variable Cl a content comprised between 0.01 and 0.47 wt.%, which is compatible with products from Sabatini.
408 Indeed, data of the newly acquired TR-CR-2, TR-CR-1 and Vigna di Valle Sabatini units sampled in proximal
409 outcrops perfectly overlap with TF-17a, TF-18, TF-19, TF-27, and TF-30 ([Fig. 4b](#); [Fig. S2a](#)). TF-28, TF-29 and
410 TF-37 show similarly high CaO/FeO ratios (e.g., TF-28 up to 1.79) and Cl contents (TF-28 = 0.05-0.21 wt.%;
411 TF-29 = 0.02-0.14 wt.%; TF-37 = 0.04-0.37 wt.%), thus at the intersection between the Sabatini and Vulsini-
412 Vico fields ([Fig. 4b](#)). Nevertheless, these Cl contents are compatible with that of Pizzo Prato unit (i.e., 0.05-
413 0.14 wt.%), which extends the field of the Sabatini products in the CaO vs Cl diagram ([Fig. 4b](#); [Fig. S2b](#)).
414 Henceforth, one of the possible sources for these samples could be the SVD. Finally, the measured $^{87}\text{Sr}/^{86}\text{Sr}$
415 and $^{143}\text{Nd}/^{144}\text{Nd}$ values ([Fig. 6a-b](#)) for TF-18, TF-19, and TF-27 samples are compatible with isotopic variation
416 displayed by SVD proximal samples ([Fig. 6b](#); [Sottili et al., 2019](#)) and overlap with those of the SVD units TR-
417 CR-2, TR-CR-1, and Vigna di Valle, confirming their attribution to the SVD.

418 Tephra layers TF-22, TF-31, TF-32, TF-33, TF-35b, and TF-43 are characterised by variable CaO/FeO ratios
419 (overall between 0.70-1.50) and low Cl contents, generally ≤ 0.10 wt.% ([Fig. 4b](#)), overlapping with products of
420 the LVC here investigated, thus suggesting an origin from this volcano. Furthermore, $^{87}\text{Sr}/^{86}\text{Sr}$ and $^{143}\text{Nd}/^{144}\text{Nd}$
421 ratios ([Fig. 6a-b](#)) measured for TF-22, TF-31, TF-32, and TF-43 match those of the proximal LVC units (i.e.,
422 Pitigliano, Onano, Grotte di Castro, Sorano, Farnese, and Canino Fall-C).

423 Finally, the two phonolitic tephra TF-24 and TF-25 are characterised by very similar CaO/FeO ratios (0.72-
424 1.43 and 0.81-1.37 respectively) and Cl contents (Cl = 0.13-0.22 and 0.11-0.20 wt.%), which are compatible
425 with products of both Vico and Vulsini volcanoes. However, considering that LVC products of this period have
426 Cl contents generally ≤ 0.10 wt.% ([Fig. 4b](#); [Fig. S2b](#)), we are more inclined to consider Vico as the source of
427 these two tephra layers, which is also suggested by the peculiar TE composition of TF-24 and TF-25 which is
428 clearly distinguished from that of the LVC and SVD units ([Fig. 5](#)).

429

430 5.2. Other tephra repositories spanning the late MIS 8-early MIS 6 interval

431 Only few tephra records, both in continental and marine sedimentary environments, covering the 250-170
432 ka time interval here considered are documented in the literature. In southern Italy, the lacustrine succession
433 of San Gregorio Magno Basin (Fig. 1a) covers the ~240-15 ka interval (Munno and Petrosino, 2007; Petrosino
434 et al., 2019), with the uppermost tephra (i.e., tephra layer S21) correlated to the Neapolitan Yellow Tuff eruption
435 (NYT, 14.9 ± 0.4 ka; Deino et al., 2004) whilst tephra S4 was directly $^{40}\text{Ar}/^{39}\text{Ar}$ dated by Ascione et al. (2013)
436 at 239.0 ± 8.0 ka, thus implying that the lowermost three tephra (i.e., S3, S2, and S1) are all older than 240
437 ka.

438 In the Adriatic Sea, marine core PRAD 1-2 (Fig. 1a) hosts tephra layers dated back to ~200 ka (Bourne et al.,
439 2010, 2015). Of these, PRAD-3225 was confidently correlated to Ohrid tephra OH-DP-0624 (Leicher et al.,
440 2016) and Fucino tephra TF-17 (Giaccio et al., 2017a). This leaves only the lowermost two tephra (i.e., PRAD-
441 3586 and PRAD-3666) as potential correlatives to the F4-F5 Fucino tephra.

442 In the Tyrrhenian Sea, the marine core KET 80-04/DED 87-08 (Fig. 1a) spans the 200-90 kyr time interval
443 (Paterne et al., 2008) and hosts several tephra layers ascribed to eruptive activity of Italian volcanoes. Giaccio
444 et al. (2017a) proposed a tentative correlation between either C-52 or C-54 (~189-192 ka) with the Ischian-like
445 tephra TF-21.

446 The long succession of Lake Ohrid (Albania, North Macedonia; Fig. 1a) hosts a rich tephra sequence that
447 continuously spans the last 1.36 Ma (Wagner et al., 2019). Leicher et al. (2016, 2019, 2021) presented data
448 relative to the last 630 ka, and identified at least 8 tephra layers, attributed to the Neapolitan volcanic area
449 (NVA), Pantelleria and Roccamonfina volcanic systems, covering the time interval of ~241-160 ka, based on
450 the Lake Ohrid age-depth model. Of these, OH-DP-0624 was confidently attributed to TF-17 (Giaccio et al.,
451 2017a), $^{40}\text{Ar}/^{39}\text{Ar}$ dated at 158.8 ± 3.0 ka.

452 In Greece, the peatland sequence of Tenaghi Philippon (Fig. 1a) is reported to span also the last 1.36 Ma
453 (Tzedakis et al., 2006), but so far detailed tephra studies are available only for the MIS 1-MIS 5 (Wulf et al.,
454 2018), MIS 9-MIS 7e (Vakhrameeva et al. 2019) and MIS 10-MIS 12 (Vakhrameeva et al., 2018), thus covering
455 only marginally the interval of interest of this study. Specifically, Vakhrameeva et al. (2019) reported four tephra
456 layers (i.e., TP05-50.05, TP05-50.45, TP05-50.55, and TP05-50.75) with a modelled age between 240-235
457 ka. However, these four tephra layers have a peculiar rhyolitic composition of an unknown source, which is
458 not observed in any of the Fucino tephra presented in this study, thus ruling out any possible counterpart
459 candidate from this sequence.

460 Finally, in the Ionian Sea, cryptotephra investigations from ODP Site 964 (Fig. 1a; Vakhrameeva et al., 2021)
461 allowed land-to-sea correlation for the last 800 ka. Two visible tephra layers, with an orbital age of ~168 ka
462 (964A-2H-3-78) and ~238 ka (964A-2H-5-59a and 964A-2H-5-59b), were tentatively correlated with tephra
463 from the above-mentioned Lake Ohrid and San Gregorio Magno successions, but discarded based on TE
464 data. Of these, tephra layers 964A-2H-3-78 and 964A-2H-5-59a both have a Pantelleria-like composition
465 (Vakhrameeva et al., 2021), which is not observed among the Fucino tephra and can thus be confidently
466 discarded as potential correlatives. Instead, tephra layer 964A-2H-5-59b has a Campanian like composition
467 that can be tentatively correlated to one of the Fucino tephra. All the other cryptotephra have an age older than
468 300 ka (Vakhrameeva et al., 2021) and can thus be discarded as well.

469 To summarize, potential F4-F5 tephra counterparts could be hosted at San Gregorio Magno, PRAD 1-2, DED-
470 87-08, Lake Ohrid, and ODP Site 964 successions.

471

472 5.3. Individual tephra correlation

473 5.3.1. Correlation of Fucino tephra found in F4-F5 and F1-F3 cores

474 The uppermost interval of the investigated F4-F5 core overlaps with the lowermost interval of the
475 previously investigated shorter core F1-F3 core (Giaccio et al., 2017a). In fact, based on the stratigraphic
476 features and order, tephra layers TF-18, TF-19, TF-21, and TF-22 from the F4-F5 core can be easily linked
477 to the equivalent tephra from F1-F3 core, which were attributed to a Latium-undefined source (TF-18/TF-19,
478 TF-20, and TF-22) and Ischia volcano (TF-21) (Giaccio et al., 2017a). Direct comparison between the F1-F3
479 and F4-F5 tephra shows consistent geochemical data between the two sets of tephra, corroborating their
480 correlation (Figs. 8a, 9a, 10a).

481

482 5.3.2. F4-F5 tephra correlation

483 5.3.2.1. Tephra from Vulsini-Latera Volcanic Complex

484 **TF-22 - Vulsini unknown.** This Vulsini tephra (Fig. 4b) has a variable geochemical composition, with
485 a silica content ranging from 52 wt.% to 61 wt.%, an alkali sum of 8-15 wt.%, and a variable alkali ratio (i.e.,
486 K₂O/Na₂O) of 1.3-3.9 (Fig. S3a). In the TAS diagram (Fig. 4a) it occupies various fields and can be classified
487 as a potassic tephriphonolite, phonolite, and latite. Sr and Nd isotope ranges (Fig. 6a-b) indicate a Latium
488 origin as well, corroborating this attribution. None of the analysed Vulsini units has an age compatible with that
489 of TF-22 (i.e., 194.5 ± 2.0 ka; Fig. 7), thus it can be attributed to an undefined Vulsini unit yet to be identified
490 in proximal settings.

491 A comparison between TF-22 and Adriatic Sea core PRAD 1-2 (Fig. 1a) tephra PRAD-3586 shows a good
492 geochemical matching (Fig. 8a). This layer was originally correlated with V-2/Sutri Formation (Bourne et al.,
493 2015) dated at 151 ± 3 ka (Laurenzi and Villa, 1987). However, this correlation is stratigraphically and
494 geochronologically inconsistent with the convincing correlation of the younger PRAD-3225 with TF-17/Taurano
495 Ignimbrite dated at 158.3 ± 3.0 ka proposed by Giaccio et al. (2017a), who also correlates the Vico-C/Sutri
496 eruption to the overlying TF-15. Therefore, the correlation of PRAD-3586 with TF-22 appears fully supported by
497 geochemical data and in agreement with tephrostratigraphical evidence, which places it below PRAD-3225
498 correlated to TF-17/Taurano Ignimbrite.

499 In the Tyrrhenian Sea core DED-87-08 (Fig. 1a), Paterne et al. (2008) reported the occurrence of five tephra
500 layers with Roman and/or Campanian like composition, with either a High or Low Alkali Ratio (HAR and LAR
501 respectively), with an age comprised between ~205-183 ka. Of these, C-56 occurs just after the end of MIS 7
502 (~196 ka in Paterne et al., 2008), with an estimated age of 196.4 ka, which corresponds to that of TF-22 (194.5
503 ± 2.0 ka). The EDS geochemical composition, reported as mean and standard deviation values, provided for
504 this tephra by Paterne et al. (2008) is consistent with that of TF-22 and PRAD-3586 (Fig. 8a). However, the
505 lack of individual WDS glass composition prevents us from any conclusive correlation between C-56 and TF-
506 22/PRAD-3586.

507 **TF-31 - Onano.** This tephra falls in the middle of the period of increasing Ca content correlated to the MIS 7
508 period (Giaccio et al., 2019; Fig. 3), a climatostratigraphic position that allows us to estimate its age around
509 220 ka (Fig. 3), in agreement with its position between TF-27 and TF-32, here $^{40}\text{Ar}/^{39}\text{Ar}$ dated at 205.1 ± 1.4
510 ka and 224.9 ± 1.0 ka, respectively (Fig. 7).

511 TF-31 displays a very heterogeneous composition, ranging from tephrite to phonolite-trachyte with a
512 compositional gap separating a less evolved tephritic-phonotephritic-tephriphonolitic population from a more
513 evolved phonolitic-trachytic component (Fig. 4b). Among the LVC proximal pyroclastic units, the Onano
514 eruption (Palladino and Simei, 2005) similarly consists of a heterogeneous composition (Fig. 4a), and
515 comparison between TF-31 and Onano shows a good geochemical matching (Fig. 8b). Here the Onano unit
516 is $^{40}\text{Ar}/^{39}\text{Ar}$ dated at 225.7 ± 2.6 ka, in agreement with the climatostratigraphic position of TF-31 and thus
517 corroborating this correlation.

518 **TF-32 - Grotte di Castro.** This tephra is located ~1 m below TF-31/Onano and is directly dated by $^{40}\text{Ar}/^{39}\text{Ar}$ at
519 224.9 ± 1.0 ka, i.e., an age indistinguishable from that TF-31/Onano (Fig. 7). It is characterised by a peculiar
520 composition that occupies various fields of the TAS diagram (Fig. 4a), classifiable as a tephriphonolite-
521 phonolite-trachyte-latitude. In terms of TE composition, TF-32 shows REE concentrations (e.g., Y = 23-34 ppm,

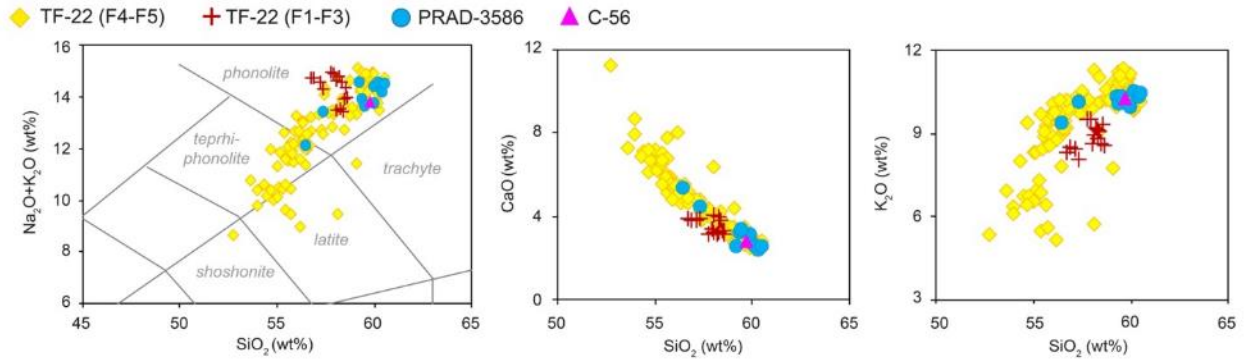
522 Fig. S4a; La = 95-128 ppm; Ce = 184-234 ppm) similar to GdC (Y = 26-40 ppm, Fig. S4b; La = 105-184 ppm;
523 Ce = 183-286 ppm), although the composition of the latter has a wider spectrum (i.e., more enriched in
524 incompatible elements). Based on these stratigraphic, geochronological, and geochemical constraints, the
525 Grotte di Castro unit (Colucci et al., 2013) arises as the best correlation candidate for TF-32. ME bi-plots
526 diagrams (Fig. 8b) show a good geochemical matching between TF-32 and Grotte di Castro. Furthermore, in
527 proximal settings the GdC is overlain by deposits of Onano (e.g., Palladino et al., 2010; Colucci et al., 2013),
528 here correlated with the overlying TF-31. Finally, the $^{40}\text{Ar}/^{39}\text{Ar}$ dating at 224.9 ± 1.0 ka for TF-32 matches very
529 well that of 225.3 ± 1.2 ka of the Grotte di Castro (Fig. 7). Therefore, the stratigraphic position and the
530 geochemical and geochronological data consistently confirm this correlation.

531 **TF-33 - Sovana.** TF-33 is found less than one meter below TF-32/Grotte di Castro and should be thus slightly
532 older than 224.9 ± 1.0 ka, which places it in the middle of the MIS 7 period (Fig. 3). This phonolitic tephra is
533 characterised by a homogeneous composition, with SiO_2 ranging between 57-61 wt.% and alkali sum of 12-
534 15 wt.% (Fig. 4a), falling at the boundary with the trachyte field. The LVC units of Sorano and Sovana, which
535 in proximal settings underlie the Grotte di Castro unit (Palladino and Taddeucci, 1998; Palladino et al., 2010,
536 2014; Valentine et al., 2019), here correlated to the overlying TF-32, represent the two most likely candidates
537 for correlating with TF-33. A comparison with the Sovana glass data shows a good geochemical matching with
538 TF-33 (Fig. 8c), to which it can thus be correlated. Here, the Sovana unit is $^{40}\text{Ar}/^{39}\text{Ar}$ dated at 226.4 ± 0.7 ka
539 (Fig. 7), thus in agreement with the immediately overlying TF-32 correlated to Grotte di Castro, here $^{40}\text{Ar}/^{39}\text{Ar}$
540 dated at 224.9 ± 1.0 ka and 225.3 ± 1.2 ka (weighted mean age: 225.1 ± 0.8 ka), respectively (Fig. 7). In
541 proximal settings, the Sovana unit was dated at 215 ± 6.0 ka (Turbeville, 1992), highlighting that previous age
542 determinations of some Latera units were substantially underestimated.

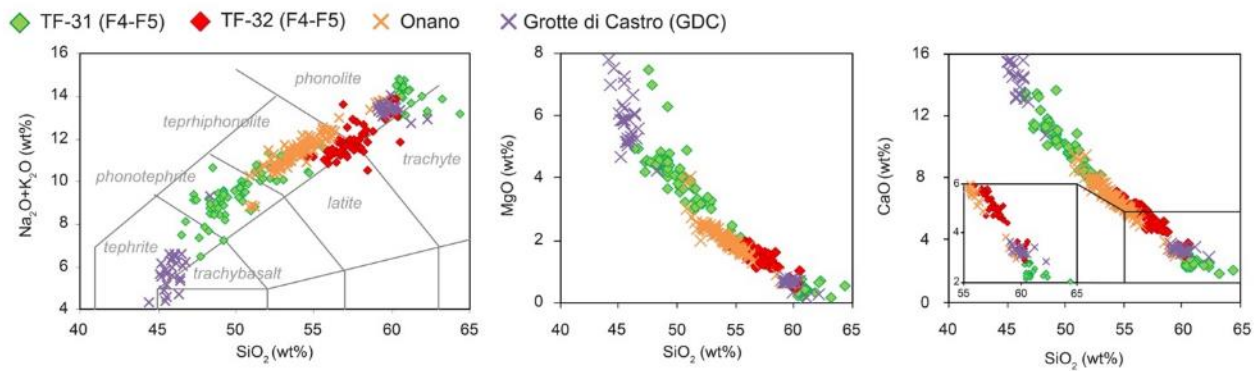
543 **TF-35b - Farnese.** This LVC tephra falls at end of the first peak of Ca content, likely corresponding to the end
544 of the MIS 7e sub-stage (Fig. 3), astronomically dated between ~ 244 and ~ 234 ka (Lisiecki and Raymo, 2005).
545 For this tephra, due to its crypto nature, we managed to acquire only 3 analytical points, which likely are
546 insufficient for expressing the full geochemical variability of the tephra. Among the remaining LVC units, the
547 only one with a phonolitic composition and a chronology consistent with TF-35b is Farnese (Fig. 4a; Palladino
548 and Valentine, 1995). A comparison with TF-35b shows a good, although poorly constrained, geochemical
549 matching (Fig. 8d), supporting the correlation of TF-35b with Farnese. Here the Farnese unit is $^{40}\text{Ar}/^{39}\text{Ar}$ dated
550 at 235.6 ± 0.6 ka, which is consistent with the climatostratigraphic position of TF-35b, thus supporting the
551 correlation. The new age we obtained for Farnese is also consistent with the less precise age of 242 ± 8 ka

552 previously determined for this unit (Turbeville, 1992). The correlation allows us to transfer the new high
 553 precision $^{40}\text{Ar}/^{39}\text{Ar}$ age of Farnese to the Fucino succession.
 554

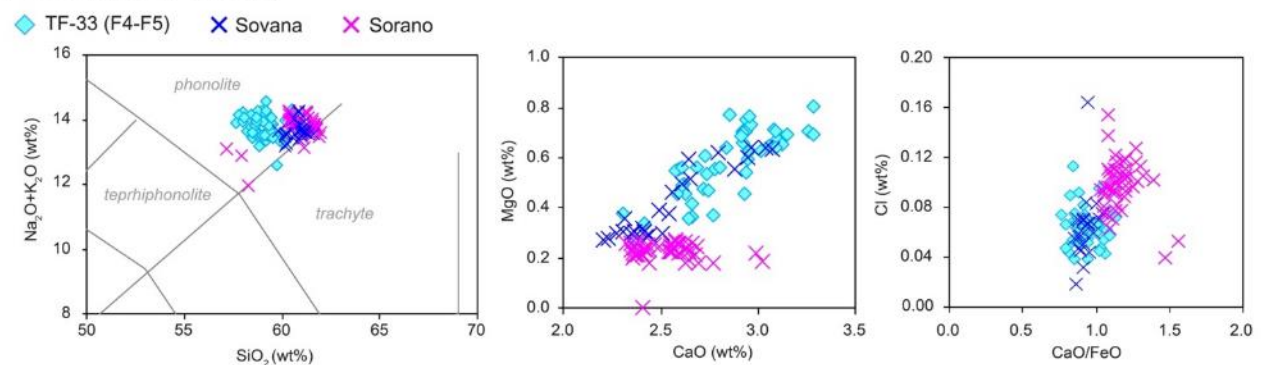
a) Vulsini unknown (194.5 ± 2.0 ka)



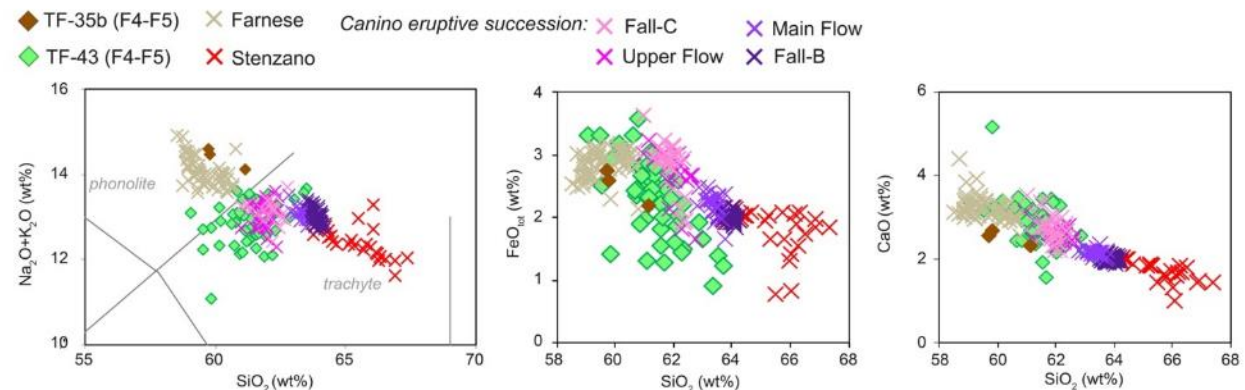
b) Onano (224.7 ± 2.6 ka) + Grotte di Castro (225.3 ± 1.2 ka)



c) Sovana (226.4 ± 0.7 ka)



d) Farnese (235.6 ± 0.6 ka) + Canino (253.4 ± 0.8 ka)



555

556 **Figure 8.** *Total alkali vs silica* (TAS) classification diagram (Le Maitre et al., 2002) and representative major element biplots for TF-22,
557 TF-31, TF-32, TF-33, TF-35b, and TF-43 from the F4-F5 record compared with proximal Latera Volcanic Complex (LVC) units. Data
558 source: WDS glass composition of TF-22, TF-31, TF-32, TF-33, TF-35b, TF-43 (F4-F5), Onano, Grotte di Castro, Sorano, Sovana,
559 Farnese, Stenzano, and Canino (Fall-C, Upper Flow, Main Flow and Fall-B): this study; TF-22 (F1-F3): Giaccio et al. (2017a); PRAD-
560 3586: Bourne et al. (2015); whole-rock mean composition of DED-87-08 C-56 tephra: Paterne et al. (2008); $^{40}\text{Ar}/^{39}\text{Ar}$ age of TF-22, TF-
561 32, Onano, Grotte di Castro, Sovana, Farnese, and Fall-C: this study.
562

563 **TF-43 - Canino.** This LVC tephra, the lowermost investigated in this study, falls towards the end of an interval
564 of low Ca content (Fig. 3) that is interpreted as the expression of the MIS 8 glacial period (Giaccio et al., 2019)
565 and thus has an estimated climatostratigraphic age of ~250 ka. It is mainly characterised by a slightly variable
566 trachytic composition, with 59-64 wt.% SiO_2 and 11-14 wt.% alkali sum (Fig. 4a). Among the LVC units
567 stratigraphically and chronologically compatible with TF-43, both the Stenzano (Taddeucci and Palladino,
568 2002) and Canino (Palladino and Agosta, 1997; Palladino et al., 2010) units are characterised by a trachytic
569 composition (Fig. 4a). A comparison with these units reveals a convincing geochemical matching between
570 Canino and TF-43 (Fig. 8d). The $^{87}\text{Sr}/^{86}\text{Sr}$ ratio obtained for TF-43 (i.e., 0.7106), although being perfectly in
571 line with the values of the other Vulsini units (Fig. 6a), is somewhat lower than the values obtained for Canino
572 (i.e., 0.7108). This discrepancy can be attributed to either an isotopic variability within the feeding system that
573 fed the eruption or a not completely clean feldspar fraction. Here Canino Fall-C has been dated at 253.1 ± 0.8
574 ka, an age virtually indistinguishable from that of Canino Fall-B (253.8 ± 0.8 ka; Fig. 7) and fully in agreement
575 with previous $^{40}\text{Ar}/^{39}\text{Ar}$ age of 253 ± 6.0 ka here recalibrated for this unit (Turbeville, 1992). The Canino
576 chronology is also consistent with the late MIS 8 climatostratigraphic position of TF-43. The correlation of
577 Canino with TF-43 allows us to transfer its high-precision $^{40}\text{Ar}/^{39}\text{Ar}$ age to the Fucino succession, providing an
578 age control point for the lower part of the interval here investigated.
579

580 5.3.2.2. Tephra from Sabatini

581 **TF-17a - Trevignano Romano TR-CR-2.** This Sabatini tephra occurs ~2 m below TF-17, $^{40}\text{Ar}/^{39}\text{Ar}$
582 dated at 158.8 ± 3.0 ka (Giaccio et al., 2017a), and in the early part of the MIS 6 glacial (Fig. 3). It is phonolitic
583 in composition (Fig. 4a) with variable silica (56.1-61.3 wt.%) and alkali sum (14.1-16.1 wt.%). It has a major
584 element geochemical composition similar to the newly investigated TR-CR-2 unit from Trevignano Romano
585 (Tables 1, 3; Fig. 9a), to which it is correlated. In proximal settings, TR-CR-2 is stratigraphically located under
586 deposits of the S. Bernardino Maar (Sottili et al., 2010; Sottili et al., 2012), which has an inferred age of ≤ 172
587 ka, compatible with the stratigraphic position of TF-17a.

588 **TF-18/TF-19 - Trevignano Romano TR-CR-1.** These couple of Sabatini tephra, like TF-17a, occurs in the
589 early part of the period characterised by low Ca content correlated to the MIS 6 glacial (Fig. 3) and are
590 bracketed between tephra TF-17 and TF-22, $^{40}\text{Ar}/^{39}\text{Ar}$ dated at 158.8 ± 3.0 ka (Giaccio et al., 2017a) and 194.4

591 ± 2.0 ka (this study; Fig. 7), respectively. They stratigraphically match the couplet of the geochemically
592 indistinguishable tephra TF-18+TF-19 found in F1-F3 core that was ascribed to an undefined Latium source
593 (Giaccio et al., 2017a). Here we correlate TF-18+TF-19 to the TR-CR-1 unit from Trevignano Romano (Tables
594 1, 3; Fig. 1), which displays similar ME and TE compositions (Figs. 5, 9a). For instance, TF-18 and TF-19 have
595 HFSE ratios to Y (i.e., Nb/Y = 0.89-1.22 [TF-18] and 1.02-1.34 [TF-19]; Zr/Y = 14.34-19.75 [TF-18] and 14.41-
596 20.22 [TF-19]; Fig. S5a) similar to TR-CR-1 (Nb/Y = 0.99-2.58; Zr/Y = 18.15-42.23; Fig. S5b). $^{87}\text{Sr}/^{86}\text{Sr}$ and
597 $^{143}\text{Nd}/^{144}\text{Nd}$ ratios determined on TF-18 and TF-19 overlap with those of TR-CR-1 and the other SVD units
598 (Fig. 6a-b), corroborating these correlations. In proximal settings, TR-CR-1 occurs below TR-CR-2, which is
599 overlaid by deposits of the S. Bernardino Maar (≤ 172 ka; Sottili et al., 2010; Sottili et al., 2012), consistently
600 with the correlation of TF-17a with TR-CR-2.

601 **TF-27 - Vigna di Valle.** This Sabatini tephra occurs in a stadial pulsation of the late MIS 7, likely corresponding
602 to the MIS 7d sub-stage dated at ~ 205 ka in LR04 Benthic Stack (Fig. 3), and just below the Iceland Basin
603 geomagnetic excursion (Giaccio et al., 2019). It is characterised by a variable composition, mainly phonolitic,
604 and can be classified as tephriphonolite-phonolite-latitude-trachyte according to the TAS diagram (Fig. 4a).
605 Comparison with the proximal SVD pyroclastic units shows a convincing geochemical matching with the Vigna
606 di Valle unit (Fig. 9b), dated at 193.0 ± 7.0 ka (FCt 28.02; Sottili et al., 2010), equivalent to 195.0 ± 7.0 using
607 FCt at 28.294 Ma or ACs at 1.1891 Ma (Niespolo et al., 2017), thus in disagreement with the age of $205.1 \pm$
608 1.4 ka (Fig. 7) determined here for TF-27. However, in Sottili et al. (2010), only 4 crystals were used for
609 calculating the weighted mean age of Vigna di Valle, whilst other 4 crystals were excluded, being interpreted
610 as xenocrysts. Of these, 3 out of the 4 rejected crystals have ages that at 1-sigma overlap that of the 4 accepted
611 ones. Thus, by reintegrating these 3 previously rejected but consistent crystals, the weighted mean age of
612 Vigna di Valle becomes 205.9 ± 5.0 ka, i.e., in agreement with the more precise $^{40}\text{Ar}/^{39}\text{Ar}$ age of 205.1 ± 1.4
613 ka we obtained for TF-27 (Fig. 7), which supports our correlation and substantially reduces the chronological
614 uncertainty for the Vigna di Valle eruption. $^{87}\text{Sr}/^{86}\text{Sr}$ and $^{143}\text{Nd}/^{144}\text{Nd}$ ratios determined on TF-27 also support
615 an origin from Sabatini as these values overlap with those of the other SVD units (Fig. 6a-b).

616 **TF-28 - Sabatini unknown.** This tephra occurs in the second half of the MIS 7, at the end of a period of high
617 Ca content likely corresponding to the end of MIS 7c, and thus with an estimated age of ~ 210 ka (Fig. 3). It is
618 characterised by a dominant phonolitic composition (Fig. 4a; Fig. S1b), with a SiO_2 content of 55-63 wt.% and
619 alkali sum of ~ 11 -16 wt.%. According to the CaO/FeO vs Cl classification diagram, TF-28 falls between the
620 Vulsini+Vico and Sabatini fields, making its attribution to one of these three potential volcanic sources
621 challenging. However, the newly acquired glass-WDS data from proximal Pizzo Prato unit perfectly overlaps

622 with TF-28, allowing it to be ascribed to the Sabatini volcano (Figs. 4b, 9c). However, the age of 251 ± 16 ka
623 available for the Pizzo Prato unit (Sottili et al., 2010), although associated with a large error, appears not
624 compatible with the position of TF-28, which occurs less than 1 m below TF-27/Vigna di Valle, dated at 205.1
625 ± 1.4 ka. This large age discrepancy would suggest either a correlation with another, currently undocumented,
626 Sabatini unit younger than Pizzo Prato, or a substantial ageing (due to xenocryst contamination?) of the
627 available age for Pizzo Prato. We thus conservatively propose to consider TF-28 as an undocumented Sabatini
628 unit, deferring its definitive confirmation or rejection to future investigations.

629 **TF-30 - Sabatini unknown.** This tephra is located closely below the previously described TF-28 and thus
630 shares with it a similar climatostratigraphic position and age (Fig. 3). Its phonolitic composition (Fig. 4a) does
631 not match that of the Pizzo Prato unit (Fig. 9c) or those of other geochronologically compatible known Sabatini
632 units (e.g., Sottili et al., 2019; Marra et al., 2020). Nevertheless, the geochemical composition of TF-30, similar
633 to those of the other Sabatini units here investigated, suggests an origin from this volcano and this tephra is
634 therefore here ascribed to an undefined Sabatini eruption.

635

636 5.3.2.3. Tephra from Vico

637 **TF-24 and TF-25 - Vico unknown.** These two chemically related tephra layers are
638 climatostratigraphically associated to the early stage of MIS 6 (Fig. 3). They are characterised by a similar and
639 homogeneous phonolitic composition, with SiO₂ ranging between 56-60 wt.% (TF-24) and 57-60 wt.% (TF-25)
640 and an alkali sum of 12-15 wt.% (both). The almost identical geochemical composition could suggest that
641 these two layers refer to an individual eruption, with uppermost of the two tephra being reworked. However,
642 these layers are separated by ~10 cm of lacustrine sediments (Table 2) and are characterised by sharp bottom
643 boundaries that exclude a possible reworking of the second layer. According to the CaO/FeO vs Cl
644 discriminating diagram, these two tephra layers can be attributed to either Vulsini or Vico (Fig. 4b; Fig. S2a).
645 However, TE biplots highlighted a marked difference between these two tephra with respect to the LVC units
646 (Fig. 5), with higher Th contents and thus lower ratios of Th to HFSE and LREE. For instance, ratios of Ta to
647 Th for TF-24 and TF-25 ranges respectively from 0.012 to 0.015 ppm, and from 0.011 to 0.017 ppm (Fig. S6a),
648 whilst LVC units have Ta/Th ratios generally > 0.020 ppm (Fig. S6b). These TE concentrations, however, are
649 compatible with TE contents of Vico Period I units (Fig. 9d), supporting an origin from this volcano. TF-24 and
650 TF-25 are positioned between TF-22 and TF-27, dated at 194.4 ± 2.0 ka and 205.1 ± 1.4 ka respectively,
651 collocating them between the caldera-forming eruptions of Vico Ignimbrite A (or Farine Formation, ~250 ka;
652 Sollevanti, 1983) and Ignimbrite B (or Ronciglione Formation, 157 ± 3 ka; Laurenzi and Villa, 1987).

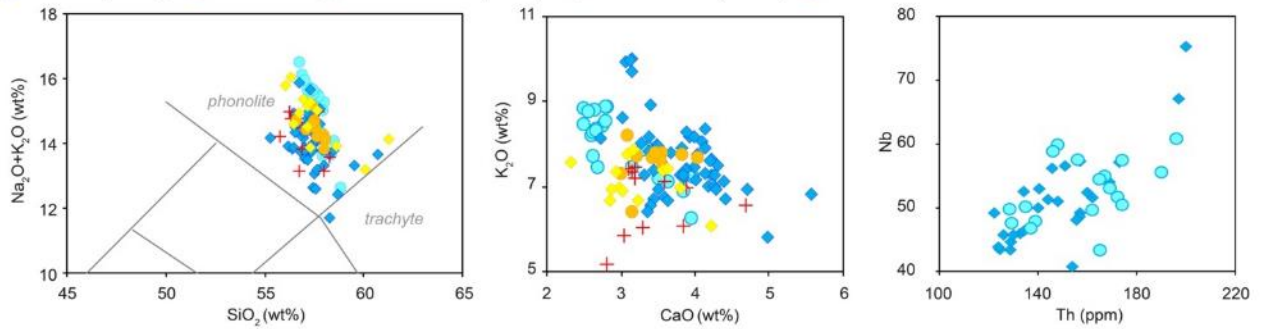
653 Comparison with the newly acquired glass-WDS composition of Vico-A/Farine Formation unit ([Fig. 9d](#)) shows
654 geochemical similarities with the two Fucino tephra (i.e., similar CaO/FeO ratio), which furtherly supports an
655 origin from Vico volcano. However, no eruption is reported between the Vico-A and Vico-B Ignimbrites (e.g.,
656 [Perini et al., 2004](#)), preventing us from any tentative correlation and suggesting that the two Fucino tephra
657 represent deposits of an explosive activity currently undocumented in proximal settings.

658 On the other hand, we find a good geochemical matching between TF-24/TF-25 and the Adriatic tephra PRAD-
659 3666 ([Fig. 10a](#)). The layer PRAD-3666 was originally attributed to an undefined Latium volcano ([Bourne et al.,](#)
660 [2015](#)) and was geochronologically poorly constrained between 181 and 156. ka. However, as already
661 discussed above (see section 5.3.2.1.) and in previous studies (e.g., [Giaccio et al., 2017a](#)), the age model for
662 the Middle Pleistocene section of PRAD 1-2 is biased by erroneous correlations and thus PRAD-3666 is here
663 proposed as a correlative tephra for TF-24 and/or TF-25 tephra, which is fully consistent with the above
664 proposed correlation of PRAD-3586 with TF-22 (see section 5.3.2.1).

665

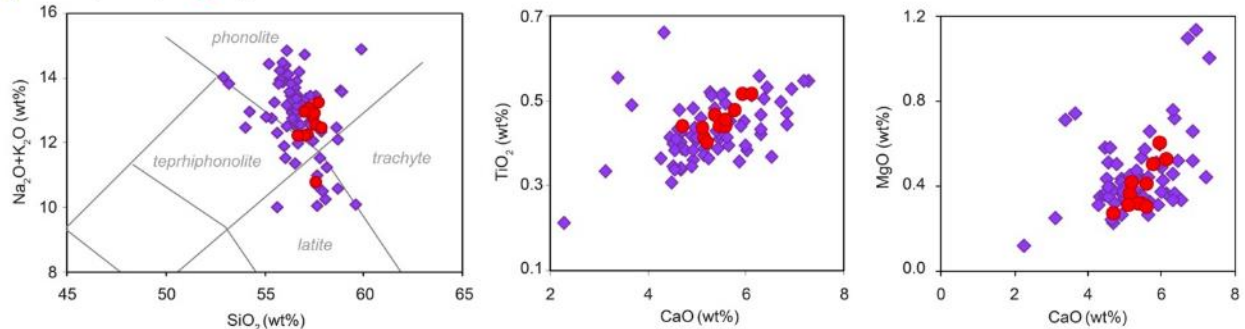
a) TR-CR-2 (182.5 ± 8.5 ka) and TR-CR-1 (183.4 ± 8.4 ka)

◆ TF-17a (F4-F5) ● TR-CR-2 ◆ TF-18 + TF-19 (F4-F5) + TF-18+TF-19 (F1-F3) ● TR-CR-1



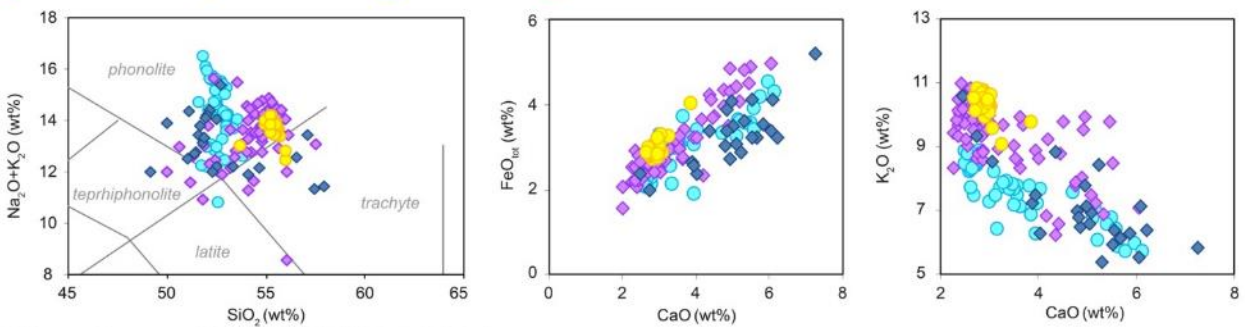
b) Tufo di Vigna di Valle (205.1 ± 1.4 ka)

◆ TF-27 (F4-F5) ● Vigna di Valle



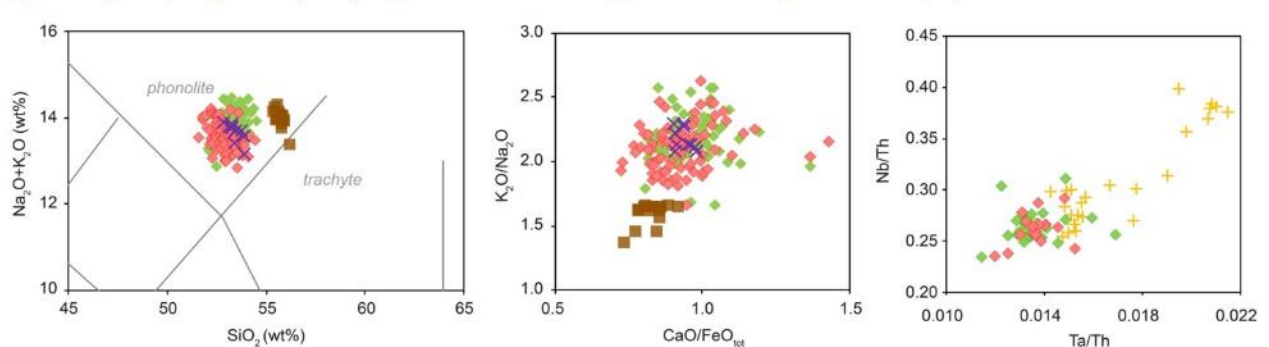
c) Sabatini unknowns (210.0 ± 4.1 - 213.0 ± 5.8 ka)

◆ TF-28 (F4-F5) ◆ TF-30 (F4-F5) ● Pizzo Prato ● Sabatini proximal



d) Vico unknowns (196.3 ± 3.1 - 196.6 ± 3.2 ka)

◆ TF-24 (F4-F5) ◆ TF-25 (F4-F5) ■ Farine Formation ✕ PRAD-3666 + Vico Period I (TE)



666

667
668
669
670
671
672
673

Figure 9. Total alkali vs silica (TAS) classification diagram (Le Maitre et al., 2002) and representative major (ME) and trace element (TE) bi-plots for TF-17a, TF-18, TF-19, TF-24, TF-25, TF-27, TF-28, and TF-30 from the F4-F5 record compared with proximal Sabatini Volcanic District (SVD) and Vico (i.e., Farine formation) units. Data source: WDS glass composition of TF-17a, TF-18, TF-19, TF-24, TF-25, TF-27, TF-28, TF-30 (F4-F5), TR-CR-2, TR-CR-1, Vigna di Valle, Pizzo Prato (Sabatini proximal data), and Farine Formation (Vico): this study; TF-18 + TF-19 (F1-F3): Giaccio et al. (2017a); PRAD-3666: Bourne et al. (2015); TE glass composition of TF-18+TF-19, TF-24, and TF-25: this study; TE glass composition of Vico Period I: Monaco et al. (2021); $^{40}\text{Ar}/^{39}\text{Ar}$ age of TF-27: this study.

674 5.3.2.4. *Latium-undefined tephra*

675 **TF-29 and TF-37.** TF-29, in the late part of the MIS 7 period (Fig. 3), is characterised by a latitic-
676 trachytic composition, with SiO₂ ranging from 55 to 65 wt.% and alkali sum of 9-12 wt.%, whilst TF-37 has a
677 polymodal composition (Fig. 4a; Fig. S1a), ranging from phonotephrite to phonolite-trachyte, with increasing
678 alkali sum at increasing SiO₂. The limited number of analytical points obtained for these two tephra layers (9
679 and 11 respectively) makes their attribution to one of the peri-Tyrrhenian volcanic sources challenging. In the
680 CaO/FeO vs Cl classification diagram (Fig. 4b) they fall at the Sabatini and Vulsini+Vico boundary. The low Cl
681 content of TF-29 (mean of 0.08 wt.%) and TF-37 (mean of 0.11 wt.%) surely point out to a Latium origin, the
682 specific source of which is however not confidently determinable. For these reasons, these two tephras will be
683 ascribed to a Latium-undefined volcanic source.

684

685 5.3.2.5. *Tephra from Ischia*

686 **TF-21 and TF-23.** Both Ischia tephra TF-21 and TF-23 are climatostratigraphically placed in the early
687 MIS 6 glacial period and are located respectively above and below TF-22, here ⁴⁰Ar/³⁹Ar dated at 194.4 ± 2.0
688 ka. They are characterised by a homogeneous trachytic composition (Fig. 4a), with SiO₂ ranging between 62-
689 64 wt.% (TF-21) and 62-65 wt.% (TF-23) and identical alkali sum (~13-15 wt.%). It is worth mentioning the
690 possibility that TF-21 or TF-23 might be a reworked layer: however, we excluded such hypothesis, as these
691 two layers are separated by another one (i.e., TF-22). In Giaccio et al. (2017a), tephra layer TF-21 was
692 tentatively correlated to either the C-52 or C-54 tephra layers from the Tyrrhenian marine core KET 80-04/DED-
693 87-08 of Paterne et al. (2008). Although the geochemical composition of TF-21 and TF-23 is compatible with
694 that of the Tyrrhenian layers C-52 and C-54 (Fig. 10a), the lack of individual glass analysis for these marine
695 tephras still leaves this potential correlation uncertain.

696

697 5.3.2.6. *Tephra from Roccamonfina/Neapolitan volcanic area?*

698 **TF-35.** This tephra is characterised by a homogeneous trachytic composition, with 61-64 wt.% SiO₂,
699 11-13 wt.% alkali sum, and mean K₂O/Na₂O ratio of 1.63 ± 0.25 (2σ). The relatively high Cl content (up to 0.36
700 wt.%) and CaO/FeO ratio of 0.74-0.88 suggest either a Roccamonfina or NVA origin for this tephra (Fig. 4b-l).
701 It is located between TF-33/Sovana (226.4 ± 0.7 ka) and TF-35b/Farnese (235.6 ± 0.6 ka). In proximal settings,
702 deposits of the caldera-forming eruptions of the Upper White Trachytic Tuff (UWTT, Subunit G of Giannetti
703 and De Casa, 2000) and Yellow Trachytic Tuff (YTT) were respectively dated at 234.0 ± 9.0 ka (recalculated
704 age from Giannetti and De Casa, 2000) and 231 ± 6.0 ka (recalculated age from Giannetti, 1996), which are

705 compatible with that of ~230 ka estimated for TF-35. [Rouchon et al. \(2008\)](#) provided whole-rock composition
706 of two WTT samples (i.e., RMF96 and RMF11), both trachytic in composition. However, it is not specified by
707 the authors to which sub-units the two samples refer, preventing us from any tentative correlation with these
708 units. Nevertheless, based on chronological constraints, TF-35 might represent one of the two above-
709 mentioned eruptions of the UWTT-YTT.

710 At Lake Ohrid ([Fig. 1a](#)), [Leicher et al. \(2019\)](#) reported the occurrence of some tephra with uncertain Campi
711 Flegrei (NVA)/Roccamonfina-like (i.e., OH-DP-0997, OH-DP-1055) or Campi Flegrei geochemical signature
712 (OH-DP-1006). Of these, the older OH-DP1055 (241.2 ± 6.2 ka) is roughly consistent with the oldest activity
713 documented in the Campanian area related to the Seiano Ignimbrites and dated between ~250 ka and ~290
714 ka ([Rolandi et al., 2003](#)), which precedes the Taurano-Moschiano phase (~190-160 ka; [Rolandi et al., 2003](#)).
715 The younger OH-DP-0997 and OH-DP-1006, with modelled ages of 228.9 ± 5.7 and 230.9 ± 6.3 ka,
716 respectively ([Leicher et al., 2021](#)), are chronologically compatible with TF-35. The comparison between TF-35
717 and these two Ohrid tephra shows remarkable geochemical differences with OH-DP-0997, while some degree
718 of similarity with OH-DP-1006 can be noted, although OH-DP-1006 shows a wider compositional variability
719 ([Fig. 10b](#)). [Leicher et al. \(2021\)](#) correlated OH-DP-1006 to S2 tephra from San Gregorio Magno ([Munno and](#)
720 [Petrosino, 2007](#)), which, like TF-35, shows a more homogenous composition, and thus TF-35 and S2 are more
721 similar to each other than to OH-DP-1006 ([Fig. 10b](#)). TF-35 might be thus correlated to S2 layer and possibly
722 to OH-DP-1006 as well, even though S2 lays immediately below tephra S4, $^{40}\text{Ar}/^{39}\text{Ar}$ dated at 239 ± 8 ka
723 ([Ascione et al., 2013](#)), thus chronologically barely compatible with age of TF-35. Therefore, we consider this
724 as a tentative correlation only.

725

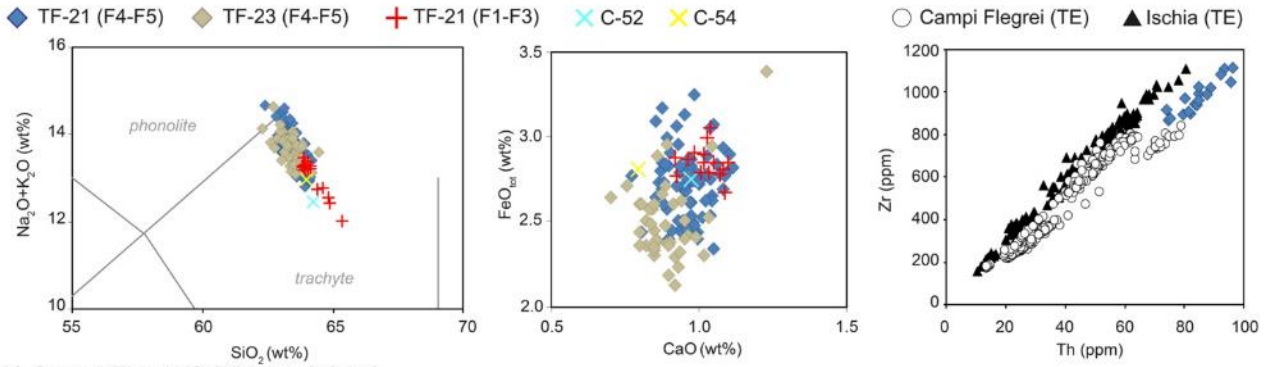
726 5.3.2.7. Tephra from Neapolitan volcanic area (NVA)

727 **TF-21a and TF-26.** Both TF-21a and TF-26 are MIS 6 tephra, that were emplaced at the very onset
728 of this glacial period and have an estimated age of ~190-180 ka ([Fig. 3](#)). They are characterised by a phonolitic-
729 trachytic composition ([Fig. 4a](#)), with a similar increase of the alkali content at increasing silica, which ranges
730 between 58-62 wt.% (TF-21a) and 56-63 wt.% (TF-26). The high Cl content (TF-21a = 0.23-0.63 wt.%; TF-26
731 = 0.19-0.65 wt.%), the CaO/FeO ratios ([Fig. 4b](#), [Fig. S1a](#)) and the Sr-Nd isotope composition ([Fig. 6b](#)) clearly
732 points to a NVA origin for both tephra. Specifically, the low $^{87}\text{Sr}/^{86}\text{Sr}$ (0.706-0.707) and simultaneously high
733 $^{143}\text{Nd}/^{144}\text{Nd}$ ratio (i.e., 0.5126) fro TF-26 is a typical feature of the old Campi Flegrei products (e.g., [D'Antonio](#)
734 [et al., 2007](#); [Monaco et al., 2022](#)) preceding the Campanian Ignimbrite eruption (39.85 ± 0.14 ka; [Giaccio et](#)
735 [al., 2017b](#)). According to former studies, several late Middle Pleistocene ignimbrite deposits were emplaced in

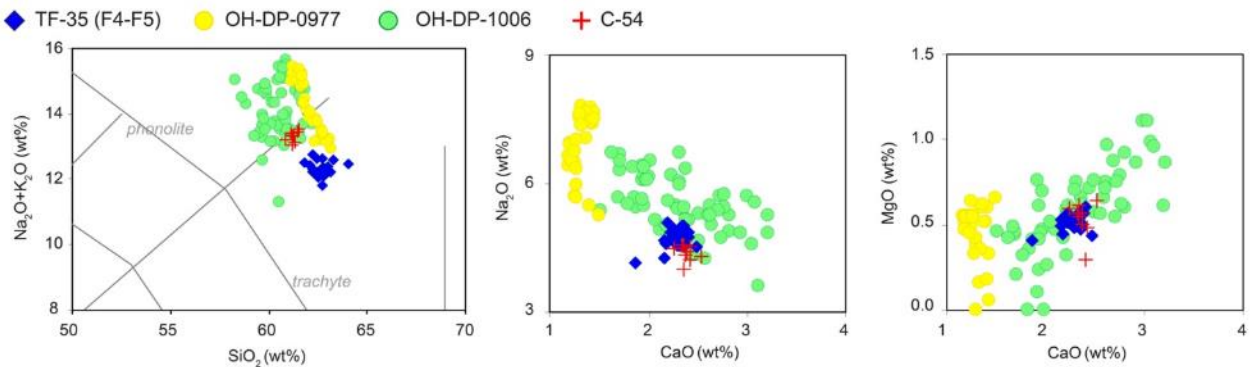
736 the Campanian Plain (e.g., [De Vivo et al., 2001](#); [Rolandi et al., 2003](#); [Belkin et al., 2016](#)), which are ascribed
737 to the so-called Campanian Volcanic Zone (CVZ; [Rolandi et al., 2003](#)), dating as back as 290 ka (i.e., Seiano
738 Ignimbrite; [Rolandi et al., 2003](#)). Specifically, the Moschiano Ignimbrite ([Rolandi et al., 2003](#)), with a poorly
739 constrained age of 188.0 ± 7.4 ka, could represent a possible candidate for correlation with TF-21a ([Fig. 11](#),
740 [Table 5](#)). So far, the only available glass composition of these late Middle Pleistocene units refers to the
741 Taurano Ignimbrite (TI, sample AF-Y1-13; [Amato et al., 2018](#)) dated at 160.2 ± 2.0 ka (recalculated; [De Vivo](#)
742 [et al., 2001](#)) and correlated to the Fucino tephra TF-17, dated to 158.3 ± 3.0 ka, and other equivalent tephra
743 layers in the Adriatic Sea and Lake Ohrid ([Giaccio et al., 2017a](#)). Overall, the composition of TF-21a and TF-
744 26 is consistent with that of TI/TF-17, including all its distal equivalents ([Fig. 10c](#)). Thus, TF-21a and TF-26
745 can be similarly ascribed to this late Middle Pleistocene NVA activity, which, in relatively proximal setting, is
746 sporadically documented by ignimbrite-like and ash-fall deposits occurring in suitable depositional settings.
747 In the Mediterranean area, late Middle Pleistocene Neapolitan-like tephra layers are reported in several
748 repositories. At Lake Ohrid ([Fig. 1a](#)), at least seven tephra with Neapolitan-Roccamonfina like composition are
749 recorded in the time interval of 241-160 ka ([Leicher et al., 2019, 2021](#)). Of these, Ohrid tephra OH-DP-0725
750 ([Leicher et al., 2021](#); new glass-EPMA-WDS data presented also in this study) shows a good geochemical
751 matching with both TF-21a and TF-26 based on major element composition ([Fig. 10d](#)). However, OH-DP-0725
752 has a modelled age of 174.4 ± 5.2 ka ([Leicher et al., 2021](#)), which is geochronologically incompatible with both
753 TF-21a and TF-26, excluding a possible correlation.
754 Reliable geochemical matching is also observed between TF-21a and S7 tephras from San Gregorio Magno
755 Basin ([Munno and Petrosino, 2007](#)), which occurs just below tephra S8, correlated to OH-DP-0710 ([Leicher](#)
756 [et al., 2019](#)) dated to 172.3 ± 5.6 ka ([Leicher et al., 2021](#)). TF-21a can be thus tentatively correlated with S7
757 ([Fig. 10d](#)). In the Tyrrhenian core DED-87-08 other Neapolitan-like tephra, chronologically compatible with TF-
758 21a and TF-26, such as C-49/C-51 (178-183 ka) and C-53/C-55 (~189-196 ka), have been reported by [Paterne](#)
759 [et al. \(2008\)](#), and show a composition compatible with both TF-21a and TF-26 ([Fig. 10c-d](#)). Again, the lack of
760 individual glass analysis prevents us from any definitive correlation. Notably, in the core DED-87-08 a couple
761 of younger tephra (C-41 and C-42; ~150 ka; [Paterne et al., 2008](#)) are geochronologically and geochemically
762 roughly consistent with the Taurano Ignimbrite/TF-17 ([Fig. 10c](#)).
763 Finally, at ODP Site 964 ([Vakhrameeva et al., 2021](#)), tephra layer 964A-2H-5-59b has a Campanian like
764 composition. However, both geochemical (major and minor elements) and geochronological (orbital age of
765 ~238 ka) data rule out a correlation with any of the two Fucino tephra layers.

766

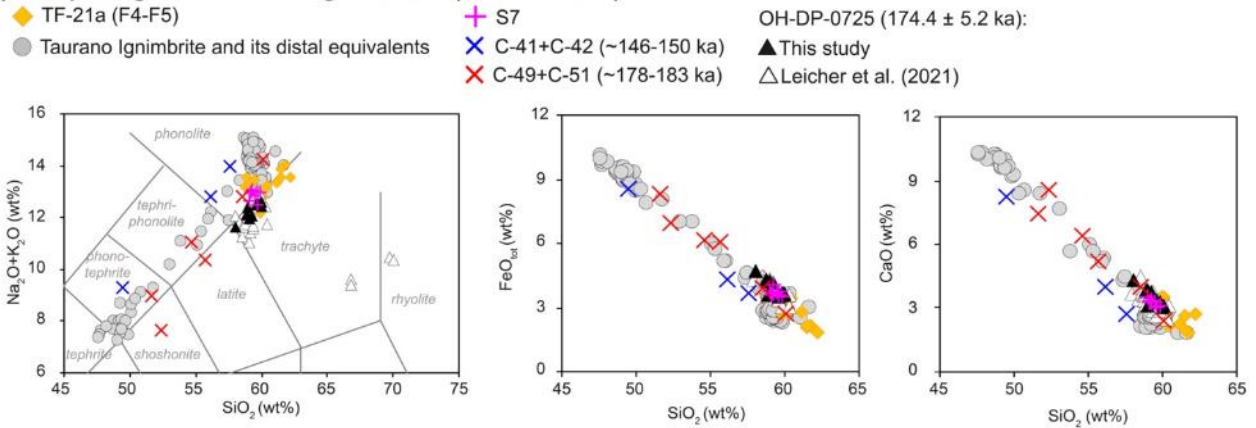
a) Ischia unknowns (187.7 ± 7.7 - 194.9 ± 2.9 ka)



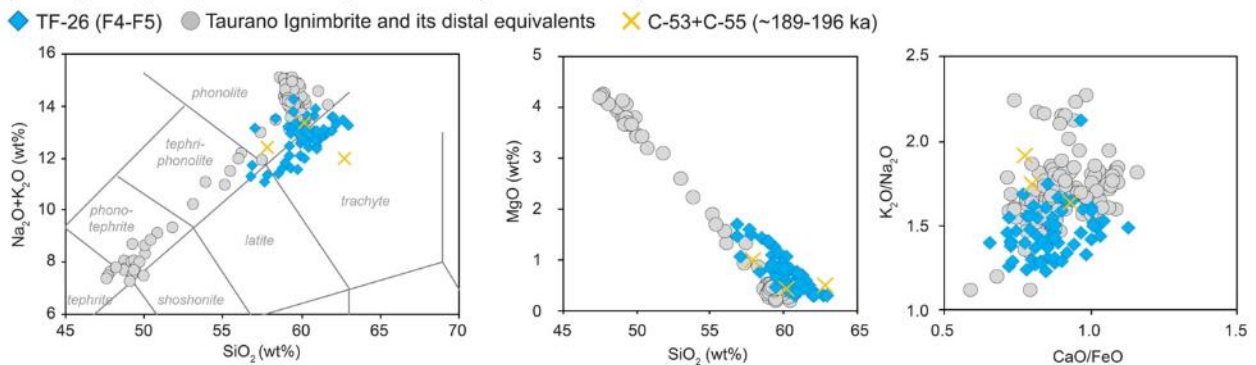
b) Campi Flegrei? (229.0 ± 2.2 ka)



c) Campi Flegrei Moschiano Ignimbrite? (189.5 ± 7.0 ka)



d) Campi Flegrei pre-Taurano Ignimbrite? (198.3 ± 3.4 ka)



767

768
769
770
771
772
773
774
775

Figure 10. Total alkali vs silica (TAS) classification diagram (Le Maitre et al., 2002) and representative major (ME) and trace element (TE) bi-plots for TF-21, TF-21a, TF-23, TF-26, and TF-35 from the F4-F5 record compared with OH-DP-0725, OH-DP-0977, OH-DP-1006 and tephra layers from the literature. Data source: WDS glass composition of TF-21, TF-21a, TF-23, TF-26, and TF-35 (F4-F5), and OH-DP-0725: this study; TF-21 (F1-F3): Giaccio et al. (2017a); OH-DP-0725, OH-DP-0977, OH-DP-1006: Leicher et al. (2021); EDS composition of S2 and S7: Munno and Petrosino (2007); WR composition of C-52 and C-54: Paterne et al. (2008). Taurano Ignimbrite literature data: TF-17 (Giaccio et al., 2017a), OH-DP-0624 (Leicher et al., 2021), PRAD-3225 (Bourne et al., 2015), AF-Y1-13 and S11-PAUP (Amato et al., 2018). TE glass composition of TF-21 (F4-F5): this study; TE glass composition of proximal Ischia and Campi Flegrei pyroclastic units: Tomlinson et al. (2012, 2015).

776

777 5.4. Age model

778 Using the $^{40}\text{Ar}/^{39}\text{Ar}$ ages of the Fucino tephra (Fig. 7) and those derived from the above-discussed
779 correlations of these tephra with the newly dated proximal counterparts (Fig. 7), we developed a Bayesian
780 age-depth model for the interval of ~160-250 ka (Fig. 11a) using the Bacon software (Blaauw and Christen,
781 2011). Specifically, eleven $^{40}\text{Ar}/^{39}\text{Ar}$ ages related to eight tephra layers were used (i.e., for TF-17, TF-27, and
782 TF-32 also the ages of correlated units have been used for the age-depth model), as shown in Figure 11a. For
783 three of them (TF-17, TF-27, and TF-32) we used the weighted mean ages resulting from both the direct dating
784 of the Fucino tephra and the related proximal equivalents, in one case only the direct $^{40}\text{Ar}/^{39}\text{Ar}$ age of the
785 Fucino tephra (TF-22), while for the remaining 4 tephra (TF-31, TF-33, TF35b and TF-43) only the age of the
786 correlated proximal equivalents (Fig 11a).

787 The chronological constraints are quite well distributed along the succession, with a higher density of the
788 control points between 224 ka and 235 ka (Fig. 11a). Overall, the resulting curve shows a quite homogeneous
789 long-term sedimentation rate and history of sediment accumulation (Fig. 11b). The age-depth model allows us
790 to reliably assess the age of each individual late MIS 8-early MIS 6 investigated tephra as modelled ages, with
791 their own statistically significant uncertainty, as shown in Figure 11b and summarized in Table 5.

792

793 5.5. Implications for volcanology and Quaternary sciences

794 5.5.1. Mediterranean tephrochronology and peri-Tyrrhenian explosive activity during MIS 6-8 reevaluated in 795 light of the Fucino record

796 The detailed late MIS 8-early MIS 6 tephra record from Fucino basin significantly enriches the
797 Mediterranean tephrochronology and allows a substantial refinement of the peri-Tyrrhenian eruptive history in
798 the time interval of 250-170 ka (Fig. 11).

799 As summarized in section 5.2., very few Mediterranean records cover, totally or partially, the investigated
800 interval and sometimes the related data are not provided as full geochemical dataset (e.g., core DED 87-08),
801 thus currently limiting a full exploitation of the Fucino record for possible correlations.

802 Here we proposed two potential new correlations between the Adriatic Sea PRAD 1-2 and the F4-F5 Fucino
803 tephra (i.e., TF-22=PRAD-3586 and TF-24/TF-25=PRAD-3666) that substantially improve the chronology for
804 the lowermost interval of the PRAD 1-2 sediment core. Specifically, TF-22=PRAD-3586 is here precisely
805 $^{40}\text{Ar}/^{39}\text{Ar}$ dated at 194.5 ± 2.0 ka, while the modelled age for TF-24/TF-25=PRAD-3666 is 196.3 ± 3.1 - $196.6 \pm$
806 3.2 ka (Table 5). We also presented a tentative correlation of tephra layer S7 from the San Gregorio Magno

807 Basin succession ([Munno and Petrosino, 2007](#); [Petrosino et al., 2019](#)) with the CF-like Fucino tephra TF-21a,
808 which has a modelled age of 189.5 ± 7.0 ka ([Table 5](#)). The former is also geochemically similar to Ohrid tephra
809 OH-DP-0725, for which here we have provided new glass-WDS analysis. However, both the modelled age, at
810 174.4 ± 5.2 ka, and the climatostratigraphic position of OH-DP-0725 ([Leicher et al., 2021](#)) appear incompatible
811 with a correlation with TF-21a ([Fig. 12](#)). A quite convincing correlation has instead been proposed between
812 TF-35, with a modelled age of 229.2 ± 2.2 ka ([Table 5](#); [Fig. 11b](#)), and the likely NVA tephra S2/OH-DP-
813 1006, from San Gregorio and Lake Ohrid, respectively. Therefore, for the 160-260 ka interval, in addition to
814 TF-17/OH-DP-0624 ([Fig. 12](#)) correlated to the Taurano Ignimbrite ([Giaccio et al., 2017a](#)), TF-35/OH-DP-1006
815 might represent a second tie point for synchronizing Fucino and Ohrid lake successions ([Fig. 12](#)).
816 Finally, some possible correlations might exist between the Fucino and DED 87-08 tephra layers. However,
817 the potential correlations (i.e., TF-21=C-52/C-54, TF-21a=C-53/55, TF-22=C-56) cannot be here definitively
818 proposed due to the lack of individual glass compositions and glass-WDS analysis of the DED-87-08 tephra
819 layers, leaving these correlations open to future investigations. Unfortunately, no tephra correlation has been
820 determined between the Fucino paleolake sequence and the Tenaghi Philippon ([Wulf et al., 2018](#);
821 [Vakhrameeva et al., 2018, 2019](#)) or ODP Site 964 ([Vakhrameeva et al., 2021](#)). However, currently the MIS 6-
822 7d at Tenaghi Philippon has not been investigated yet, thus correlations between the two tephra repositories
823 might emerge in the future.
824

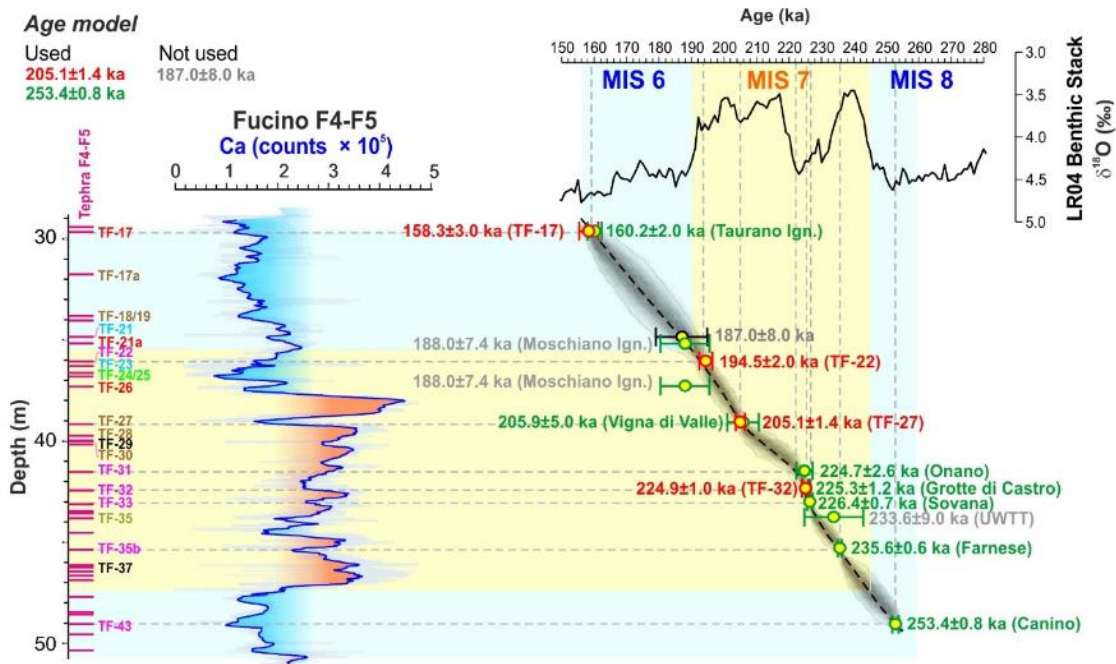
a)

Dating

○ $^{40}\text{Ar}/^{39}\text{Ar}$ age of Fucino tephra
 ○ $^{40}\text{Ar}/^{39}\text{Ar}$ age of correlated tephra
 ○ Orbital age of correlated tephra

Age model

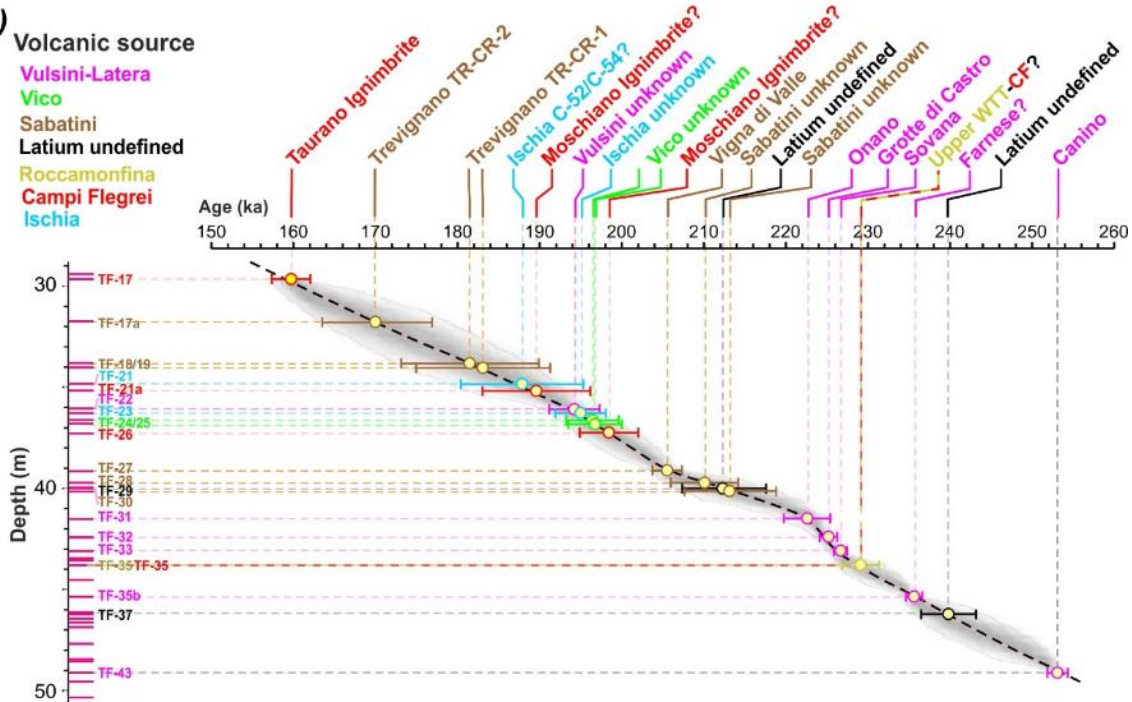
Used: 205.1±1.4 ka, 253.4±0.8 ka
 Not used: 187.0±8.0 ka



b)

Volcanic source

■ Vulsini-Latera
■ Vico
■ Sabatini
■ Latium undefined
■ Roccamonfina
■ Campi Flegrei
■ Ischia



825

826
827
828
829

Figure 11. Summary of the tephrochronological constrains and results for the late MIS 8-early MIS 6 Fucino record. **a)** Age-depth model. For comparison, the resulting Fucino Ca time-series is shown together to the LR04 Benthic Stack (Lisiecki and Raymo, 2005). **b)** Volcanic sources, individual correlation a modelled age (2σ error) for the F4-F5 investigated tephras.

830

On the other hand, as far as the history of the peri-Tyrrhenian volcanism is concerned, our results provide

831

more important insights. Notably, for the Latera caldera activity in the Vulsini volcanic district, here we provided

832

new $^{40}\text{Ar}/^{39}\text{Ar}$ dating for the eruption succession of Sovana, Grotte di Castro and Onano (Fig. 7; Table 5).

833 However, while the $^{40}\text{Ar}/^{39}\text{Ar}$ chronology resulted unable to resolve the inter-eruptive intervals between these
834 events, being the ages statistically undistinguishable from each other, the Fucino record provided modelled
835 ages that allow an estimation of the time elapsed between two subsequent eruptions (Table 5; Fig. 11).
836 Furthermore, the Vulsini-like TF-22 tephra, here $^{40}\text{Ar}/^{39}\text{Ar}$ dated at 194.5 ± 2.0 ka (Fig. 7), could provide a
837 precise chronological constraint for the minor Latera activity between Onano and Pitigliano, which is
838 documented in proximal settings, but still yet not fully characterised. Finally, although no other previously
839 undocumented Latera-like tephra has been identified in the investigated interval, we cannot exclude that the
840 two Latium-undefined tephra layers (i.e., TF-29 and TF-37), here not associated to a specific volcanic source,
841 could be potentially attributed to other LVC or coeval eastern Vulsini (Nappi et al., 1994) units after further
842 investigation.

843 At Sabatini volcano, proximal deposits discontinuously document explosive activity between the eruptions of
844 Vigna di Valle and Pizzo Prato (Sottili et al., 2019). At Fucino, at least two tephra layers (TF-28 and TF-30)
845 with Sabatini like composition document so far unknown explosive activity at ~ 210 -213 ka (210.0 ± 4.1 ka and
846 213.0 ± 5.8 ka). The Fucino record also provides a new, more precise $^{40}\text{Ar}/^{39}\text{Ar}$ age of 205.1 ± 1.4 ka for the
847 previously poorly dated Vigna di Valle unit, and modelled ages of 171.1 ± 7.1 ka and 183.4 ± 8.4 ka/ $182.5 \pm$
848 8.5 ka for the undated Trevignano Romano units TR-CR-2 and TR-CR-1, respectively (Table 5; Fig. 11b).

849 At Vico volcano, a ~ 90 ka interval is reported between the Vico Ignimbrite A (or Farine Formation, ca. ~ 250
850 ka; Sollevanti, 1983) and Ignimbrite B (or Ronciglione Formation, 157 ± 3 ka; Laurenzi and Villa, 1987) in the
851 literature. However, at Fucino two tephra layers (i.e., TF-24 and TF-25) with a Vico-like geochemical
852 composition occur in a time interval of 205.1 ± 1.4 ka (TF-27/Vigna di Valle) and 194.5 ± 2.0 ka (TF-22/Vulsini
853 unknown; Table 5; Fig. 11b), thus halving (from ~ 90 to ~ 45 ka) the supposed quiescence period.

854 At Ischia volcano, proximal deposits outcropping in the SE sector of the island are reported to date as back as
855 > 150 ka (e.g., Poli et al., 1987; Sbrana et al., 2018). At Fucino, the two Ischia tephra TF-21 and TF-23, with
856 a modelled age of 187.8 ± 7.5 ka and 195.0 ± 3.1 ka, respectively (Table 5; Fig. 11), testify, in agreement with
857 previous tephra studies (e.g., Paterno et al., 2008), that the island has been volcanically active since the late
858 Middle Pleistocene period at least.

859 At Campi Flegrei, explosive activity preceding the Campanian Ignimbrite eruption (39.85 ± 0.14 ka; Giaccio et
860 al., 2017b) has been erased and/or covered by deposits of the most recent activity, and is still poorly
861 documented (e.g., Pappalardo et al., 1999; De Vivo et al., 2001; Rolandi et al., 2003; Di Renzo et al., 2007; Di
862 Vito et al., 2008; Belkin et al., 2016). However, recent investigations of relatively proximal sections in the
863 Campania plain allowed the recognition of a relevant Campi Flegrei explosive activity between ~ 92 ka and

864 ~109 ka (Monaco et al., 2022), also linking it to widespread tephra, as the X-6, X-5 (Keller et al., 1978) and C-
865 22 (Paterne et al., 1986), which act as relevant markers for the Mediterranean MIS 5 successions (e.g., Wulf
866 et al., 2012, 2018; Giaccio et al., 2012a; Regattieri et al., 2015; Leicher et al., 2016; Petrosino et al., 2016). At
867 Fucino, two or three Campi Flegrei-like tephra, i.e., TF-21a, TF-26 and, possibly, TF-35, represent activity at
868 this volcano at ~189, ~199 ka and ~230 ka (Table 5; Fig. 11). TF-21a in particular is chronologically consistent
869 with the Moschiano Ignimbrite, dated at 188.0 ± 7.4 ka and attributed to the so-called Campanian Volcanic
870 Zone (CVZ; Rolandi et al., 2003). Although individual correlations currently are either hampered by the lack of
871 geochemical data or not supported by geochronological-geochemical evidence, a chronologically and
872 geochemically similar activity is documented in the Tyrrhenian Sea, at San Gregorio Magno and Lake Ohrid
873 (Table 5; Fig. 11). Noteworthy, the comparison of the Taurano Ignimbrite distal equivalents (Fig. 10c-d) with
874 TF-21a/TF-26, and similar tephra in Tyrrhenian Sea, San Gregorio Magno and Lake Ohrid, shows good
875 geochemical similarities, highlighting a significant late Middle Pleistocene explosive activity at Campi Flegrei,
876 which calls for further detailed investigations in both proximal and distal settings.

877 Finally, in the time interval here considered, only one potential tephra layer is documented with an uncertain
878 Roccamonfina signature (TF-35), possibly linked with the Upper White Trachytic Tuff eruptive cycle (e.g.,
879 Giannetti and De Casa, 2000). However, as discussed above, although we cannot exclude Roccamonfina, an
880 attribution of TF-35 to the Campi Flegrei tephra from San Gregorio Magno and Ohrid (S2/OH-DP-1006) seems
881 more likely.

882 In conclusion, the tephra succession from the Fucino Basin here presented hosts deposits of explosive activity
883 currently undocumented (or yet not correlated) at Vulsini (TF-22), Vico (TF-24, TF-25), Sabatini (TF-28, TF-
884 30), and Ischia (TF-21, TF-23) volcanoes, confirming previous evidence of a conspicuous Middle Pleistocene
885 activity at NVA as well (TF-21a, TF-26, TF-35). Our record also provides precise chronological constraints for
886 many of the undated or poorly dated eruptions of the Middle Pleistocene peri-Tyrrhenian volcanoes identified
887 in the Fucino record.

888

889 **Table 5.** Summary of the proposed correlations of the F1-F3 (Giaccio et al., 2017a) and F4-F5 Fucino tephra with tephra layers from other
890 repositories across central-southern Italy and the Mediterranean.

Fucino tephra				Source		Distal archives			
Label	Age (ka \pm 2 σ)			Volcano	Unit	PRAD1-2	Ohrid	SGM	DED-87-08
	Direct	Correlated	Modelled						
TF-17	158.8 \pm 3.0 ¹	160.2 \pm 2.0 ²	159.6 \pm 2.4	CF/NVA*	Taurano Ignimbrite	PRAD-3225	OH-DP-0624		C-41/ C-42?
TF-17a			171.1 \pm 7.1	Sabatini	TR.CR-2				
TF-18			182.5 \pm 8.5	Sabatini	TR-CR-1				
TF-19			183.4 \pm 8.4						
TF-21			187.7 \pm 7.7	Ischia	Unknown				C-52/ C-54?
TF-21a		188.0 \pm 7.4 ³	189.5 \pm 7.0	CF/NVA*	Moschiano		OH-DP-0725?	S7	C-53/

TF-22	194.5±2.0 ⁴	194.2±2.8	Vulsini	Ignimbrite?		C-55?
TF-23		194.9±2.9	Ischia	Unknown	PRAD-3586	C-56?
TF-24		196.3±3.1	Vico	Unknown		
TF-25		196.6±3.2	Vico	Unknown	PRAD-3666	
TF-26		198.3±3.4	CF/CVZ*	Pre-Taurano Ignimbrite?		C-53/ C-55?
TF-27	205.1±1.4 ⁴	205.9±5.0 ⁵	Sabatini	Vigna di Valle		
TF-28		210.0±4.1	Sabatini	Unknown		
TF-29		212.2±5.2	Latium	Unknown		
TF-30		213.0±5.8	Sabatini	Unknown		
TF-31		224.7±2.6 ⁴	Vulsini	Onano		
TF-32	224.9±1.0 ⁴	225.3±1.2 ⁴	Vulsini	Grotte di Castro		
TF-33		226.4±0.7 ⁴	Vulsini	Sovana		
TF-35		229.0±2.2	CF/Roccamon?	Unknown/UWTT?	OH-DP-1006?	S2?
TF-35b		235.6±0.6 ⁴	Vulsini	Farnese		
TF-37		240.0±3.4	Latium	Unknown		
TF-43		253.4±0.8 ⁴	Vulsini	Canino		

*CF/NVA = Campi Flegrei/Neapolitan Volcanic Area. ⁴⁰Ar/³⁹Ar age data source: ¹: [Giaccio et al. \(2017a\)](#); ²: [De Vivo et al. \(2001\)](#); ³: [Rolandi et al. \(2003\)](#); ⁴: this study; ⁵: recalculated from [Sottili et al. \(2010\)](#). All ⁴⁰Ar/³⁹Ar are reported using the age for Alder Creek sanidine standard (ACs-2) at 1.1891 Ma ([Niespolo et al., 2017](#)).

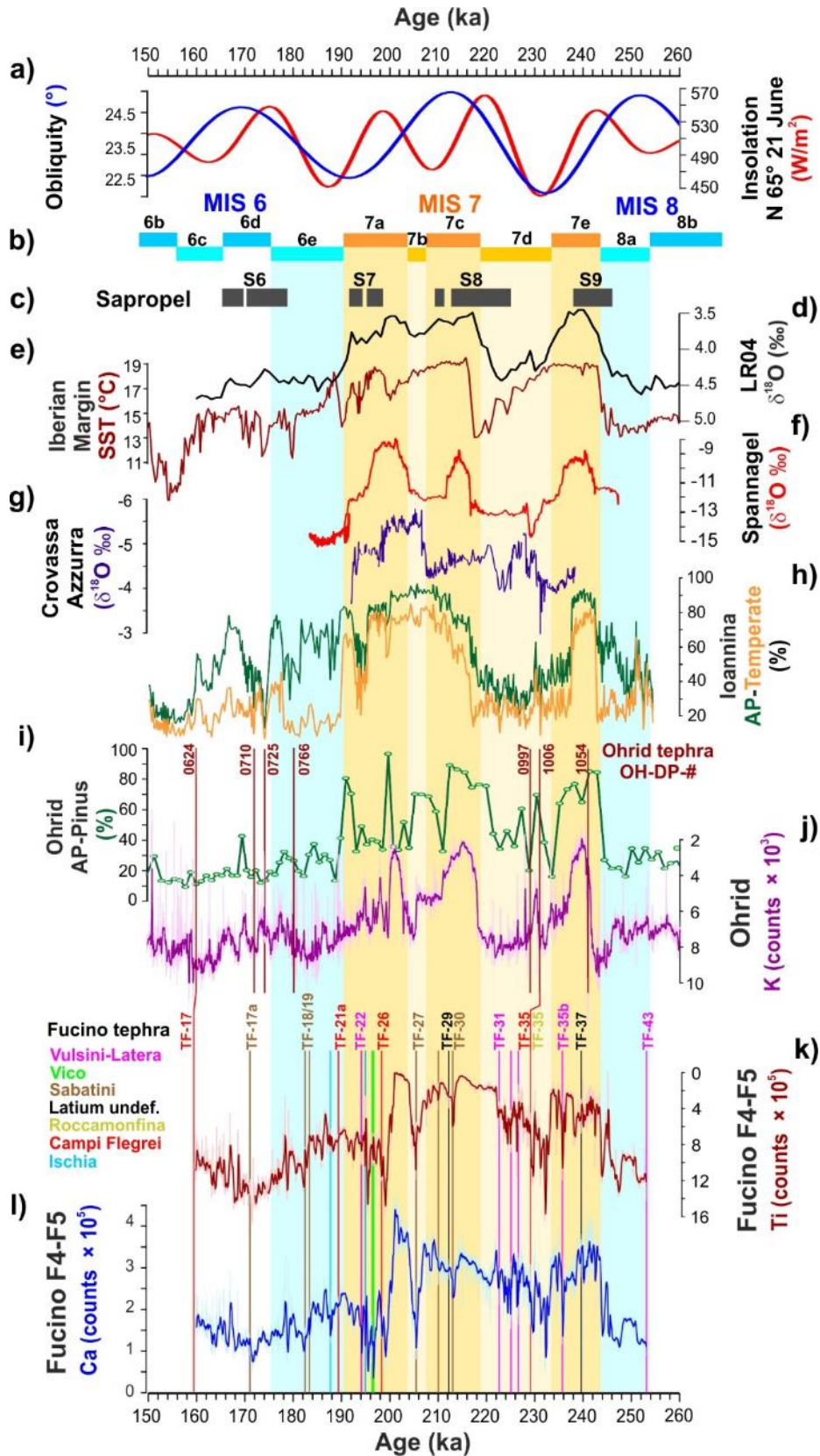
891
892
893
894

895 5.5.2. Tephra climatostratigraphy and MIS 7 paleoclimatic proxy record chronology

896 Overall, the resulting Fucino Ca and Ti time series (depth series from [Giaccio et al., 2019](#)), which are
897 proxies of the lake primary productivity and of the catchment erosion, respectively, and by extension of
898 temperature and precipitation (e.g., [Mannella et al., 2019](#)), reflect the climate variability of the late MIS 8-early
899 MIS 7 glacial-interglacial at both glacial-interglacial and millennial timescales ([Fig. 12](#)). The MIS 7 period
900 includes three warm substages, MIS 7e, 7c and 7a. The first two have been assigned interglacial status, while
901 the third is considered a ‘continued interglacial’ as it was not preceded by any substantial ice-sheet expansion
902 during MIS 7b ([Tzedakis et al., 2017](#)). In terms of interglacial intensity, sea level and global surface temperature
903 reconstructions suggest that MIS 7e, 7c and 7a were weaker compared to the MIS 5e, 9e, 11c and 1
904 interglacials (e.g., [Past Interglacials Working Group, 2016](#); [Snyder, 2016](#)). The independent ⁴⁰Ar/³⁹Ar
905 chronology of Fucino record places the beginning of MIS 7e at 243.6 ± 4.7 ka, i.e., very close to the maximum
906 insolation at 243.5 ka, in line with the canonical view of Milankovitch forcing pacing the timing of interglacials
907 ([Hays et al., 1976](#); [Tzedakis et al., 2012](#)) ([Fig. 12](#)). The MIS 8-MIS 7e transition is marked by an abrupt
908 decrease (increase) of the Ti (Ca) and is preceded by a late MIS 8 interstadial oscillation centered at ~245
909 ka ([Fig. 12](#)). Although the timing of the deglacial transition is bracketed by two high-precision ⁴⁰Ar/³⁹Ar ages of
910 TF-43 (Canino, 253.4 ± 0.8 ka) and TF-35b (Farnese, 235.6 ± 0.6 ka) that are 18 kyr apart, the emerging
911 chronology is in good agreement with astrochronologically-calibrated Mediterranean records (e.g., Lake Ohrid
912 pollen: [Sadori et al., 2016, 2018](#); [Donders et al., 2021](#); Ioannina I-284 pollen: [Roucoux et al., 2007](#)) and the
913 U/Th-dated stalagmites from continental Europe ([Wendt et al., 2021](#)).

914 According to the Ti and Ca data, the MIS 7e interglacial shows evidence of climate instability, which may have
915 correlatives in other Mediterranean records ([Fig. 12](#)). Compared to the marine sequence, a number of

916 terrestrial records indicate a shorter interglacial duration, ending around 236 ka (e.g., Tzedakis et al., 2004;
 917 Roucoux et al., 2007; Sadori et al., 2016; Wendt et al., 2021), though this is not as clear in the Fucino Ca and
 918 Ti timeseries (Fig. 12).



919

920 **Figure 12.** Comparison between Fucino and regional and extra-regional selected late MIS 8-early MIS 6 paleoclimatic records. **a)-b)**
921 obliquity and 65°N insolation (Berger and Lutre, 1991). **c)** Mediterranean sapropel stratigraphy (Ziegler et al., 2010). **d)** LR04 Benthic
922 Stack (Lisiecki and Raymo, 2005). **e)** Portuguese margin sea surface temperature (SST, Martrat et al., 2007). **f)** Stalagmite $\delta^{18}\text{O}$ record
923 from Spannagel Cave (Austria; Wendt et al., 2021). **g)** Stalagmite $\delta^{18}\text{O}$ record from Crovassa Azzurra Cave (Sardina; Columbu et al.,
924 2019). **h)** Total arboreal pollen (AP) and Temperate tree pollen (Eurosiberian and Mediterranean taxa) percentages from Ioannina I-284
925 lacustrine succession (Greece, Roucoux et al., 2007). **i-j)** Arboreal Pollen (-Pinus) percentages (Sadori et al., 2016; Donders et al., 2021)
926 and K XRF scanning data (Wagner et al., 2019) from Lake Ohrid (Albania, North Macedonia). **k)-l)** Fucino Ti and Ca XRF scanning data
927 (Giaccio et al., 2019).
928

929 The following MIS 7d sub-stage, containing a deep boreal summer insolation minimum, arising from the
930 confluence of an obliquity minimum and a precession maximum, and associated with a rapid pulse of ice-sheet
931 expansion (Ruddiman & McIntyre, 1982), is well-expressed by an abrupt increase in Ti at ~234 ka in Fucino.
932 This interval is characterised by the occurrence of four tephras, including TF-35, likely sourced in Campi
933 Flegrei, and the Latera series of Sovana-Grotte di Castro-Onano (TF-33, TF-32, and TF-31), from Vulcini (Fig.
934 12). Of note, the likely equivalent TF-35 (229.0 ± 2.2 ka) and OH-DP-1006 tephra, in Fucino and Ohrid
935 successions, share a similar climatostratigraphic position, at the very onset of an interstadial oscillation within
936 the MIS 7d glacial sub-stage, thus supporting the tentative correlation (Fig. 12). A similar pronounced
937 interstadial oscillation centred at ~230 ka is also evident in the high-resolution Ioannina pollen record (Fig. 12).
938 Among the Latera tephras, Onano (TF-31), here dated at 224.7 ± 2.6 ka ($^{40}\text{Ar}/^{39}\text{Ar}$ age) or 222.5 ± 2.8 ka
939 (modelled age; Table 5), immediately precedes an abrupt decrease in Ti at ~222.0 ka, which could correspond
940 to the wide increase in Lake Ohrid AP at ~221 ka and that, in turn, could represent the regional expression of
941 the MIS 7d-MIS 7c, glacial-interglacial transition (Fig. 12). However, in agreement with other records, the
942 Fucino Ca profile suggests a later onset of the MIS 7c (~218 ka; Fig. 12), leaving open the definition/chronology
943 of this major climatic transition in Fucino record until more, multiproxy evidence (e.g., pollen analyses) is
944 available.
945 The MIS 7c interglacial appears as a more stable period, according to the Ti record of Fucino, with the notable
946 exception of a stadial oscillation at ~214-212 ka, which may be correlative with a drop of the Lake Ohrid AP at
947 212-210 ka (Fig. 12). This oscillation is marked by the occurrence of tephras TF-29 and TF-30, of unknown
948 Latium and Sabatini origin, respectively, which can be thus considered as good potential markers for this event
949 (Fig. 12). Starting from 210 ka, the Ti becomes less stable and shows a general increasing trend that
950 culminates in an abrupt increase at ~207 ka, likely corresponding to the beginning of MIS 7b (Fig. 12). This
951 short stadial is marked by the occurrence of the Sabatini tephra TF-27/Vigna di Valle, here precisely dated to
952 205.1 ± 1.4 ka (Table 5).

953 At ~204 ka, Ti and Ca are characterised by a rapid decrease and increase, respectively, that may represent
954 the onset of the MIS 7a sub-stage (Fig. 12). This interpretation is in good chronological agreement with
955 speleothem records from Austria (Wendt et al., 2021) and Sardinia (Columbu et al., 2019), which show an
956 abrupt increase in temperature, in central Europe, and precipitation, in the Mediterranean, at ~204 ka and 206
957 ka, respectively (Fig. 12). Ti remains very low only up to ~200 ka, while it abruptly increases and remains
958 generally higher and unstable between 200 ka and 190 ka, suggesting a short duration of the stable MIS 7a
959 conditions, as previously observed in marine and terrestrial records from the Portuguese Margin and southern
960 Europe (Tzedakis et al., 2004; Martrat et al., 2007; Roucoux et al., 2008) (Fig. 12). This is also in agreement
961 with Austrian and Sardinian speleothem evidence, indicating a significant climatic worsening at ~197 ka and
962 199 ka, respectively (Fig. 12). Lake Ohrid AP and XRF record also indicates unstable conditions during the
963 MIS 7a, with only two isolated peaks of high AP concentration, at ~192 ka and ~200 ka, the earliest one likely
964 correlated with Fucino low-Ti at 200-204 ka (Fig. 12). The unstable phase of the late MIS 7a is marked by a
965 series of tephra layers, including the Campi Flegrei-like TF-26, the Vico TF-24 and TF-25, the Ischia TF-23,
966 and the Vulsini TF-22, here $^{40}\text{Ar}/^{39}\text{Ar}$ dated to 194.5 ± 2.0 ka (Fig. 7; Table 5).
967 As far as the MIS 7/MIS 6 transition is concerned, either Ti or Ca profiles show no clear expression of this
968 boundary in the Fucino record, which could be placed at ~190 ka, close the CF-like tephra TF-21a, possibly
969 correlated to the Moschiano Ignimbrite (Fig. 12). However, this must be considered only as a preliminary and
970 tentative remark as more multiproxy records, especially pollen, are needed to establish the expression and
971 the age of this transition in the Fucino record.

972
973

974 **6. Summary and concluding remarks**

975 In this study, we presented a new tephra record from Fucino Basin, central Italy, spanning the ~250-170
976 ka time interval or the late Marine Isotope Stage (MIS) 8-early MIS 6. Twentyone Fucino tephra layers identified
977 in this time-interval, along with one tephra from Lake Ohrid succession, thirteen pyroclastic units from near
978 vent sections of Latera Volcanic Complex (LVC, Vulsini Volcanic District), Vico volcano, and Sabatini Volcanic
979 District (SVD) have been characterised in terms of major, minor (EPMA-WDS) and trace element contents
980 (LA-ICP-MS), Sr-Nd isotopic composition (TIMS), and $^{40}\text{Ar}/^{39}\text{Ar}$ dating.

981 The results provide new data to refine the history of explosive volcanism in the peri-Tyrrhenian magmatic
982 systems during the 250-170 ka interval and enrich the MIS 8-6 Mediterranean tephrostratigraphy. The

983 combination of the new $^{40}\text{Ar}/^{39}\text{Ar}$ ages for Latera units (Onano, Grotte di Castro, Sovana, Farnese and Canino),
984 which have been identified in the Fucino record, with $^{40}\text{Ar}/^{39}\text{Ar}$ ages of the Fucino tephras, allowed us to
985 develop a robust Bayesian age-depth model that provides statistically reliable modelled ages for the
986 investigated tephra succession. In turn, this not only yields new ages for the previously undated tephras, but
987 also allowed us to better estimate the ages of the closely spaced Onano, Grotte di Castro and Sovana major
988 eruptions, chronologically poorly distinguishable using $^{40}\text{Ar}/^{39}\text{Ar}$ dating of the proximal units alone. This
989 highlights the great potential of the approach of integrating proximal and distal data for a better assessment of
990 the dynamics and tempo of the explosive volcanism also in the perspective of hazard evaluation.

991 The Fucino tephrochronological record also provides the first ages for the previously undated Trevignano
992 Romano eruptions TR-CR-1 and TR-CR-2 of the Sabatini Volcanic District, and possibly (i.e., if the correlation
993 was confirmed) an improved age for the Upper White Trachytic Tuff of the Roccamonfina volcano. Finally, the
994 Fucino record evidenced currently undocumented or poorly known explosive activity at Vico, Sabatini, Ischia
995 and Campi Flegrei volcanoes, providing new fundamental insights into the eruptive history at these volcanic
996 systems. Notably, we identified three NVA-like tephras at ~ 190 ka, ~ 198 ka and ~ 230 ka, i.e., preceding the
997 already known Taurano Ignimbrite (158.8 ± 3.0 ka), which, together with other distal tephra evidence (e.g.,
998 Tyrrhenian Sea, Lake Ohrid), suggest a significant activity in the Campi Flegrei volcanic area between 160
999 and 250 ka. However, more investigations are needed in both proximal and distal setting to better define the
1000 volcanological features and history of this late Middle Pleistocene explosive activity.

1001 Regarding the development of the Mediterranean tephrochronology, we noticed a significant paucity of records
1002 spanning the MIS 8-6 interval. Some potential correlative layers have been found only in the Adriatic Sea core
1003 PRAD 1-2, the San Gregorio Magno Basin, southern Italy, and Lake Ohrid, Albania-North Macedonia. In this
1004 regard, the rich and detailed Fucino record can provide a reference dataset for future tephra studies in the
1005 Mediterranean region of this poorly investigated period.

1006 Finally, the preliminary analysis of the Fucino paleoclimatic proxy records (Ti and Ca XRF data), anchored to
1007 a robust radioisotopic-based chronology, indicated a coherent pattern of the late MIS 8-early MIS 6 climatic
1008 variability with respect to other regional and extraregional reference records. This sets the basis for the
1009 assemblage of high-resolution paleoenvironmental and paleoclimatic multiproxy records, which will allow
1010 exploring the timing and dynamics of the climatic change independently of any assumption of the orbital tuning.

1011 What emerges is the importance of the Fucino Basin as a key sedimentary archive for reconstructing the
1012 history of the Quaternary peri-Tyrrhenian explosive volcanism, the development of the Central Mediterranean

013 tephrochronology and for consolidating an independent, $^{40}\text{Ar}/^{39}\text{Ar}$ -based chronology of Quaternary climate
014 variability.

015

016 Acknowledgments

017 R. Jedlička is thanked for providing valuable technical assistance during EPMA analysis at Prague University.
018 This article is a contribution to project “FUCINO Tephrochronology Unites Quaternary Records (FUTURE)”,
019 financed by the Italian Research Ministry (MUR, PRIN 2017, grant 20177TKBXZ_003, project “FUTURE”, G.
020 Zanchetta, coordinator), issued to B.G., D.P., M.D., and G.Z. The Fucino project is co-funded by DFG (German
021 Research Foundation) grant WA 2109/16. $^{40}\text{Ar}/^{39}\text{Ar}$ dating also received complementary contribution from the
022 CNRS INSU-LEFE 2018-2020 action to S.N. The INGV-OV laboratories have been also financially supported
023 by the EPOS Research Infrastructure through the contribution of the Italian Ministry of University and Research
024 (MUR). P.C.T. acknowledges funding from NERC research grant NE/V001620/1.

025

026

027 References

- 028 Albert, P.G., Giaccio, B., Isaia, R., Costa, A., Niespolo, E.M., Nomade, S., Pereira, A., Renne, P.R., Hinchliffe, A., Mark, D.F., Brown,
029 R.J., Smith, V.C., 2019. Evidence for a large-magnitude eruption from Campi Flegrei Caldera (Italy) at 29 ka. *Geology*. **47** (7), 595-
030 599. <https://doi.org/10.1130/G45805.1>.
- 031 Albert, P.G., Smith, V.C., Suzuki, T., Tomlinson, E.L., Nakagawa, T., McLean, D., Yamada, M., Staff, R.A., Scholaut, G., Takemura, T.,
032 Nagahashi, Y., Kimura, J., Suigetsu 2006 Project Members, 2018. Constraints on the frequency and dispersal of explosive eruptions
033 at Sambe and Daisen volcanoes (South-West Japan Arc) from the distal Lake Suigetsu record (SG06 core). *Earth Sci. Rev.* **185**,
034 1004-1028. <https://doi.org/10.1016/j.earscirev.2018.07.003>.
- 035 Amato, V., Aucelli, P.P.C., Cesarano, M., Filocamo, F., Leone, N., Petrosino, P., Roskopf, C.M., Valente, E., Casciello, E., Giral, S.,
036 Jicha, B.R., 2018. Geomorphic response to late Quaternary tectonics in the axial portion of the Southern Apennines (Italy): A case
037 study from the Calore River valley. *Earth Surf. Process. Landf.* **43** 2463-2480. <https://doi.org/10.1002/esp.4390>.
- 038 Amato, V., Aucelli, P.P.C., Cesarano, M., Jicha, B.R., Lebreton, V., Orain, R., Pappone, G., Petrosino, P., Russo Ermolli, E., 2014.
039 Quaternary evolution of the largest intermontane basin of the Molise Apennine (Central Southern Italy). *Rend. Fis. Acc. Lincei* **25**,
040 197-216. <https://doi.org/10.1007/s12210-014-0324-y>.
- 041 Appleton, J.D., 1972. Petrogenesis of Potassium-rich Lavas from the Roccamonfina Volcano, Roman Region, Italy. *J. Petrol.* **13** (3), 425-
042 456. <https://doi.org/10.1093/petrology/13.3.425>.
- 043 Arienzo, I., Civetta, L., Heumann, A., Wörner, G., Orsi, G., 2009. Isotopic evidence for open system processes within the Campanian
044 Ignimbrite (Campi Flegrei-Italy) magma chamber. *Bull. Volcanol.* **71**, 285-300. <https://doi.org/10.1007/s00445-008-0223-0>.
- 045 Arienzo, I., D'Antonio, M., Di Renzo, V., Tonarini, S., Minolfi, G., Orsi, G., Carandente, A., Belviso, P., Civetta, L., 2015. Isotopic
046 microanalysis sheds light on the magmatic endmembers feeding volcanic eruptions: The Astroni 6 case study (Campi Flegrei, Italy).
047 *J. Volcanol. Geotherm. Res.* **304**, 24–37. <https://doi.org/10.1016/j.jvolgeores.2015.08.003>.
- 048 Arienzo, I., Mazzeo, F.C., Moretti, R., Cavallo, A., D'Antonio, M., 2016. Open-system magma evolution and fluid transfer at Campi Flegrei
049 caldera (Southern Italy) during the past 5 ka as revealed by geochemical and isotopic data: the archetype of Nisida eruption. *Chem.*
050 *Geol.* **427**, 109-124. <https://doi.org/10.1016/j.chemgeo.2016.02.007>.
- 051 Arienzo, I., Moretti, R., Civetta, L., Orsi, G., Papale, P., 2010. The feeding system of the Agnano-Monte Spina eruption Campi Flegrei,
052 Italy): dragging the past into present activity and future scenarios. *Chem. Geol.* **270** (1-4), 135-147.
053 <https://doi.org/10.1016/j.chemgeo.2009.11.012>.
- 054 Ascione, A., Mazzoli, S., Petrosino, P., Valente, E., 2013. A decoupled kinematic model for active normal faults: Insights from the 1980,
055 Ms = 6.9 Irpinia earthquake, southern Italy. *Geol. Soc. Amer. Bull.* **125** (7-8), 1239-1259. <https://doi.org/10.1130/B30814.1>.
- 056 Balbas, A., Koppers, A.A.P., Kent, D.V., Konrad, K., Clark, P.U., 2016. Identification of the short-lived Santa Rosa geomagnetic excursion
057 in lavas on Floreana Island (Galapagos) by $^{40}\text{Ar}/^{39}\text{Ar}$ geochronology. *Geology* **44** (5), 359-362 (2016).
058 <https://doi.org/10.1130/G37569.1>.
- 059 Bear, A.N., Cas, R.A.F., Giordano, G., 2009. The implications of spatter, pumice and lithic clast rich proximal co-ignimbrite lag breccias
060 on the dynamics of caldera forming eruptions: The 151 ka Sutri eruption, Vico Volcano, Central Italy. *J. Volcanol. Geotherm. Res.* **181**
061 (1-2), 1-24. <https://doi.org/10.1016/j.jvolgeores.2008.11.032>.

- 062 Belkin, H.E., Rolandi, G., Jackson, J.C., Cannatelli, C., Doherty, A.L., Petrosino, P., De Vivo, B., 2016. Mineralogy and geochemistry of
063 the older (>40 ka) ignimbrites in the Campanian Plain, southern Italy. *J. Volcanol. Geotherm. Res.* **323**, 1-18.
064 <https://doi.org/10.1016/j.jvolgeores.2016.05.002>.
- 065 Berger, A. & Lautre, M.F., 1991. Insolation values for the climate of the last 10 million years. *Quat. Sci. Rev.* **10**, 297-317.
066 [https://doi.org/10.1016/0277-3791\(91\)90033-Q](https://doi.org/10.1016/0277-3791(91)90033-Q).
- 067 Bertagnini, A. & Sbrana, A., 1986. Il vulcano di Vico: stratigrafia del complesso vulcanico e sequenze eruttive delle formazioni piroclastiche
068 (in Italian). *Mem. Soc. Geol. It.* **35**, 699-713.
- 069 Bini M., Zanchetta G., Drysdale R.N., Giaccio B., Stocchi P., Vacchi M., Hellstrom J.C., Couchoud I., Monaco L., Ratti A., Martini, F., Sarti
070 L., 2020. An end to the Last Interglacial highstand before 120 ka: Relative sea-level evidence from Infreschi Cave (Southern Italy).
071 *Quat. Sci. Rev.* **250**, 106658. <https://doi.org/10.1016/j.quascirev.2020.106658>.
- 072 Blaauw, M., Christen, J.A., 2011. Flexible palaeoclimate age-depth models using an autoregressive gamma process. *Bayesian analysis*
073 **6** (3), 457-474. <https://doi.org/10.1214/11-BA618>.
- 074 Blockley, S.P.E., Bourne, A.J., Brauer, A., Davies, S.M., Hardiman, M., Harding, P.R., Lane, C.S., MacLeod, A., Matthews, I.P., Pyne-
075 O'Donnel, S.D.F., Rasmussen, S.O., Wulf, S., Zanchetta, G., 2014. Tephrochronology and the extended intimate (integration of ice-
076 core, marine and terrestrial records) event stratigraphy 8-128 ka 2bk. *Quat. Sci. Rev.* **106**, 88-100.
077 <https://doi.org/10.1016/j.quascirev.2014.11.002>.
- 078 Boncio, P., Lavecchia, G., Pace, B., 2004. Defining a model of 3D seismogenic sources for seismic hazard assessment applications: The
079 case of central Apennines (Italy). *J. Seismol.* **8** (3), 407-425. <https://doi.org/10.1023/B:JOSE.0000038449.78801.05>.
- 080 Bourne, A.J., Albert, P.G., Matthews, I.P., Trincardi, F., Wulf, S., Asioli, A., Blockley, S.P.E., Keller, J., Lowe, J.J., 2015. Tephrochronology
081 of core PRAD 1-2 from the Adriatic Sea: insights into Italian explosive volcanism for the period 200-80 ka. *Quat. Sci. Rev.* **116**, 28-
082 43. <https://doi.org/10.1016/j.quascirev.2015.03.006>.
- 083 Bourne, A.J., Lowe, J.J., Trincardi, F., Asioli, A., Blockley, S.P.E., Wulf, S., Matthews, I.P., Piva, A., Vigliotti, L., 2010. Distal tephra record
084 for the last ca 105,000 years from core PRAD 1-2 in the central Adriatic Sea: implications for the marine tephrostratigraphy. *Quat. Sci.*
085 *Rev.* **29**, 3079-3094. <https://doi.org/10.1016/j.quascirev.2010.07.021>.
- 086 Brown, R.J., Civetta, L., Arienzo, I., D'Antonio, M., Moretti, R., Orsi, G., Tomlinson, E.L., Albert, P.G., Menzies, M.A., 2014. Geochemical
087 and isotopic insights into the assembly, evolution and disruption of a magmatic plumbing system before and after cataclysmic caldera-
088 collapse eruption at Ischia volcano (Italy). *Contrib. Mineral. Petrol.* **168**: 1035. <https://doi.org/10.1007/s00410-014-1035-1>.
- 089 Brown, R.J., Orsi, G., de Vita, S., 2008. New insights into Late Pleistocene explosive volcanic activity and caldera formation on Ischia.
090 *Bull. Volcanol.* **70**, 583-603. <https://doi.org/10.1007/s00445-007-0155-0>.
- 091 Casalini, M., Heumann, A., Marchionni, S., Conticelli, S., Avanzinelli, R., Tommasini, S., 2018. Inverse modelling to unravel the radiogenic
092 isotope signature of mantle sources from evolved magmas: the case-study of Ischia volcano. *Ital. J. Geosci.* **137**, pp. 00.
093 <https://doi.org/10.33011/IJG.2018.05>.
- 094 Cavinato, G.P., Carusi, C., Dell'Asta, M., Miccadei, E., Piacentini T., 2002. Sedimentary and tectonic evolution of Plio-Pleistocene alluvial
095 and lacustrine deposits of Fucino Basin (central Italy). *Sediment. Geol.* **148**, 29-59. [https://doi.org/10.1016/S0037-0738\(01\)00209-3](https://doi.org/10.1016/S0037-0738(01)00209-3).
- 096 Chen, X.-Y., Blockley, S.P.E., Fletcher, R., Zhang, S., Kim, J.-H., Park, M.-O., Chen, C., Yin, J., Xu, Y.-G., 2022. Holocene
097 tephrostratigraphy in the East-Sea/Japan Sea: Implications for eruptive history of Ulleungdo volcano and potential for hemispheric
098 synchronization of sedimentary archives. *J. Geophys. Res. Solid Earth* **127**, e2021JB023243. <https://doi.org/10.1029/2021JB023243>.
- 099 Cox, S.E., Hemming, S.R., Tootell, D., 2020 The Isotopx NGX and ATONA Faraday amplifiers. *Geochronology* **2**, 231-243.
100 <https://doi.org/10.5194/gchron-2-231-2020>.
- 101 Colucci, S., Palladino, D.M., Mulukutla, G.K., Proussevitch, A.A., 2013. 3-D Reconstruction of ash vesicularity: insights into the origin of
102 ash-rich explosive eruptions. *J. Volcanol. Geotherm. Res.* **255**, 98-107. <https://doi.org/10.1016/j.jvolgeores.2013.02.002>.
- 103 Columbu, A., Spötl, C., De Waele, J., Yu, T.-L., Shen, C.-C., Gázquez, F., 2019. A long record of MIS 7 and MIS 5 climate and environment
104 from a western Mediterranean speleothem (SW Sardinia, Italy). *Quat. Sci. Rev.* **220**, 230-243.
105 <https://doi.org/10.1016/j.quascirev.2019.07.023>.
- 106 D'Agostino, N., Jackson, J. A., Dramis, F., Funicello, R., 2001. Interactions between mantle upwelling, drainage evolution and active
107 normal faulting: an example from the central Apennines (Italy). *Geophys. J. Inter.* **147** (2), 475-497. <https://doi.org/10.1046/j.1365-246X.2001.00539.x>.
- 108 D'Antonio, M., Tonarini, S., Arienzo, I., Civetta, L., Dallai, L., Moretti, R., Orsi, G., Andria, M., Trecalli, A., 2013. Mantle and crustal
109 processes in the magmatism of the Campania region: inferences from mineralogy, geochemistry, and Sr-Nd-O isotopes of young
110 hybrid volcanics of the Ischia island (South Italy). *Contrib. Mineral. Petrol.* **165**, 1173-1194. <https://doi.org/10.1007/s00410-013-0853-x>.
- 111 D'Antonio, M., Tonarini, S., Arienzo, I., Civetta, L., Di Renzo, V., 2007. Components and processes in the magma genesis of the Phlegrean
112 Volcanic District, southern Italy. In: Beccaluva, L., Bianchini, G., Wilson, M. (eds.) Cenozoic Volcanism in the Mediterranean Area.
113 *Geol. Soc. Am. Special Paper* **418**, 203-220.
- 114 Davies, S.M., Wastegård, S., Abbott, P.M., Barbante, C., Bigler, M., Johnsen, S.J., Rasmussen, T.L., Steffensen, J.P., Svensson, A.,
115 2010. Tracing volcanic events in the NGRIP ice-core and synchronising North Atlantic marine records during the last glacial period.
116 *Earth Planet. Sci. Lett.* **294** (1-2), 69-79. <https://doi.org/10.1016/j.epsl.2010.03.004>.
- 117 de Fontaine, C.S., Kaufman, D.S., Anderson, R.S., Werner, A., Waythomass, C.F., Brown, T.A., 2007. Late Quaternary distal-fall deposits
118 in lacustrine sediments, Kenai Peninsula, Alaska. *Quaternary Research*, **68**, 1, 64-78. <https://doi.org/10.1016/j.yqres.2007.03.006>.
- 119 De Maisonville, C.B. & Bergal-Kuvikas, O., 2020. Timing, magnitude and geochemistry of major Southeast Asian volcanic eruptions:
120 identifying tephrochronologic markers. *Journal of Quaternary Science*, **35**, 1-2, 272-287. <https://doi.org/10.1002/jqs.3181>.
- 121 de Rita, D., Funicello, R., Parotto, M., 1988. Carta geologica del complesso vulcanico dei Colli Albani (Vulcano Laziale) (in Italian). C.N.R.-
122 Gruppo Nazionale Vulcanologia.
- 123 De Vivo, B., Rolandi, G., Gans, P.B., Calvert, A., Bohrson, W.A., Spera, F.J., Belkin, H.E., 2001. New constraints on the pyroclastic
124 eruptive history of Campanian volcanic Plain (Italy). *Mineral. Petrol.* **73**, 47-65. <https://doi.org/10.1007/s007100170010>.
- 125 Del Carlo, P., Smedile, A., Petrelli, M., Di Roberto, A., 2020. Evidence of an unknown explosive eruption of Mt. Etna volcano (Italy) during
126 the Late Glacial. *J. Volcanol. Geotherm. Res.* **402**, 106992. <https://doi.org/10.1016/j.jvolgeores.2020.106992>.

- 129 Deino, A.L., Orsi, G., de Vita, S., Piochi, M., 2004. The age of the Neapolitan Yellow Tuff-caldera forming eruption (Campi Flegrei caldera
130 - Italy) assessed by $^{40}\text{Ar}/^{39}\text{Ar}$ dating method. *J. Volcanol. Geotherm. Res.* **133** (1-4), 157-170. [https://doi.org/10.1016/S0377-0273\(03\)00396-2](https://doi.org/10.1016/S0377-0273(03)00396-2).
- 132 Di Battistini, G., Montanini, A., Vernia, L., Bargossi, G.M., Castorina, F., 1998. Petrology and geochemistry of ultrapotassic rocks from the
133 Montefiascone Volcanic Complex (Central Italy): magmatic evolution and petrogenesis. *Lithos* **43** (3), 169-195.
134 [https://doi.org/10.1016/S0024-4937\(98\)00013-9](https://doi.org/10.1016/S0024-4937(98)00013-9).
- 135 Di Renzo, V., Arienzo, I., Civetta, L., D'Antonio, M., Tonarini, S., Di Vito, M.A., Orsi, G., 2011. The magmatic feeding system of the Campi
136 Flegrei caldera: Architecture and temporal evolution. *Chem. Geol.* **281** (3-4), 227-241. <https://doi.org/10.1016/j.chemgeo.2010.12.010>.
- 137 Di Renzo, V., Di Vito, M.A., Arienzo, I., Carandente, A., Civetta, L., D'Antonio, M., Tonarini, S., 2007. Magmatic history of Somma-Vesuvius
138 on the basis of new geochemical and isotopic data from a deep borehole (Camaldoli della Torre). *J. Petrol.* **48**, 753-784.
139 <https://doi.org/10.1093/petrology/egl081>.
- 140 Di Roberto, A., Smedile, A., Del Carlo, P., De Martini, P.M., Iorio, M., Petrelli, M., Pantosti, P., Pinzi, S., Todrani, A., 2018. Tephra and
141 cryptotephra in a ~60,000-year old lacustrine sequence from the Fucino Basin: new insights into the major explosive events in Italy.
142 *Bull. Volcanol.* **80**:20. <https://doi.org/10.1007/s00445-018-1200-x>.
- 143 Di Vito, M.A., Sulpizio, R., Zanchetta, G., D'Orazio M., 2008 The late Pleistocene pyroclastic deposits of the Campanian Plain: New
144 insights into the explosive activity of the Neapolitan volcanoes. *J. Volcanol. Geotherm. Res.* **177**, 19-48.
145 <https://doi.org/10.1016/j.jvolgeores.2007.11.019>.
- 146 Doglioni, C., Harabaglia, P., Martinelli, G., Mongelli, F., Zito, G., 1996. A geodynamic model of the Southern Apennines accretionary
147 prism. *Terra Nova* **8** (6), 540-547. <https://doi.org/10.1111/j.1365-3121.1996.tb00783.x>.
- 148 Donders, T., Panagiotopoulos, K., Koutsodendris, A., Bertini, A., Mercuri, A.M., Masi, A., Combourieu-Nebout, N., Joannin, S., Kouli, K.,
149 Kousis, I., Peyron, O., Torri, P., Florenzano, A., Francke, A., Wagner, B., Sadori, L., 2021. 1.36 million years of Mediterranean forest
150 refugium dynamics in response to glacial-interglacial cycle strenght. *PNAS* **118** (34), e2026111118.
151 <https://doi.org/10.1073/pnas.2026111118>.
- 152 Freda, C., Gaeta, M., Karner, D.B., Marra, F., Renne, P.R., Taddeucci, J., Scarlato, P., Christensen, J.N., Dallai, L., 2006. Eruptive history
153 and petrologic evolution of the Albano multiple maar (Alban Hills, Central Italy). *Bull. Volcanol.* **68**, 567-591.
154 <https://doi.org/10.1007/s00445-005-0033-6>.
- 155 Froggat, P.C. & Gosson, G.J., 1982. Techniques for the preparation of tephra samples for mineral and chemical analysis and radiometric
156 dating. *Geology Department, Victoria University of Wellington Publication* 23, 1-12.
- 157 Galadini, F. & Galli, P., 2000. Active tectonics in the Central Apennines (Italy) - Input Data for Seismic Hazard Assessment. *Nat. Haz.* **22**,
158 225-270. <https://doi.org/10.1023/A:1008149531980>.
- 159 Gaeta, M., Freda, C., Marra F., Arienzo, I., Gozzi, F., Jicha, B., Di Rocco, T., 2016. Paleozoic metasomatism at the origin of Mediterranean
160 ultrapotassic magmas: Constraints from time-dependent geochemistry of Colli Albani volcanic products (Central Italy). *Lithos* **244**,
161 151-164. <https://doi.org/10.1016/j.lithos.2015.11.034>.
- 162 Galli, P., Giaccio, B., Messina, P., Peronace, E., Amato, V., Naso, G., Nomade, S., Pereira, A., Piscitelli, S., Bellanova, J., Billi, A., Blamart,
163 D., Galderisi, A., Giocoli, A., Stabile, T., Thil, F., 2017. Middle to Late Pleistocene activity of the Matese fault system (southern
164 Apennines, Italy). *Tectonophysics* **699**, 61-81. <https://doi.org/10.1016/j.tecto.2017.01.007>.
- 165 Gasperini, D., Bilchert-Toft, J., Bosch, D., Del Moro, A., Macera, P., Albarède, F., 2002. Upwelling of deep mantle material through a plate
166 window: Evidence from the geochemistry of Italian basaltic volcanics. *J. Geophysic. Res.* **107** (B12), 2367.
167 <https://doi.org/10.1029/2001JB000418>.
- 168 Giaccio, B., Galli, P., Messina, P., Peronace, E., Scardia, G., Sottili, G., Sposato, A., Chiarini, E., Jicha, B., Silvestri, S., 2012a. Fault and
169 basin depocentre migration over the last 2Ma in the L'Aquila 2009 earthquake region, central Italian Apennines. *Quat. Sci. Rev.* **56**,
170 69-88. <https://doi.org/10.1016/j.quascirev.2012.08.016>.
- 171 Giaccio, B., Galli, P., Peronace, E., Arienzo I., Nomade, S., Cavinato, G.P., Mancini, M., Messina, P., Sottili, G., 2014. A 560-440 ka
172 tephra record from the Mercure Basin, Southern Italy: volcanological and tephrostratigraphic implications. *J. Quat. Sci.* **29**, 232-248.
173 <https://doi.org/10.1002/jqs.2696>.
- 174 Giaccio, B., Haydas, I., Isaia, R., Deino, A., Nomade, S., 2017b. High-precision ^{14}C and $^{40}\text{Ar}/^{39}\text{Ar}$ dating of Campanian Ignimbrite (Y-5)
175 reconciles the time-scales of climatic cultural processes at 40 ka. *Sci. Rep.* **7**, 45940. <https://doi.org/10.1038/srep45940>.
- 176 Giaccio, B., Leicher, N., Mannella, G., Monaco, L., Regattieri, E., Wagner, B., Zanchetta, G., Gaeta, M., Marra, F., Nomade, S., Palladino,
177 D.M., Pereira, A., Scheidt, S., Sottili, G., Wonik, T., Wulf, S., Zeeden, C., Ariztegui, D., Cavinato, G.P., Dean, R.J., Florindo, F., Leng,
178 M.J., Macri, P., Niespolo, E., Renne, P.R., Rolf, C., Sadori, L., Thomas, C., Tzedakis, P.C., 2019. Extending the tephra and
179 paleoenvironmental record of the Central Mediterranean back to 430 ka: A new core from Fucino Basin, central Italy. *Quat. Sci. Rev.*
180 **225**, 106003. <https://doi.org/10.1016/j.quascirev.2019.106003>.
- 181 Giaccio, B., Marra, F., Hajdas, I., Karner, D.B., Renne, P.R., Sposato, A., 2009. $^{40}\text{Ar}/^{39}\text{Ar}$ and ^{14}C geochronology of the Albano maar
182 deposits: Implications for defining the age and eruptive style of the most recent explosive activity at Colli Albani Volcanic District,
183 Central Italy. *J. Volcanol. Geotherm. Res.* **185**, 203-213. <https://doi.org/10.1016/j.jvolgeores.2009.05.011>.
- 184 Giaccio, B., Niespolo, E.M., Pereira, A., Nomade, S., Renne, P.R., Albert, P.G., Arienzo, I., Regattieri, E., Wagner, B., Zanchetta, G.,
185 Gaeta, M., Galli, P., Mannella, G., Peronace, E., Sottili, G., Florindo, F., Leicher, N., Marra, F., Tomlinson, E.L., 2017a. First integrated
186 tephrochronological record for the last ~190 kyr from the Fucino Quaternary lacustrine succession, central Italy. *Quat. Sci. Rev.* **158**,
187 211-234. <https://doi.org/10.1016/j.quascirev.2017.01.004>.
- 188 Giaccio, B., Nomade, S., Wulf, S., Isaia, R., Sottili, G., Cavuoto, G., Galli, P., Messina, P., Sposato, A., Sulpizio, R., Zanchetta, G., 2012b.
189 The late MIS 5 Mediterranean tephra markers: a reappraisal from peninsular Italy terrestrial records. *Quat. Sci. Rev.* **56**, 31-45.
190 <https://doi.org/10.1016/j.quascirev.2012.09.009>.
- 191 Giaccio, B., Isaia, R., Fedele, F.G., Di Canzio, E., Hoffecker, J., Ronchitelli, A., Sinitsyn, A.A., Anikovich, M., Lisitsyn, S.N., Popov, V.V.,
192 2008. The Campanian Ignimbrite and Codola tephra layers: Two temporal/stratigraphic markers for the Early Upper Palaeolithic in
193 southern Italy and eastern Europe. *J. Volcanol. Geotherm. Res.* **177** (1), 208-226. <https://doi.org/10.1016/j.jvolgeores.2007.10.007>.
- 194 Giannetti, B. & De Casa, G., 2000. Stratigraphy, chronology, and sedimentology of ignimbrites from the white trachytic tuff, Roccamonfina
195 Volcano, Italy. *J. Volcanol. Geotherm. Res.* **96**, 3-4, 243-295. [https://doi.org/10.1016/S0377-0273\(99\)00144-4](https://doi.org/10.1016/S0377-0273(99)00144-4).

- 196 Giannetti, B., 1996. The geology of the Yellow Trachytic Tuff, Roccamonfina Volcano. *J. Volcanol. Geotherm. Res.* **71** (1), 53-72.
 197 [https://doi.org/10.1016/0377-0273\(95\)00030-5](https://doi.org/10.1016/0377-0273(95)00030-5).
- 198 Giordano, G. & the CARG Team, 2010. Stratigraphy, volcano tectonics and evolution of the Colli Albani volcanic field. In: Funicello, R. &
 199 Giordano, G. (Eds.): The Colli Albani volcano. *Spec. Pub. IAVCEI* **3**, 43-97, *Geol. Soc., Lond.* (2010).
- 200 Goldstein, S.L., Denis, P., Oelkers, E.H., Rudnick, R.L., Walter, L.M., 2003. Standards for publication of isotope ratio and chemical data
 201 in chemical geology. *Chem. Geol.* **202**, 1-4. <https://doi.org/10.1016/j.chemgeo.2003.08.003>.
- 202 Hays, J.D., Imbrie, I., Shackleton, N.J., 1976. Variations in the Earth's orbit: pacemaker of the ice ages. *Science* **194**, 1121-1131.
 203 <https://doi.org/10.1126/science.194.4270.1121>.
- 204 Hayward, C., 2011. High spatial resolution electron probe microanalysis of tephra and melt inclusion without beam-induced chemical
 205 modification. *The Holocene* **22** (1), 119-125. <https://doi.org/10.1177%2F0959683611409777>.
- 206 Jicha, B.R., Singer, B.S., Sobol, P., 2016. Re-evaluation of the ages of $^{40}\text{Ar}/^{39}\text{Ar}$ sanidine standards and supereruptions in the western
 207 U.S. using a Noblesse multi-collector mass spectrometer. *Chem. Geol.* **431**, 54-66. <https://doi.org/10.1016/j.chemgeo.2016.03.024>.
- 208 Jochum, K.P., Stoll, B., Herwig, K., Willbold, M., Hofmann, A.W., Amini, M., Aarbug, S., Abouchami, W., Hellebrand, E., Mocek, B.,
 209 Raczek, I., Stracke, A., Alard, O., Bouman, C., Becker, S., Dücking, M., Brätz, H., Klemd, R., de Bruin, D., Canil, D., Cornell, D., de
 210 Hoog, C.-S., Dalpé, C., Danyushevsky, L., Eisenhauer, A., Gao, Y., Snow, J.E., Groschopf, N., Günther, D., Latkoczy, C., Guillong,
 211 M., Hauri, E.K., Höfer, H.E., Lahaye, Y., Horz, K., Jacob, D.E., Kasemann, S.A., Kent, A.J.R., Ludwig, T., Zack, T., Mason, P.R.D.,
 212 Meixner, A., Rosner, M., Kisawa, K., Nash, P.B., Pfänder, J., Premo, W.R., Sun, W.D., Tiepolo, M., Vannucci, R., Vennemann, T.,
 213 Wayne, D., Woodhead, J.D., 2006. MPI-DING reference glasses for in situ microanalysis: New reference values for element
 214 concentrations and isotope ratios. *Geochem. Geophys.* **7**:2. <https://doi.org/10.1029/2005GC001060>.
- 215 Keller, J., Ryan, W.B.F., Ninkovich, D., Altherr, R., 1978. Explosive volcanic activity in the Mediterranean over the last 200,000 yr as
 216 recorded in deep-sea sediments. *Geol. Soc. Am. Bull.* **89**, 591-604. [https://doi.org/10.1130/0016-7606\(1978\)89%3C591:EVAITM%3E2.0.CO;2](https://doi.org/10.1130/0016-7606(1978)89%3C591:EVAITM%3E2.0.CO;2).
- 217 Koppers, A.A.P., 2002. ArArCALC e software for $^{40}\text{Ar}/^{39}\text{Ar}$ age calculations. *Comput. Geosci.* **28**, 605-619. [https://doi.org/10.1016/S0098-3004\(01\)00095-4](https://doi.org/10.1016/S0098-3004(01)00095-4).
- 218 Kutterolf, S., Schindlbeck, J.C., Jegen, M., Freundt, A., Straub, S.M., 2019. Milankovitch frequencies in tephra records at volcanic arcs:
 219 The relation of kyr-scale cyclic variations in volcanism to global climatic changes. *Quat. Sci. Rev.* **204**, 1-16.
 220 <https://doi.org/10.1016/j.quascirev.2018.11.004>.
- 221 Lane, C.S., Brauer, A., Blockley, S.P.E., Dulski, P., 2013. Volcanic ash reveals time-transgressive abrupt climate change during the
 222 Younger Dryas. *Geology* **41** (12), 1251-1254. <https://doi.org/10.1130/G34867.1>.
- 223 Lane, C.S., Cullen, V.L., White, D., Bramham, C.W.F., Smith, V.C., 2014. Cryptotephra as a dating and correlation tool in
 224 archaeology. *J. Archaeol. Sci.* **42**, 42-50. <https://doi.org/10.1016/j.jas.2013.10.033>.
- 225 Lane, C.S., Lowe, D.J., Blockley, S.P.E., Suzuki, T., Smith, V.C., 2017. Advancing tephrochronology as a global dating tool: Applications
 226 in volcanology, archaeology and palaeoclimatic research. *Quat. Geochronol.* **40**, 1-7. <https://doi.org/10.1016/j.quageo.2017.04.003>.
- 227 Laurenzi, M.A. & Villa, I.M., 1987. $^{40}\text{Ar}/^{39}\text{Ar}$ chronostratigraphy of Vico ignimbrites. *Period. Mineral.* **56**, 285-293.
- 228 Le Maitre, R.W., Streckeisen, A., Zanettin, B., Le Bas, M.J., Bonin, B., Bateman, P., Bellieni, G., Dudek, A., Efremova, S., Keller, J.,
 229 Lameyre, J., Sabine, P.A., Schmid, R., Sørensen, H., Woolley, A.R., 2002. *Igneous Rocks: A Classification and Glossary of Terms.*
 230 Recommendation of the International Union of Geological Sciences Subcommittee on the Systematics of Igneous Rocks, 2nd Edition.
 231 Cambridge University Press, Cambridge. 236 pages.
- 232 Lee, J.Y., Marti, K., Severinghaus, J.P., Kawamura, K., Yoo, H.S., Lee, J.B., Kim, J.S., 2006. A redetermination of the isotopic abundances
 233 of atmospheric Ar. *Geochim. Cosmochim. Acta* **70** (17), 4507-4512. <https://doi.org/10.1016/j.gca.2006.06.1563>.
- 234 Leicher, Giaccio, B., Zanchetta, G., Sulpizio, R., Albert, P.G., Tomlinson, E.L., Lagos, M., Francke, A., Wagner, B., 2021. Lake Ohrid's
 235 tephrochronological dataset reveals 1.36 Ma of Mediterranean explosive volcanic activity. *Sci. Data* **8**, 231.
 236 <https://doi.org/10.1038/s41597-021-01013-7>.
- 237 Leicher, N., Giaccio, B., Zanchetta, G., Wagner, B., Francke, A., Palladino, D.M., Sulpizio, R., Albert, P.G., Tomlinson, E.L., 2019. Central
 238 Mediterranean explosive volcanism and tephrochronology during the last 630 ka based on the sediment record from Laker Ohrid,
 239 *Quat. Sci. Rev.* **226**, 106021. <https://doi.org/10.1016/j.quascirev.2019.106021>.
- 240 Leicher, N., Zanchetta, G., Sulpizio, R., Giaccio, B., Wagner, B., Nomade, S., Francke, A., Del Carlo, P., 2016. First tephrostratigraphic
 241 results of the DEEP site record from Lake Ohrid (Macedonia and Albania). *Biogeosciences* **13**, 2151-2178. <https://doi.org/10.5194/bg-13-2151-2016>.
- 242 Lisiecki, L.E. & Raymo, M.E., 2005. A Pliocene-Pleistocene stack of 57 globally distributed benthic $\delta^{18}\text{O}$ records. *Palaeoceanogr.*
 243 *Palaeoclimatol.* **20** (1), PA1003. <https://doi.org/10.1029/2004PA001071>.
- 244 Lowe, D.J., 2011. Tephrochronology and its application: A review. *Quat. Geochronol.* **6**, 107-153.
 245 <https://doi.org/10.1016/j.quageo.2010.08.003>.
- 246 Lowe, D.J., Pearce, N.J.G., Jorgensen, M.A., Kuhlen, S., Tyron, C.A., Hayward, C.L., 2017. Correlating tephra and cryptotephra using
 247 glass compositional analyses and numerical and statistical methods: Review and evaluation. *Quat. Sci. Rev.* **175**, 1-44.
 248 <https://doi.org/10.1016/j.quascirev.2017.08.003>.
- 249 Ludwig, K.R., 2012. User's Manual for Isoplot Version 3.75-4.15: A Geochronological Toolkit for Microsoft Excel. *Berkley Geochronological*
 250 *Centre Special Publication* **5**.
- 251 Mannella, G., Giaccio, B., Zanchetta, G., Regattieri, E., Niespolo, E.M., Pereira, A., Renne, P.R., Nomade, S., Leicher, N., Perchiazzi, N.,
 252 Wagner, B., 2019. Paleoenvironmental and paleohydrological variability of mountain areas in the central Mediterranean region: A 190-
 253 ka-long chronicle from the independently dated Fucino paleolake record (central Italy). *Quat. Sci. Rev.* **210**, 190-210.
 254 <https://doi.org/10.1016/j.quascirev.2019.02.032>.
- 255 Marianelli, P. & Sbrana, A. Risultati di misure standard di minerali e di vetri naturali in microanalisi a dispersione di energia (In Italian). *Atti*
 256 *Soc. Tosc. Sci. Nat. Resid. Pisa, Mem. Serie A* **105**, 57-63 (1998).
- 257 Marra, F., Castellano, C., Cucci, L., Florindo, F., Gaeta, M., Jicha, B., Palladino, D.M., Sottili, G., Tertulliani, A., Tolomei, C., 2020. Monti
 258 Sabatini and Colli Albani: the dormant twin volcanoes at the gates of Rome. *Sci. Rep.* **10**:8666. <https://doi.org/10.1038/s41598-02-65394-2>.

- 263 Marra, F., Freda, C., Scarlato, P., Taddeucci, J., Karner, D.B., Renne, P.R., Gaeta, M., Palladino, D.M., Triglia, R., Cavaretta, G., 2003.
 264 Post-caldera activity in the Alban Hills volcanic district (Italy): $^{40}\text{Ar}/^{39}\text{Ar}$ geochronology and insights into magma evolution. *Bull.*
 265 *Volcanol.* **65**, 227-247. <https://doi.org/10.1007/s00445-002-0255-9>.
- 266 Marra, F., Gaeta, M., Giaccio, B., Jicha, B.R., Palladino, D.M., Polcari, M., Sottili, G., Taddeucci, J., Florindo, F., Stramondo, S., 2016.
 267 Assessing the volcanic hazard for Rome: $^{40}\text{Ar}/^{39}\text{Ar}$ and In-SAR constraints on the most recent eruptive activity and present-day uplift
 268 at Colli Albani Volcanic District. *Geophys. Res. Lett.* **43**, 6898-6906. <https://doi.org/10.1002/2016GL069518>.
- 269 Marra, F., Karner, D.B., Freda, C., Gaeta, M., Renne, P., 2009. Large mafic eruptions at Alban Hills Volcanic District (Central Italy):
 270 chronostratigraphy, petrography and eruptive behavior. *J. Volcanol. Geotherm. Res.* **179**, 217-232.
 271 <https://doi.org/10.1016/j.jvolgeores.2008.11.009>.
- 272 Marra, F., Nomade, S., Pereira, A., Petronio, C., Salari, L., Sottili, G., Bahain, J.J., Boschian, G., Di Stefano, G., Falguères, C., Florindo,
 273 F., Gaeta, M., Giaccio, B., Masotta, M., 2018. A review of the geological sections and the faunal assemblages of Aurelian Mammal
 274 Age of Latium (Italy) in the light of a new chronostratigraphic framework. *Quat. Sci. Rev.* **181**, 173-199.
 275 <https://doi.org/10.1016/j.quascirev.2017.12.007>.
- 276 Martrat, B., Grimalt, J.O., Shackleton, N.J., de Abreu, L., Hutterli, M.A., Stocker, T.F., 2007. Four climate cycles of recurring deep and
 277 surface water destabilizations on the Iberian margin. *Science* **317**, 502-507. <https://www.science.org/doi/10.1126/science.1139994>.
- 278 McDonough, W.F. & Sun, S.-s., 1995. The composition of the Earth. *Chem. Geol.* **120** (3-4), 223-253. [https://doi.org/10.1016/0009-2541\(94\)00140-4](https://doi.org/10.1016/0009-2541(94)00140-4).
- 279
 280 Mixon, E.E., Jicha, B.R., Tootell, D., Singer, B.S., 2022. Optimizing $^{40}\text{Ar}/^{39}\text{Ar}$ analyses using the Isotopx NGX-600 mass spectrometer.
 281 *Chem. Geol.* **593**, 120753. <https://doi.org/10.1016/j.chemgeo.2022.120753>.
- 282 Monaco, L., Palladino, D.M., Albert, P.G., Arienzo, I., Conticelli, S., Di Vito, M., Fabbrizio, A., D'Antonio, M., Isaia, R., Manning, C.J.,
 283 Nomade, S., Pereira, A., Petrosino, P., Sottili, G., Sulpizio, R., Zanchetta, G., Giaccio, B., 2022. Linking the Mediterranean MIS 5
 284 tephra markers to Campi Flegrei (southern Italy) 109-92 ka explosive activity and refining the chronology of MIS 5c-d millennial-scale
 285 climatic variability. *Glob. Pla. Che.* **211**, 103785. <https://doi.org/10.1016/j.gloplacha.2022.103785>.
- 286 Monaco, L., Palladino, D.M., Gaeta, M., Marra, F., Sottili, G., Leicher, N., Mannella, G., Nomade, S., Pereira, A., Regattieri, E., Wagner,
 287 B., Zanchetta, G., Albert, P.G., Arienzo, I., D'Antonio, M., Petrosino, P., Manning, C., Giaccio, B., 2021. Mediterranean
 288 tephrostratigraphy and peri-Tyrrhenian explosive activity reevaluated in light of the 430-365 ka record from Fucino Basin (central Italy).
 289 *Earth Sci. Rev.* **220**, 103706. <https://doi.org/10.1016/j.earscirev.2021.103706>.
- 290 Munno, R. & Petrosino, P., 2007. The late Quaternary tephrostratigraphical record of the San Gregorio Magno basin (southern Italy). *J.*
 291 *Quat. Sci.* **22**, 247-266. <https://doi.org/10.1002/jqs.1025>.
- 292 Nappi, G., Capaccioni, B., Mattioli, M., Mancini, F., & Valentini, L., 1994. Plinian fall deposits from Vulsini Volcanic District (Central Italy).
 293 *Bull. Volcanol.* **56**, 502-515. <https://doi.org/10.1007/BF00302831>.
- 294 Niespolo, E.M., Rutte, D., Deino, A.L., Renne, P.R., 2017. Intercalibration and age of the Alder Creek Sanidine $^{40}\text{Ar}/^{39}\text{Ar}$ standard. *Quat.*
 295 *Geochronol.* **39**, 205-213. <https://doi.org/10.1016/j.quageo.2016.09.004>.
- 296 Pabst, S., Wörner, G., Civetta, L., Tesoro, R., 2007. Magma chamber evolution prior to the Campanian Ignimbrite and Neapolitan Yellow
 297 Tuff eruptions (Campi Flegrei, Italy). *Bull. Volcanol.* **70**, 961-976. <https://doi.org/10.1007/s00445-007-0180-z>.
- 298 Palladino, D.M. & Agosta, E., 1997. Pumice fall deposits of the Western Vulsini Volcanoes (Central Italy). *J. Volcanol. Geotherm. Res.* **78**
 299 (1-2), 77-102. [https://doi.org/10.1016/S0377-0273\(96\)00107-2](https://doi.org/10.1016/S0377-0273(96)00107-2).
- 300 Palladino, D.M. & Simei, S., 2005. Eruptive dynamics and caldera-collapse during the Onano eruption, Vulsini, Italy. *Bull. Volcanol.* **67**,
 301 423-440. <https://doi.org/10.1007/s00445-004-0385-3>.
- 302 Palladino, D.M. & Taddeucci, J., 1998. The basal ash deposit of the Sovana Eruption (Vulsini Volcanoes, central Italy): the product of a
 303 dilute pyroclastic density current. *J. Volcanol. Geotherm. Res.* **87** (1-4), 233-254. [https://doi.org/10.1016/S0377-0273\(98\)00095-X](https://doi.org/10.1016/S0377-0273(98)00095-X).
- 304 Palladino, D.M. & Valentine, G.A., 1995. Coarse-tail vertical and lateral grading in pyroclastic flow deposits of the Latera Volcanic Complex
 305 (Vulsini, central Italy): origin and implications for flow dynamics. *J. Volcanol. Geotherm. Res.* **69** (3-4), 343-364.
 306 [https://doi.org/10.1016/0377-0273\(95\)00036-4](https://doi.org/10.1016/0377-0273(95)00036-4).
- 307 Palladino, D.M., Gaeta, M., Giaccio, B., Sottili, G., 2014. On the anatomy of magma chamber and caldera collapse: the example of
 308 trachyphonolite explosive eruptions of the Roman province (Central Italy). *J. Volcanol. Geotherm. Res.* **281**, 12-26.
 309 <https://doi.org/10.1016/j.jvolgeores.2014.05.020>.
- 310 Palladino, D.M., Simei, S., Sottili, G., Triglia, R., 2010. Integrated approach for the reconstruction of stratigraphy and geology of Quaternary
 311 volcanic terrains: an application to the Vulsini Volcanoes (central Italy). In: Gropelli, G., Viereck, e L. (Eds.), *Stratigraphy and Geology*
 312 *in Volcanic Areas. Geol. Soc. Am. Spec. Pap.* **464**, 66-84.
- 313 Palladino, D.M., Simei, S., Triglia, R., 2016. Note illustrative della Carta geologica d'Italia alla scala 1:50.000, foglio 344 Tuscania, *ISPRA-*
 314 *Servizio Geologico d'Italia* (In Italian). https://www.isprambiente.gov.it/Media/carg/note_illustrative/344_Tuscania.pdf.
- 315 Pappalardo, L., Civetta, L., D'Antonio, M., Deino, A., Di Vito, M., Orsi, G., Carandente, A., de Vita, S., Isaia, R., Piochi, M., 1999. Chemical
 316 and Sr-isotopical evolution of the Phlegrean magmatic system before the Campanian Ignimbrite and the Neapolitan Yellow Tuff
 317 eruptions. *J. Volcanol. Geotherm. Res.* **91** (2-4), 141-166. [https://doi.org/10.1016/S0377-0273\(99\)00033-5](https://doi.org/10.1016/S0377-0273(99)00033-5).
- 318 Past Interglacials Working Group of PAGES, 2016. Interglacials of the last 800,000 years. *Rev. Geophys.* **54**, 162-219.
 319 <https://doi.org/10.1002/2015RG000482>.
- 320 Patacca, E., Scandone, P., Di Luzio, E., Cavinato, G.P., Parotto, M., 2008. Structural architecture of the central Apennines: Interpretation
 321 of the CROP 11 seismic profile from the Adriatic coast to the orographic divide. *Tectonics* **27**, TC3006.
 322 <https://doi.org/10.1029/2005TC001917>.
- 323 Paterne, M., Guichard, F., Duplessy, J.C., Siani, G., Sulpizio, R., Labeyrie, J., 2008. A 90,000-200,000 yrs marine tephra record of Italian
 324 volcanic activity in the Central Mediterranean Sea. *J. Volcanol. Geotherm. Res.* **177**, 187-196.
 325 <https://doi.org/10.1016/j.jvolgeores.2007.11.028>.
- 326 Paterne, M., Guichard, F., Labeyrie, J., 1988. Explosive activity of the south Italian volcanoes during the past 80,000 years as determined
 327 by marine tephrochronology. *J. Volcanol. Geotherm. Res.* **34**, 153-172. [https://doi.org/10.1016/0377-0273\(88\)90030-3](https://doi.org/10.1016/0377-0273(88)90030-3).
- 328 Paterne, M., Guichard, F., Labeyrie, J., Gillot, P.Y., Duplessy, J.C., 1986. Tyrrhenian Sea tephrochronology of the oxygen isotope record
 329 for the past 60,000 years. *Mar. Geol.* **72**, 259-285. [https://doi.org/10.1016/0025-3227\(86\)90123-4](https://doi.org/10.1016/0025-3227(86)90123-4).

- 330 Pearce, N.J.G., Alloway, B., Wickham, C., 2019. Correlating weathered, microphenocryst-rich, intermediate tephra: An approach
 331 combining bulk and single shard analyses from the Lepu  Tephra, Chile and Argentina. *Quat. Internat.* **500**, 71-82.
 332 <https://doi.org/10.1016/j.quaint.2019.01.017>.
- 333 Pearce, N.J.G., Perkins, W.T., Westgate, J.A., Gorton, M.P., Jackson, S.E., Neal, C.R., Chenery, S.P., 1997. A Compilation of New and
 334 Published Major and Trace Element Data for NIST SRM 610 and NIST SRM 612 Glass Reference Materials. *Geostand. Newslett.* **21**
 335 (1), 115-144. <https://doi.org/10.1111/j.1751-908X.1997.tb00538.x>.
- 336 Peccerillo, A., 2017. Cenozoic Volcanism in the Tyrrhenian Sea Region. In: IAVCEI, Advances in Volcanology, 2 ed. Springer, p. 400.
- 337 Pelullo, C., Cirillo, G., Iovine, R.S., Arienzo, I., Aulinas, M., Pappalardo, L., Petrosino P., Fernandez-Turiel, J.L., D'Antonio, M., 2020.
 338 Geochemical and Sr-Nd isotopic features of the Zaro volcanic complex: insights on the magmatic processes triggering a small-scale
 339 prehistoric eruption at Ischia island (south Italy). *Int. J. Earth Sci.* **109** (8), 2829-2849. <https://doi.org/10.1007/s00531-020-01933-6>.
- 340 Pereira, A., Nomade, S., Moncel, M.-H., Voinchet, P., Bahain, J.-J., Biddittu, I., Falgu eres, C., Giaccio, B., Manzi, G., Parenti, F., Scardia,
 341 G., Scao, V., Sottili, G., Vietti, A., 2018. Geochronological evidences of a MIS 11 to MIS 10 age for several landmark Acheulian sites
 342 from the Frosinone province (Lazio, Italy): Archaeological implications. *Quat. Sci. Rev.* **187**, 112-129.
 343 <https://doi.org/10.1016/j.quascirev.2018.03.021>.
- 344 Perini, G., Conticelli, S., Francalanci, L., 1997. Inferences on the volcanic history of the Vico volcano, Roman Magmatic Province, central
 345 Italy: stratigraphic, petrographic and geochemical data. *Mineral. Petrograph. Acta* **40**, 67-93.
- 346 Perini, G., Francalanci, L., Davidson, J.P., Conticelli, S., 2004. Evolution and Genesis of Magmas from Vico Volcano, Central Italy: Multiple
 347 Differentiation Pathways and Variable Parental Magmas. *J. Petrol.* **45** (1), 139-182. <https://doi.org/10.1093/petrology/egg084>.
- 348 Petrelli, M., Laeger, K., Perugini, D., 2016. High spatial resolution trace element determination of geological samples by laser ablation
 349 quadrupole plasma mass spectrometry: implications for glass analysis in volcanic products. *Geosci. J.* **20** (851-863).
 350 <https://doi.org/10.1007/s12303-016-0007-z>.
- 351 Petrosino, P., Arienzo, I., Mazzeo, F.C., Natale, J., Petrelli, M., Milia, A., Perugini, D., D'Antonio, M., 2019. The San Gregorio Magno
 352 lacustrine basin (Campania, southern Italy): improved characterization of the tephrostratigraphic markers based on trace elements
 353 and isotopic data. *J. Quat. Sci.* **34**, 393-404. <https://doi.org/10.1002/jqs.3107>.
- 354 Petrosino, P., Morabito, S., Jicha, B.R., Milia, A., Sprovieri, M., Tamburrino, S., 2016. Multidisciplinary tephrochronological correlation of
 355 marker events in the eastern Tyrrhenian Sea between 48 and 105 ka. *J. Volcanol. Geotherm. Res.* **315**, 79-99.
 356 <https://doi.org/10.1016/j.jvolgeores.2016.02.001>.
- 357 Poli, S., Chiesa, S., Gillot, P.-Y., Gregnanin, A., Guichard, F., 1987. Chemistry versus time in the volcanic complex of Ischia (Gulf of
 358 Naples, Italy): evidence of successive magmatic cycles. *Contrib. Mineral. Petrol.* **95**, 322-335.
- 359 Ponomareva, V.V., Portnyagin, M., Davies, S.M., 2015. Tephra without borders: far-reaching clues into past explosive eruptions. *Front.*
 360 *Earth Sci.* **3** (83). <https://doi.org/10.3389/feart.2015.00083>.
- 361 Regattieri, E., Giaccio, B., Zanchetta, G., Drysdale, R.N., Galli, P., Nomade, S., Peronace, E., Wulf, S., 2015. Hydrological variability over
 362 the Apennines during the Early Last Glacial precession minimum, as revealed by a stable isotope record from Sulmona basin, Central
 363 Italy. *J. Quat. Sci.* **30**, 19-31. <https://doi.org/10.1002/jqs.2755>.
- 364 Reimer, P.J., Austin, W.E.N., Bard, E., Bayliss, A., Blackwell, P.G., Bronk Ramsey, C., Butzin, M., Cheng, H., Edwards, R.L., Friedrich,
 365 M., Grootes, P.M., Guilderson, T.P., Hajdas, I., Heaton, T.J., Hogg, A.G., Hughen, H.A., Kromer, B., Manning, S.W., Muscheler, R.,
 366 Palmer, J.G., Pearson, C., van der Plicht, J., Reimer, R.W., Richards, D.A., Scott, E.M., Southon, J.R., Turney, C.S.M., Wacker, L.,
 367 Adolphi, F., B untgen, U., Capano, M., Fahrni, S.M., Fogtmann-Schulz, A., Friedrich, R., K hler, P., Kudsk, S., Miyake, F., Olsen, J.,
 368 Reinig, F., Sakamoto, M., Sookdeo, A., Talamo, S., 2020. The Intcal20 northern hemisphere radiocarbon age calibration curve (0-55
 369 cal kBP). *Radiocarbon* **62** (4), 725-757. <https://doi.org/10.1017/RDC.2020.41>.
- 370 Renne, P.R., Balco, G., Ludwig, K.R., Mundil, R., Min, K., 2011. Response to the comment by WH Schwarz et al. on "Joint determination
 371 of 40 K decay constants and ⁴⁰Ar*/⁴⁰K for the Fish Canyon sanidine standard, and improved accuracy for ⁴⁰Ar/³⁹Ar geochronology" by
 372 PR Renne et al. (2010). *Geochim. Cosmochim. Acta* **75**, 5097-5100.
- 373 Rolandi, G., Bellucci, F., Heizler, M.T., Belkin, H.E., De Vivo, B., 2003. Tectonic controls on the genesis of ignimbrite from the Campanian
 374 Volcanic Zone, southern Italy. *Mineral. Petrol.* **79**, 3-31. <https://doi.org/10.1007/s00710-003-0014-4>.
- 375 Ross, J., 2019. NMGRL/pychron v18.2: Zenodo. <https://doi.org/10.5281/zenodo.3237834>.
- 376 Rouchon, V., Gillot, P.Y., Quidelleur, X., Chiesa, S., Floris, B., 2008. Temporal evolution of the Roccamonfina volcanic complex
 377 (Pleistocene), Central Italy. *J. Volcanol. Geotherm. Res.* **177**, 500-514. <https://doi.org/10.1016/j.jvolgeores.2008.07.016>.
- 378 Roucoux, K.H., Tzedakis, P.C., Frogley, M.R., Lawson, I.T., Preece, R.C., 2008. Vegetation history of the marine isotope stage 7
 379 interglacial complex at Ioannina, NW Greece. *Quat. Sci. Rev.* **27**, 1378-1395. <https://doi.org/10.1016/j.quascirev.2008.04.002>.
- 380 Ruddiman, W.F., McIntyre, A., 1982. Severity and speed of Northern Hemisphere glaciation pulses: The limiting case? *Geol. Soc. Am.*
 381 *Bull.* **93**, 1273-1279. [https://doi.org/10.1130/0016-7606\(1982\)93%3C1273:SASONH%3E2.0.CO;2](https://doi.org/10.1130/0016-7606(1982)93%3C1273:SASONH%3E2.0.CO;2).
- 382 Sadori, L., Koutsodendris, A., Panagiotopoulos, K., Masi, A., Bertini, A., Combourieu-Nebout, N., Francke, A., Koull, K., Joannin, S.,
 383 Mercuri, A.M., Peyron, O., Torri, P., Wagner, B., Sinopoli, G., Donders, T.H., 2016. Pollen-based paleoenvironmental and
 384 paleoclimatic change at Lake Ohrid (south-eastern Europe) during the past 500 ka. *Biogeosciences* **13**, 1423-1437.
 385 <https://doi.org/10.5194/bg-13-1424-2016>.
- 386 Sadori, L., Koutsodendris, A., Panagiotopoulos, K., Masi, A., Bertini, A., Combourieu-Nebout, N., Francke, A., Koull, K., Kousis, I., Joannin,
 387 S., Mercuri, A.M., Peyron, O., Torri, P., Wagner, B., Sinopoli, G., Donders, T.H., 2018. Pollen data of the last 500 ka BP at Lake Ohrid
 388 (south-eastern Europe). *PANGAEA*. <https://doi.org/10.1594/PANGAEA.892362>.
- 389 Satow, C., Tomlinson, E.L., Grant, K.M., Albert, P.G., Smith, V.C., Manning, C.J., Ottoloni, L., Wulf, S., Rohling, E.J., Lowe, J.J., Blockley,
 390 S.P.E., Menzies, M.A., 2015. A new contribution to the Late Quaternary tephrostratigraphy of the Mediterranean: Aegean Sea core
 391 LC21. *Quat. Sci. Rev.* **117**, 96-112. <https://doi.org/10.1016/j.quascirev.2015.04.005>.
- 392 Sbrana, A., Marianelli, P., Pasquini, G., 2018. Volcanology of Ischia. *J. Maps* **14** (2) 494-503.
 393 <https://doi.org/10.1080/17445647.2018.1498811>.
- 394 Shane, P., 2000. Tephrochronology, a New Zealand case study. *Earth-Science Reviews*, **49**, 1-4, 223-259. [https://doi.org/10.1016/S0012-8252\(99\)00058-6](https://doi.org/10.1016/S0012-8252(99)00058-6).

- 396 Smith, D.G.W. & Westgate, J.A., 1968. Electron probe technique for characterising pyroclastic deposits. *Earth Planet. Sci. Lett.* **5**, 313-
397 319. [https://doi.org/10.1016/S0012-821X\(68\)80058-5](https://doi.org/10.1016/S0012-821X(68)80058-5).
- 398 Snyder, C.W., 2016. Evolution of global temperature over the past two million years. *Nature* **538**, 226-228.
399 <https://doi.org/10.1038/nature19798>.
- 400 Sollevanti, F., 1983. Geologic, volcanologic, and tectonic setting of the Vico-Cimino area, Italy. *J. Volcanol. Geotherm. Res.* **17** (1-4), 203-
401 217. [https://doi.org/10.1016/0377-0273\(83\)90068-9](https://doi.org/10.1016/0377-0273(83)90068-9).
- 402 Sottili, G., Arienzo, I., Castorina, F., Gaeta, M., Giaccio, B., Marra, F., Palladino, D.M., 2019. Time-dependent Sr and Nd isotope variations
403 during the evolution of ultrapotassic Sabatini Volcanic District (Roman Province, Central Italy). *Bull. Volcanol.* **81**:67.
404 <https://doi.org/10.1007/s00445-019-1324-7>.
- 405 Sottili, G., Palladino, D.M., Gaeta, M., Masotta, M., 2012. Origins and energetics of maar volcanoes: examples from the ultrapotassic
406 Sabatini Volcanic District (Roman Province, Central Italy). *Bull. Volcanol.* **74**, 163-186. <https://doi.org/10.1007/s00445-011-0506-8>.
- 407 Sottili, G., Palladino, D.M., Marra, F., Jicha, B., Karner, D.B., Renne, P., 2010. Geochronology of the most recent activity in the Sabatini
408 volcanic district, Roman Province, central Italy. *J. Volcanol. Geotherm. Res.* **196**, 20-30.
409 <https://doi.org/10.1016/j.jvolgeores.2010.07.003>.
- 410 Sparks, R.S.J., 1975. Stratigraphy and geology of the ignimbrites of Vulsini Volcano, central Italy. *Geologische Rundschau* **64** (1), 497-
411 523. <https://doi.org/10.1007/BF01820680>.
- 412 Sunyé-Puchol, I., Hodgetts, A.G.E., Watt, S.F.L., Arce, J.L., Barfod, D.N., Mark, D.F., Sosa-Ceballos, G., Siebe, C., Dymock, R.C.,
413 Blaauw, M., Smith, V.C., 2022. Reconstructing the middle to late Pleistocene explosive eruption histories of Popocatepetl, Itzacihuatl
414 and Tláloc-Telapón volcanoes in central México. *J. Volcanol. Geotherm. Res.* **421**, 107413.
415 <https://doi.org/10.1016/j.jvolgeores.2021.107413>.
- 416 Taddeucci, J. & Palladino, D.M., 2002. Particle size-density relationships in pyroclastic deposits: inferences from emplacement processes.
417 *Bull. Volcanol.* **64**, 273-284. <https://doi.org/10.1007/s00445-002-0205-6>.
- 418 Thorarinsson, S., 1944. Tefrokronologiska Studier På Island. Þjórsárdalur Och Dess Förödelse. *Geografiska Annaler* **26** (1-2), 1-217.
419 <https://doi.org/10.1080/20014422.1944.11880727>.
- 420 Thorarinsson, S., 1981a. Greetings from Iceland. *Geografiska Annaler: Series A, Physical Geography*, 63:3-4, 109-118.
- 421 Thorarinsson, S., 1981b. Tephra studies and tephrochronology: a historical review with special reference to Iceland. In: S. Self, R.S.J.,
422 Sparks (Eds.), *Tephra Studies*, Reidel, Dordrecht (1981), pp. 1-12. https://doi.org/10.1007/978-94-009-8537-1_1.
- 423 Tomlinson, E.L., Arienzo, I., Civetta, L., Wulf, S., Smith, V.C., Hardiman, M., Lane, C.S., Carandente, A., Orsi, G., Rosi, M., Müller, W.,
424 Menzies, M.A., 2012. Geochemistry of the Phlegrean Fields (Italy) proximal sources for major Mediterranean tephras: Implications for
425 the dispersal of Plinian and co-ignimbritic components of explosive eruptions. *Geochim. Cosmochim. Acta* **93**, 102-128.
426 <https://doi.org/10.1016/j.gca.2012.05.043>.
- 427 Tomlinson, E.L., Smith, V.C., Albert, P.G., Aydar, E., Civetta, L., Cioni, R., Çubukçu, E., Gertisser, R., Isaia, R., Menzies, M.A., Orsi, G.,
428 Rosi, M., Zanchetta, G., 2015. The major and trace element glass compositions of the productive Mediterranean volcanic sources:
429 tools for correlating distal tephra layers in and around Europe. *Quat. Sci. Rev.* **118**, 48-66.
430 <https://doi.org/10.1016/j.quascirev.2014.10.028>.
- 431 Tonarini, S., D'Antonio, M., Di Vito, M.A., Orsi, G., Carandente, A., 2009. Geochemical and Ba-Sr-Nd isotopic evidence for mingling and
432 mixing processes in the magmatic system that fed the Astroni volcano (4.1-3.8 ka) within the Campi Flegrei caldera (southern Italy).
433 *Lithos* **107** (3-4), 135-151. <https://doi.org/10.1016/j.lithos.2008.09.012>.
- 434 Turbeville, B.N., 1992. ⁴⁰Ar/³⁹Ar ages and Stratigraphy of the Latera caldera, Italy. *Bull. Volcanol.* **55**, 110-118.
435 <https://doi.org/10.1007/BF00301124>.
- 436 Tzedakis, P.C., Crucifix, M., Mitsui, T., Wolff, E.W., 2017. A simple rule to determine which insolation cycles lead to interglacials. *Nature*
437 **542**, 427-432. <https://doi.org/10.1038/nature21364>.
- 438 Tzedakis, P.C., Hooghiemstra, H., Pälike, H., 2006. The last 1.35 million years at Tenaghi Philippon: revised chronostratigraphy and long-
439 term vegetation trends. *Quat. Sci. Rev.* **25** (23-24), 3416-3430. <https://doi.org/10.1016/j.quascirev.2006.09.002>.
- 440 Tzedakis, P.C., Roucoux, K. H., de Abreu, L., Shackleton, N. J., 2004. The duration of forest stages in southern Europe and interglacial
441 climate variability. *Science* **306**, 2231-2235. <https://doi.org/10.1126/science.1102398>.
- 442 Tzedakis, P.C., Wolff, E.W., Skinner, L.C., Brovkin, V., Hodell, D.A., McManus, J.F., Raynaud, D., 2012. Can we predict the duration of
443 an interglacial? *Clim. Past* **8**, 1473-1485. <https://doi.org/10.5194/cp-8-1473-2012>.
- 444 Vakhrameeva, P., Koutsodendris, A., Wulf, S., Fletcher, W.J., Appelt, O., Knipping, M., Gertisser, R., Trieloff, M., Pross, J., 2018. The
445 cryptotephra record of the Marine Isotope Stage 12 to 10 interval (460-335 ka) at Tenaghi Philippon, Greece: Exploring chronological
446 markers for the Middle Pleistocene of the Mediterranean region. *Quat. Sci. Rev.* **200**, 313-333.
447 <https://doi.org/10.1016/j.quascirev.2018.09.019>.
- 448 Vakhrameeva, P., Koutsodendris, A., Wulf, S., Portnyagin, M., Appelt, O., Ludwig, T., Trieloff, M., Pross, J., 2021. Land-sea correlations
449 in the Eastern Mediterranean region over the past c. 800 kyr based on macro- and cryptotephras from ODP Site 964 (Ionian Basin).
450 *Quat. Sci. Rev.* **255**, 106811. <https://doi.org/10.1016/j.quascirev.2021.106811>.
- 451 Vakhrameeva, P., Wulf, S., Koutsodendris, A., Tjallingii, R., Fletcher, W.J., Appelt, O., Ludwig, T., Knipping, M., Trieloff, M., Pross, J.,
452 2019. Eastern Mediterranean volcanism during Marine isotope stages 9 to 7e (335-235 ka): Insights based on cryptotephra layers at
453 Tenaghi Philippon, Greece. *J. Volcanol. Geotherm. Res.* **380**, 31-47. <https://doi.org/10.1016/j.jvolgeores.2019.05.016>.
- 454 Valentine, G.A., Palladino, D.M., DiemKaye, K., Fletcher, C., 2019. Lithic-rich and lithic-poor ignimbrites and their basal deposits: Sovana
455 and Sorano formations (Latera caldera, Italy). *Bull. Volcanol.* **81**, 29. <https://doi.org/10.1007/s00445-019-1288-7>.
- 456 Vezzoli, L., Conticelli, S., Innocenti, F., Landi, P., Manetti, P., Palladino, D.M., Trigila, R., 1987. Stratigraphy of the Latera Volcanic
457 Complex: proposals for a new nomenclature. *Period. Mineral.* **56**, 89-110.
- 458 Villa, P., Soriano, S., Pollarolo, L., Smiriglio, C., Gaeta, M., D'Orazio, M., Conforti, J., Tozzi, C., 2020. Neandertals on the beach: Use of
459 marine resources at Grotta dei Moscerini (Latium, Italy). *PLoS ONE* **15** (1), e0226690. <https://doi.org/10.1371/journal.pone.0226690>.
- 460 Wagner, B., Vogel, H., Francke, A., Friederich, T., Donders, T., Lacey, J.H., Leng, M.J., Regattieri, E., Sadori, L., Wilke, T., Zanchetta,
461 G., Albrecht, C., Bertini, A., Combourieu-Nebout, N., Cvetkoska, A., Giaccio, B., Grazhdani, A., Hauffe, T., Holtvoeth, J., Joannin, S.,
462 Lagoos, M., Leicher, N., Levkov, Z., Lindhorst, K., Masi, A., Melles, M., Mercuri, A.M., Nomade, S., Nowaczyk, N., Panagiotopoulos,
463 K., Peyron, O., reed, J.M., Sagnotti, L., Sinopoli, G., Stellbrink, B., Sulpizio, R., Timmermann, A., Tofilovska, S., Torri, P., Wagner-

- 464 Cremer, F., Wonik, T., Zhang, X., 2019. Mediterranean winter rainfall in phase with African monsoons during the past 1.36 million
465 years. *Nature* **573**, 256-260. <https://doi.org/10.1038/s41586-019-1529-0>.
- 466 Wastegård, S., Veres, D., Kliem, P., Hahn, A., Ohlendorf, C., Zolitschka, B., The PASADO Science Team, 2013. Towards a late
467 Quaternary tephrochronological framework for the southernmost part of South America – the Laguna Potrok Aike tephra record.
468 *Quat. Sci. Rev.* **71**, 81-90. <https://doi.org/10.1016/j.quascirev.2012.10.019>.
- 469 Wendt, K.A., Li, X., Edwards, R.L., Cheng, H., Spötl, C., 2021. Precise timing of MIS 7 substages from the Austrian Alps. *Clim. Past* **17**,
470 1443-1454. <https://doi.org/10.5194/cp-17-1443-2021>.
- 471 Wilson, M. & Bianchini, G., 1999. Tertiary-Quaternary magmatism within the Mediterranean and surroundings regions. In: Durand, B.,
472 Jolivet, L., Horváth, F., Séranne, M. (eds.) *The Mediterranean Basins: Tertiary extension within the Alpine Orogen. Geol. Soc. Lond. Spec. Publ.* **156**, 141-169.
- 473
474 Wulf, S., Hardiman, M.J., Staff, R.A., Koutsodendris, A., Appelt, O., Blockley, S.P.E., Lowe, J.J., Manning, C.J., Ottolini, L., Schmitt, A.K.,
475 Smith, V.C., Tomlinson, E.L., Vakhrameeva, P., Knipping, M., Kotthoff, U., Milner, A.M., Müller, U.C., Christanis, K., Kalaitzidis, S.,
476 Tzedakis, P.C., Schmiedl, G., Pross, J., 2018. The Marine isotope stage 1-5 cryptotephra record of Tenaghi Philippon, Greece:
477 Towards a detailed tephrostratigraphic framework for the Eastern Mediterranean region. *Quat. Sci. Rev.* **186**, 236-262.
478 <https://doi.org/10.1016/j.quascirev.2018.03.011>.
- 479 Wulf, S., Keller, J., Paterne, M., Mingram, J., Lauterbach, S., Opitz, S., Sottili, G., Giaccio, B., Albert, P.G., Satow, C., Tomlinson, E.L.,
480 Viccaro, M., Brauer, A., 2012. The 100-133 ka record of Italian explosive volcanism and revised tephrochronology of Lago Grande di
481 Monticchio. *Quat. Sci. Rev.* **58**, 104-123. <https://doi.org/10.1016/j.quascirev.2012.10.020>.
- 482 Wulf, S., Keller, J., Satow, C., Gertisser, R., Kraml M., Grant, K.M., Appelt, O., Vakhrameeva, P., Koutsodendris, A., Hardiman, M., Schulz,
483 H., Pross, J., 2020. Advancing Santorini's tephrostratigraphy: New glass geochemical data and improved marine-terrestrial tephra
484 correlations for the past ~360 kyrs. *Earth Sci. Rev.* **200**, 102964. <https://doi.org/10.1016/j.earscirev.2019.102964>.
- 485 Wulf, S., Kraml, M., Brauer, A., Keller, J., Negendank, J.F.W., 2004. Tephrochronology of the 100 ka lacustrine sediment record of Lago
486 Grande di Monticchio (Southern Italy). *Quat. Int.* **122**, 7-30. <https://doi.org/10.1016/j.quaint.2004.01.028>.
- 487 Wulf, S., Kraml, M., Keller, J., 2008. Towards a detailed tephrostratigraphy in the Central Mediterranean: The last 20,000 yrs record of
488 Lago Grande di Monticchio. *J. Volcanol. Geotherm. Res.* **177**, 118-132. <https://doi.org/10.1016/j.jvolgeores.2007.10.009>.
- 489 Zanchetta, G., Giaccio, B., Bini, M., Sarti, L., 2018. Tephrostratigraphy of Grotta del Cavallo, Southern Italy: insights of the chronology of
490 Middle to Upper Paleolithic transition in the Mediterranean. *Quat. Sci. Rev.* **182**, 65-77.
491 <https://doi.org/10.1016/j.quascirev.2017.12.014>.
- 492 Ziegler, M., Tuenter, E., Lourens, L.J., 2010. The precession phase of the boreal summer monsoon as viewed from the eastern
493 Mediterranean (ODP Site 968). *Quat. Sci. Rev.* **29**, 1481-1490. <https://doi.org/10.1016/j.quascirev.2010.03.011>.